**Generation and Rearrangement of Thioethers for Self-Reinforcing Thermosets and Semi-crystalline Thermoplastic Photopolymers**

by

Alex Commisso

A dissertation submitted in partial fulfillment
of the requirements for the degree of
Doctor of Philosophy
(Chemical Engineering)
in the University of Michigan
2023

Doctoral Committee:

Associate Professor Timothy Scott, Monash University. Co-Chair
Associate Professor Greg Thurber, Co-Chair
Professor Brian J. Love
Professor Robert Ziff

Alex Commisso

alexcomm@umich.edu

ORCID iD: 0000-0002-8825-5029

© Alex Commisso 2023

**Acknowledgements**

I would like to thank my advisor Tim Scott for guidance and advice through my PhD. As well as my committee for their time to give advice and feedback.

I would like to thank everyone that I have worked with in the Scott lab at the University of Michigan and at Monash University for the support and insights they have provided throughout this process including Harry van der Laan, Megan Dunn, Max Ma, Abdulla Alqubati, Sam Leguizamon, Austin Bingham, Futianyi Wang, Gopal Sama Reddy, Ryan Mulvenna, Davood Khoeini, Abdi Khosravanian, Michael Scalzo, Nizam Khan, and Lois Appiagyei.

I appreciate Monash University and the Chemical and Biological Engineering department at Monash for taking me in and allowing me to complete my research during lockdowns and a difficult global pandemic situation.

Lastly, I appreciate the unconditional love and support of my family that helped me through my doctoral studies while being locked down on the other side of the world during a global pandemic and drove me to pursue my doctorate and for that I am very grateful.

## Table of Contents

## List of Tables

## List of Figures

## List of Schemes

## Abstract

In an effort toward long-term sustainability of plastics, the development of robust polymeric materials with longer lifespans is required. The life cycle of polymeric materials can be expanded by programming polymers with chemical functionalities that afford recyclability or the ability to self-heal and self-reinforce. The versatile nature of thioether chemistry enables facile coupling and rearrangement of covalent bonds due to the reactivity of thiolate anions and thiyl radicals. In this thesis, I will detail two approaches using the versatile thioether chemistry to improve sustainability of polymers: the design of stimuli-responsive self-reinforcing thiol-ene thermosets and the development of recyclable thermoplastic cyclic allylic sulfide resins for stereolithographic additive manufacturing.

To produce sustainable polymers that can respond to their environment, two-stage self-reinforcing films incorporating hexaarylbimidazole (HABI) as a mechanophore were investigated. Using orthogonal thiol-ene chemistries, we first generated thioethers through selective polymerization of the thiol/acrylate using nucleophilic thiol-Michael addition. Then, the network-bound HABI was activated to initiate the *in situ* thiol/allyl radical thiol-ene addition to yield cross-linking *via* locally generated thioethers. This two-stage network was demonstrated first using light as a stimulus with HABI acting as a thiol-ene photoinitiator. Then demonstrated the mechanically labile nature of HABI for use as a mechanophore in the two-stage polymer. The modification of monomer types and stoichiometric ratios affords almost limitless possibilities for the properties of the first and second stage polymer which can be tailored to a wide variety of applications.

Facile generation of thioethers is possible through thiol-ene chemistry but thioethers also possess the ability to be rearranged using addition-fragmentation chain transfer in allyl sulfide functionalities. Here, we evaluated cyclic allylic sulfide (CAS) monomers in thermoplastic stereolithography for their ability to use rearrangeable thioethers to enhance layer adhesion in the light-based additive manufacturing technique. The 7- and 8-membered CAS ring-opening monomers were demonstrated as being effective photopolymers and subsequently crystallized in tens of seconds, making them capable monomers for thermoplastic stereolithography. The advantageous properties of CAS-based resins were demonstrated in stereolithography with a range of complex geometries printed at high resolution using a standard DLP stereolithographic 3D printer. To counteract the brittleness of the homopolymers, copolymers of different sized CAS monomers were produced and assessed. Initially between the 7- and 8-membered, the copolymers were found to produce overall tougher polymers. These copolymer combinations were expanded through the synthesis of 11- and 15-membered semi-crystalline CAS monomers, affording a wider variety of copolymer properties including extremely tough copolymers made from 8- and 11-membered CAS comonomers. To increase the overall print speed, CAS monomers were evaluated for their compatibility with two color photoinitiation/photoinhibition systems used in continuous stereolithographic additive manufacturing. However, the visible light photoinitiators that were evaluated, camphorquinone and H-Nu-640, produced lower quality films than near-UV photoinitiator, Irgacure 819. Additionally, the photoinhibition of CAS was unable to be achieved with readily attainable UV-active photoinhibitors; hexaarylbimidazole, butyl nitrite, and tetraethylthiuram disulfide.

# Chapter 1 Introduction

## 1.1 Stimuli-Responsive Polymers

### *1.1.1 Healing Mechanisms in Polymeric Materials*

Polymeric materials all sustain macroscopic damage over their lifetime as they are constantly exposed to environmental stresses. Strategies to overcome the lifespan deficiency of polymeric materials typically don't involve repair but instead focus on material crack visualization or designing robust materials with longer lifespans.[1,2] Macroscopic repair methods like welding or mending with adhesives can often be used as a temporary solution to restore some mechanical properties but doesn't replace the broken bonds at the molecular level. Moreover, fracturing of covalent bonds in crosslinked polymers requires (re)generation of covalent bonds to restore the original mechanical properties.[3]

Healable polymers are designed with mechanisms to replace broken covalent bonds and regain mechanical properties of the original polymer. Although many strategies to afford self-healing polymers have been reported, they can be classified into either extrinsic or intrinsic healing. The strategies have either necessitated an external stimulus to initiate healing or healing occurs autonomously. The extrinsic self-healing mechanism uses external liquid self-healing agents encapsulated in microcapsules or vasculature which can be autonomously triggered by microcrack formation which releases the healing agent into the damaged area to initiate a repairing mechanism.[4,5] Conversely, the intrinsic healing

approach uses reversible bonds that enable rejoining after a bond scission event to enable repeated healing after multiple damage events.[6,7] The reversible bonds can vary from dynamic covalent bonds to non-covalent supramolecular interactions including hydrogen bonding, ionic bonding, and π- π interactions.[8]

Extrinsic healing embeds healing agents into the bulk polymer which autonomously release in response to localized damage. Extrinsic self-healing can be traced back to 2001 with the first incorporation of microcapsules for autonomous self-healing,[9] where the healing agent is autonomously released into a microcrack when the capsules are severed. The healing agent then mixes with catalyst within the polymer matrix and polymerization occurs to afford healing. After the localized polymerization, the healing agent is locally depleted hindering the ability to self-heal multiple times. Improving the self-healing mechanism, White et al. proposed a biologically inspired vasculature healing system. This method flows healing agent through vasculature below the surface which can rush to the surface in response to a puncture in the material and effectively clot the wound similar to the biological healing system.[10] While the delivery mechanism can be varied, the basic idea of all extrinsic healing systems is a release of healing agents into a crack and polymerize in the void to slow or stop crack propagation. Extrinsic healing provides healing that occurs autonomously but is limited due to its inability to heal multiple times in the same area. Moreover, the long-term stability and reduced load-bearing effects of the liquid-filled inclusions are not ideal.

Intrinsic healing, unlike extrinsic, employs reversible bonding strategies to afford infinitely reversible healing. These reversible cross-links are driven by certain external stimuli (light, heat, pH, mechanical stress, etc.) that control the bond breaking and

reforming reactions. The bonds may be reversible covalent bonds (dynamic covalent bonds) or simple supramolecular interactions (hydrogen bonds, ionic interactions, pi-pi interactions, etc.).[11] Reversible dynamic covalent bonds provide greater mechanical strength than simple supramolecular interactions. These covalent bonds can be thermally reversible like the cycloaddition between a conjugated diene and a dienophile, known as a Diels-Alder reaction. Specifically, the furan and maleimide Diels-Alder reaction has been widely used in thermally reversible networks.[12] Other reaction pairs require higher temperatures for the reverse reaction leading to undesired side-reactions.[13] High temperatures and poor spatiotemporal resolution for healing limit the capabilities of thermally reversible covalent bonding systems.

Photoreversible dynamic covalent bonds are more desirable for their ability to be controlled with high spatial and temporal resolution using irradiation. Dynamic exchange reactions, which occur spontaneously, can cause creep and yield materials with weakened mechanical properties[14] but photochemical approaches only undergo exchange reactions under irradiation conditions leading to greatly minimized creep. Several photochemical approaches have been studied including photoinduced cyclization, photo-mediated metathesis, and photodissociation.[15–17] These types of approaches are still limited by slow healing rates and thus require prolonged periods of irradiation.[18–21] The need for an external stimulus, overall slow healing rates, and long irradiation times limit the practicality of this approach. Moreover, due to imperfect bond reformation, intrinsic self-healing has less than ideal healing efficiencies.[22]

### *1.1.2 Mechanophores in Polymeric Materials*

Using mechanical stress in chemical reactions was found to unlock chemical synthesis pathways that were previously unattainable. The study of using mechanical stress to drive chemical reactivity changes, or mechanochemistry, has been applied to inorganic, organic, and polymeric materials. While mechanochemistry in inorganic materials has been well established,[23,24] more work remains on the study of polymer mechanochemistry.[25]

In polymer materials, the application of a mechanical stress that exceeds the elastic limit affects scission events at the weakest bonds in the network, the accumulation of which causes macroscopic plastic deformation and mechanical property degradation. However, this mechanical energy can be captured in the form of predictable changes in the chemical reactivity.[26] Due to their chain-like structure, polymers are perfectly suited for capturing this mechanical energy and transferring it along the backbone to specific weak bonds in the polymer.[27,28] Termed mechanophores, when bound in a polymer these chemical species afford a predictable change in chemical reactivity through a specific mechanically labile bond or mechanically-initiated conformation change.[29] These controlled bond scissions allow for dissipation of typically destructive mechanical energy into controlled reactions.

Reactivity changes within polymers have historically been initiated by an external stimulus like light and/or heat, however, the opportunity of creating force-induced reactivity changes opens new doors for improved stress-responsive materials. Mechanophores have been specially developed to unlock various chemistries that can be used in functional polymers. Mechanocatalysis was one of the earliest mechanically activated reactions with applications in polymer materials when Sijbesma developed mechanocatalysts for transition metal coordination polymers.[30,31] Further development of

mechanocatalysts by Sijbesma identified new latent catalysts for transesterification or ring-opening metathesis polymerization (ROMP).[32] The extensive mechanophore development that followed led to an assortment of useful mechanophores in polymer materials from the release of small molecules[33] or acid initiators[34] to polymer force sensors.[35,36] Boydston's work on creating force sensors was even applied to fused filament fabrication 3D printed polymers to 3D print force sensors.[37]

The activation of mechanophores in the solid state is more complex than the initial proof of concept demonstrations of mechanophore activation in stretched linear polymers in solution. The complexity is confirmed by Imato *et al.* who showed that different modes of mechanical stress can activate different mechanophores in the solid state. The diarylbibenzofuranone (DABBF) mechanophore could be activated by grinding but not by tension, compression, shear, or swelling. They found that this result was a combination of a poorly optimized network for energy transfer to the mechanophore and the fast recombination of radicals that prevent optical changes from lasting long enough to notice.[38] Robb *et al.* further confirmed the importance of connectivity of the network by comparing regioisomers of a napthopyran mechanophore in a PDMS film under tension. They found that the angle of the weak C-O bond determined if the mechanophore was activated in the film with the smallest angle to the force being the only film to display mechanochromism.[39] While the choice of mechanophore is important, these demonstrations highlight the importance of the network design around the mechanophore to optimize energy transfer.[40]

Self-healing polymers often require the use of polymer volume dedicated to healing agents or the use external stimuli to initiate healing mechanisms that require additional time and energy to the system. Conversely, the molecular-scale self-reinforcement can be

achieved by harnessing the energy of typically destructive mechanical stress. Mechanophore activation can be used to generate additional cross-linking that can serve to locally self-protect and self-reinforce polymers.

Self-reinforcing mechanisms require a chemical change under mechanical stress to produce a reactive functional group that can undergo subsequent bond forming reactions. The reactivity change in the group must be substantial and the resulting functionality must be able to readily undergo solid-state bimolecular reactions.[41] In the first instance of a mechanochemical cross-linking reaction, Ramirez *et al.* described a polymer architecture incorporating dibromocyclopropane. The application of mechanical stress *via* sonication of the polymer solution initiates a ring-opening of the strained cyclopropane ring. The ring-opening affords a new allylic bromide functional group which then undergoes nucleophilic displacement reactions to generates new crosslinks and allow the polymer solution to achieve gelation (Figure 1.1).[42] Similarly, Gordon *et al.* used a thiocarbonylthio mechanophore that is easily incorporated into the bulk polymer with a single-step RAFT polymerization.[43] As the mechanophore is also a RAFT agent, this approach allowed for both controlled RAFT polymerizations and self-reinforcing features in a single polymer.

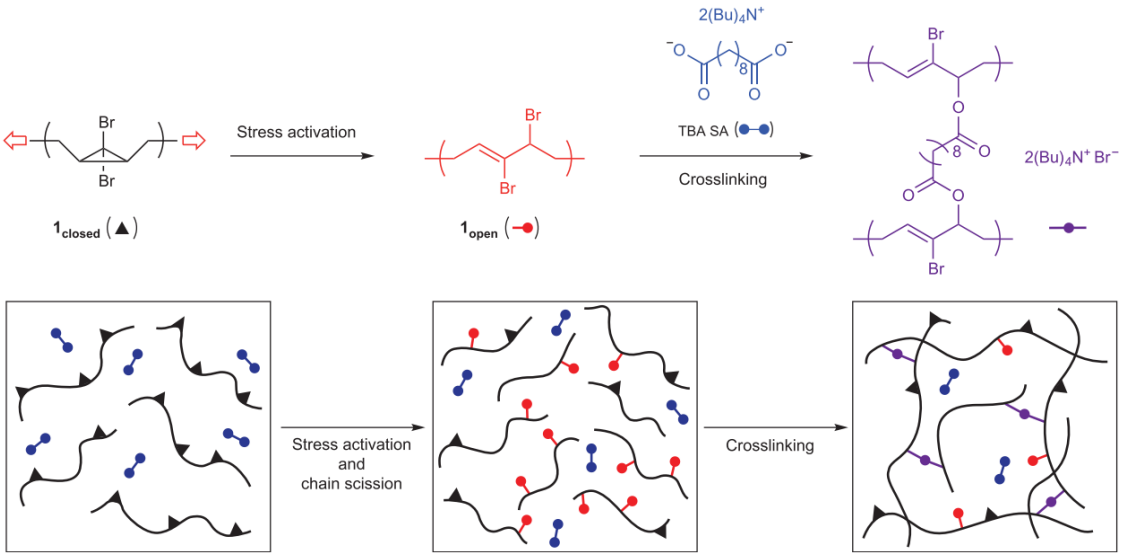


***Figure 1.1 Stress-activated crosslinking using dibromocyclopropane.***[42]

Most focus on mechanically initiated cross-linking was focused on the mechanochemistry but was less focused on producing robust solid-state materials that could undergo self-reinforcing reactions *in situ*. Polymers in solution allow for high mobility of reactive functional groups to undergo secondary cross-linking reactions whereas generating cross-linking reactions *in situ* in the solid-state is much more difficult to achieve.

Using double-network hydrogels, Matsuda *et al.* showed the ability to use self-reinforcement in the solid-state and maintain functional polymers. The double-network gels generated mechanoradicals through covalent bond scission which could initiate more polymerization with excess monomer.[44] Due to the dependence on the reaction rate of the cross-linking reaction, it was advantageous to use hydrogels which often contain >80% water and retain high mobility for diffusion. Without highly mobile polymer films, the in situ crosslinking reaction in robust solid-state films is more challenging.

## 1.2 Hexaarylbimidazoles

Although many different mechanophores have been studied, hexaarylbiimidazoles (HABIs) have many unique photo- and mechano- responsive properties. Although initially synthesized by Hayashi and Maeda in the 1960's,[45] they were first developed commercially as photoinitiators by Dupont who developed many products around them including DYLUX® proofing products.[46] Hexaarylbiimidazoles are unique in that they exist as dimers with only a weak C-N bond binding them together. Homolytic cleavage of the C-N bond using heat, light, or stress generates two stable lophyl radical species (Figure 1.2). The efficient cleaving of this carbon-nitrogen bond can be attributed to steric hindrance and the twisted structure of the HABI, making the C-N bond relatively easy to cleave with a reported bond dissociation energy of around 17 kcal/mol[47] compared to typical C-N bonds which can be about 50-100 kcal/mol. Using HABIs in functional materials has been attractive, not only due to the slow recombination time of the lophyl radicals compared to most organic free radicals,[48] attributable to their stabilization by steric hindrance and electron delocalization,[49] but also due to the low reactivity of lophyl radicals towards molecular oxygen.[50]

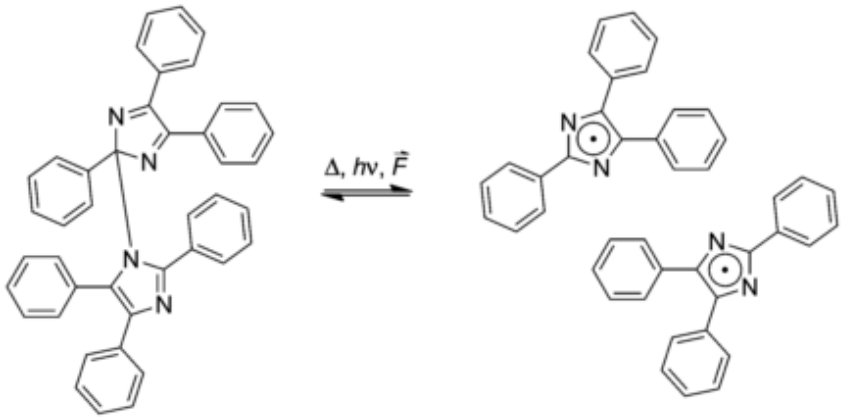


***Figure 1.2 Hexaarylbiimidazoles undergo cleavage of the carbon-nitrogen bond to produce 2 colored lophyl radicals under light, heat, or mechanical stimulus.***

Hexaarylbiimidazoles are formed by the oxidation of two 2,4,5-triarylimidazoles molecules, bonding them through a carbon-nitrogen bond. Functionalized triarylimidazoles can be readily synthesized and oxidized to functionalized HABIs. HABIs have been readily modified to overcome solubility issues by adding alkane[51] or ethylene glycol pendant groups[52]. Functionalization of HABI has also afforded facile incorporation of HABI into a variety of polymer networks using alcohol groups, methyl acrylates,[53] and alkynes.[54] This ease of modification to incorporate into polymer networks is another reason for its use in functional materials.

While HABI has been primarily studied for its photochemistry, it also can be cleaved through thermolysis or piezolysis making HABI a possible mechanophore. Like spiropyran, the lophyl radicals produced through cleavage have different optical properties to HABI due to the delocalization and aromatization of the radical species. The color change associated with this process has been used to create sensors either to light, stress, or heat.

The research of HABI in the 1960s and 70s revolved around their ability to initiate photopolymerizations under certain conditions. However, their initiation is only possible with a suitable hydrogen-donating coinitiator.[51] This makes them good candidates for thiol-ene polymerizations where the abstraction of a hydrogen from a hydrogen-donating thiol, generates a thiyl radical species that is highly reactive in thiol-ene polymerizations.[48] The exact mechanism of hydrogen abstraction and photoinitiation of HABI is complex and studies have tried to determine the mechanistic aspects of the initiation. It has been suggested that in some coinitiators the initiation doesn't proceed *via* direct hydrogen abstraction but may instead happen through an electron transfer mechanism.[55] Nevertheless, HABI is an efficient initiator of thiol-ene reactions as lophyl radicals preferentially undergo hydrogen abstraction over radical recombination (Figure 1.3).

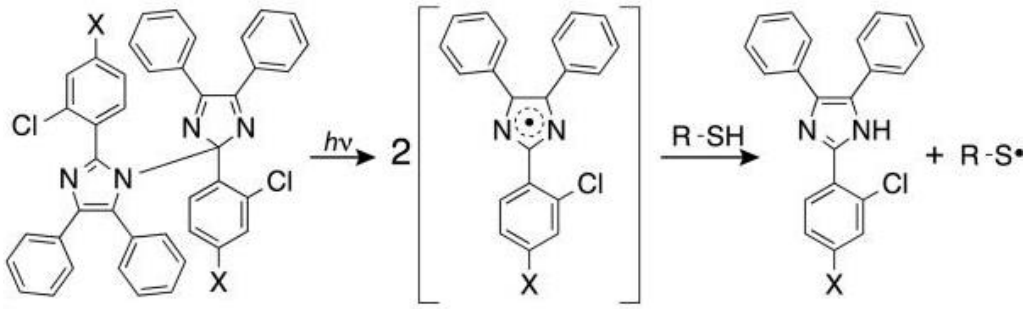


***Figure 1.3 Lophyl radicals can be used as thiol-ene initiators as the lophyl radicals abstract hydrogen from thiols to generate a propagating thiyl radical.***

### *1.2.1 Thiol-ene Chemistry*

Thiols undergo efficient reactions with reactive carbon-carbon double bonds. This thiol-ene reaction is termed a "click reaction" because of its high yields under mild conditions, lack of side reactions, and insensitivity to oxygen (Figure 1.4).[56] Thiol-ene reactions can proceed either through a radical or anionic mechanism.

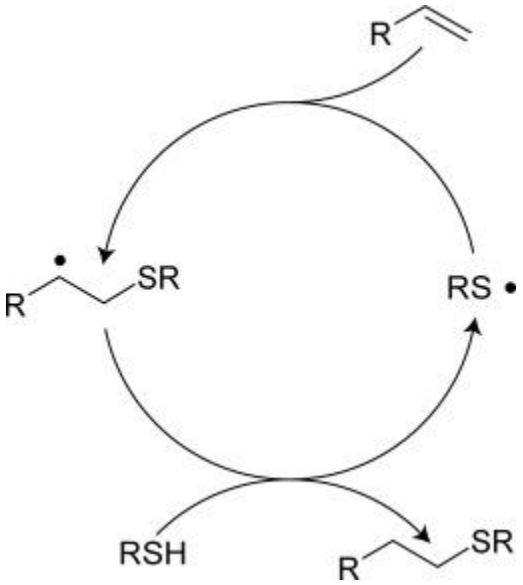


***Figure 1.4 The radical-mediated thiol-ene mechanism.***

Radical-mediated thiol-ene can proceed with almost all terminal double bonds with some preference to electron-rich double bonds. Conventional radical photopolymerizations, like (meth)acrylates, suffer from oxygen inhibition,[57] significant shrinkage,[58] and heterogenous network formation,[59] critically reducing potential applications. Therefore, radical-mediated photopolymerization of thiol-ene has been a popular method to produce more homogenous networks with less oxygen inhibition. Its adaptability to photochemistry allows for control over the spatial and temporal

polymerization like a conventional photopolymerization with all the added benefits of a click reaction.

Base-catalyzed thiol-ene polymerization is a type of nucleophilic Michael addition with thiol as the Michael donor. While it has many similarities to radical-mediated thiol-ene, the thiol-Michael addition does not self-terminate and requires an electron-deficient double bond. The double bonds used most often for nucleophilic Michael addition are maleimides, (meth)acrylates, and fumarate esters. The preference of the thiol-Michael addition for electron-deficient double bonds allows for selectivity in the presence of multiple types of double bonds. In the presence of both an electron-rich and electron-deficient double bond, the thiol-Michael addition selectively occurs only with the electron-deficient double bonds. The unreacted electron-rich double bonds are then available for subsequent radical-mediated thiol-ene polymerization to create two-stage films. This method only works if the thiol-Michael addition is performed first due to lower selectivity of the radical-mediated addition.[60] Two-stage thiol-ene films have been demonstrated using the orthogonality of different enes including acrylate/alkyne,[60] maleimide/allyl,[61] and two-stage films with different acrylate monomers.[62] Using the same functional group in orthogonal chemistry makes thiol-ene chemistry unique and a good choice for multi-stage polymer materials.

## 1.3 Stereolithography

### *1.3.1 Stereolithographic Chemistries*

Photopolymerizations afford spatiotemporal control of polymer materials not possible using thermal methods. Identifying the ability to build 3D objects in a layer by

layer fashion, Chuck Hull, was the first to patent the process and coin the term "stereolithography" in 1984.[63] Taking advantage of the ability of light to polymerize and cross-link a liquid resin, Hull and his company, 3D Systems, first developed and commercialized the laser scanning SLA machine.[64] Today, many methods of light-based additive manufacturing exist but a common method is digital light processing (DLP), which removes the need to scan point-by-point and instead cures an entire layer at once using a patterned light source.[65] DLP can be more expensive due to the intricate digital micromirror devices (DMD) required to project the patterned image, but it reduces oxygen inhibition by curing from the bottom of the liquid resin bath instead of the resin-air interface and cures entire layers in a single projection without scanning.

Stereolithographic resin consists of monomer(s), photoinitiator, photoabsorbing dyes to control light penetration, and may also consist of other reactive diluents or additives to control resin viscosity, mechanical properties, or optical properties. Monomer choice is often dictated by the combination of cure rate, long-term storage capabilities, and mechanical properties.[66] As a result of their rapid cure rate in radical photopolymerizations, (meth)acrylates are almost always employed in SLA resins. Instead of using a pure acrylate or pure methacrylate system, it is more desirable to use a mixture of both as pure acrylates cure too rapidly causing inhomogeneous networks and distortion while pure methacrylates cure too slowly.[67] Even so, the shrinkage stress during radical polymerization of (meth)acrylates typically causes deleterious effects on the mechanical properties. Radical polymerization of (meth)acrylates is also inhibited by molecular oxygen.[68,69]

Unlike radical polymerization, cationic polymerization is not affected by molecular oxygen and can be used in SLA by incorporating a photoacid generator (PAG) in the resin

as an initiator of the polymerization. Although cationic systems are slower than radical polymerization of acrylates, the cationic polymerization of epoxide monomers has significantly less shrinkage. Thus, the low shrinkage and improved mechanical properties are attractive for SLA but the low cure rate precludes them from being used on their own in SLA resins. Instead, epoxides are paired with faster curing cationic monomers like vinyl ethers to provide better properties and curing rates.[70] Conversely, they can be used in a hybrid acrylate/epoxide system, utilizing both cationic and radical polymerizations to generate a type of interpenetrating network that reduces the downsides of each polymerization method individually.[64]

SLA has been mostly restricted to resins based on multifunctional (meth)acrylates and/or epoxides. The low cost, rapid curing monomers are indeed convenient to use for low-cost rapid prototyping. However, the needs of stereolithography are evolving with increasing research and funding being focused on higher volume, and more impactful uses for SLA technology. Rapid prototyping is no longer the only use for SLA printed parts and instead more focus is placed on manufacturing for end use. For this reason, there has been significant work to develop better combinations of print speed, and mechanical properties using alternative monomeric resins.

Although most commercial resins are made of (meth)acrylates and/or epoxides, there has been interest in developing more robust materials for SLA. One such alternative, thiol-ene polymerizations attempt to overcome the limitations on acrylate systems due to oxygen inhibition and heterogeneous network formation. Thiol-ene reactions are less affected by molecular oxygen due to the strong hydrogen donating ability of thiols which allow them to be initiated by the peroxy radicals formed by oxygen. Moreover, thiol-ene

radical polymerizations are fast and occur in a step-growth process meaning that the gel point occurs at higher conversions and shrinkage stress is reduced.[71] Adding thiols to (meth)acrylate systems affords polymers with lower shrinkage stress and higher conversions and increased overall toughness compared to pure acrylate networks.[72,73] Thiol-ene usage in SLA is mainly limited by their poor storage stability, the unpleasant odor of thiols, and the softer properties that thiol-ene networks tend to have.[64]

With the goal of reducing the shrinkage stress by shifting the gel-point to higher conversions; addition-fragmentation chain transfers (AFCT) agents have been used in SLA resins. Chain-transfer agents regulate the network structure by allowing rearrangement and dissipation of internal stresses. Since AFCT agents have been used for decreasing polydispersity in linear polymers, many agents have been previously studied. β-Allyl sulfone were found as successful network regulators with dimethacrylate monomers.[74] The AFCT agents generally do not have the same storage stability issues as thiol-ene systems but reduced polymerization rates do still hinder AFCT materials.

### *1.3.2 Thermoplastic Stereolithography*

Stereolithography has been well understood as a process of photo crosslinking thermoset polymers comprised of a combination of (meth)acrylates and/or epoxides. The photocuring of crosslinked thermosets yields solid polymers almost instantaneously allowing for high resolution patterning of complex geometries. Thermoset polymers are attractive in many applications for their thermal and chemical resistance, but the highly crosslinked networks lack the desired processability or recyclability. In contrast, non-crosslinked thermoplastics, are rarely photopolymerized and often require high molecular

weights before solidification occurs. Nevertheless, thermoplastics offer a wide range of attractive properties including a wide range of mechanical properties and more processability and utility in a wide range of applications.

In the absence of cross-linking, various techniques have been developed to drive solidification of the thermoplastic polymer within the liquid resin. Using cross-linked pre-gelled structures, Hegde *et al*. described a novel method to use cross-linked pre-gelled structures for SLA printing which could be modified to form a high $T_g$ polyimide engineering thermoplastic with comparable properties to commercial Kapton® using post-print chemical modification and thermal imidization. Initially printing a cross-linked polyamic diacrylate ester organogel, the chemical modification to polyamic acid and then thermal imidization to polyimide was required post-print. Thermal processing serves as both the method of conversion to polyimide and also the method of decomposition of the acrylate cross-linking points to yield a thermoplastic.[75] While the chemistry was a clever way to print an engineering thermoplastic, the many involved steps and the significant shrinkage involved in the solvent removal and thermal imidization hinder potential commercial applications and the resulting polyimide is still not easily processable. Nevertheless, they were able to shorten the method to direct print the polyamic acid which removed the tedious chemical modification step.[76]

The direct printing of thermoplastic parts must balance the process of polymerization with the diffusion and dissolution process of the polymer in the monomeric resin. This balance of processes was explored by Deng *et al.* when they evaluated a range of photocurable thermoplastic monomers and chose to print 4-acryloylmorpholine for its fast kinetics and high $T_g$.[77] This approach makes use of fast polymerizing, high molecular

weight, high $T_g$, insoluble polymers to afford solid polymers without the need for cross-linking. While the direct approach to thermoplastic printing was simpler and less chemistry intensive, the variety of monomers suitable to this approach is extremely limited as 4-acryloylmorpholine and isobornyl acrylate are mentioned as being the only monomers that could be found to fit this strict criterion.

Instead of using high Tg polymers, Gall *et al.* created solid semi-crystalline photopolymers using thiol-ene chemistry between a difunctional thiol, 1,6-hexanedithiol, and a divinyl spirocyclic monomer.[78] Instead of the solidification of the polymer coming from crosslinks, the non-crosslinked thermoplastics solidify after crystallization which resists the polymer from further diffusion and dissolution in the monomeric resin. They further demonstrated the potential of their thermoplastic photopolymers by using them in stereolithography to 3D print geometries such as a cube and a dogbone shape.[79]

Abundant consumer thermoplastics like poly(ethylene) (PE), Poly(propylene) (PP), and poly(ethylene terephthalate) (PET) are all processed through controlled polymerizations and aren't easily photopolymerized. However, the mechanical properties and processability of these polymers would be ideal to replicate in photocurable systems. Trying to replicate the chemistry of PET, Alim *et al*. employed photocurable radical thiol-ene polymerization. Step-growth polymerization using 1,6-hexanedithiol and diallyl terephthalate afford a non-crosslinked semi-crystalline thermoplastic resembling a structure not too dissimilar to PET. The bulk polymerization afforded tough semi-crystalline polymers and complex printed structures were achieved.[80] Even though bulk properties were promising, the mechanical properties of the printed materials were significantly degraded more than a typical cross-linked resin. This was attributed to

reduced interlayer adhesion limiting the covalent bonding in linear, semi-crystalline polymers where the tight crystal structure with limited bonding sites weakens the adhesion between cured layers. Necessary modifications to the design used a multi-functional allyl crosslinker, triallyloxy-1,3,5-triazine (TAT), which allowed for post-print annealing.[81] Adding the crosslinker improves the mechanical properties through post-print annealing but the recyclability and processability of the thermoplastic is completely lost.

### *1.3.3 Cyclic Allylic Sulfides*

Cyclic allylic sulfides are a unique class of radical ring-opening monomers. The radical-initiated ring opening occurs through an allyl sulfide addition-fragmentation chain transfer mechanism and generates a propagating thiyl radical which propagates rapidly with minimal competition from hydrogen abstraction side reactions.[82] Cyclic allylic sulfides (CAS) were first described by Rizzardo and Evans at CSIRO in the 1990's and were attractive for their low volume shrinkage as a result of their radical ring-opening mechanism.[83] The initial CAS monomers studied were the 7- and 8-membered CAS monomers, CAS7 and CAS8 (Figure 1.5). While the volume shrinkage was low compared to other radical polymers, the semi-crystallinity of these monomers was still high and thus contributed to some volume shrinkage. Further development of CAS monomers was devoted more to amorphous polymers that reduced volume shrinkage further by adding substituents like methyl groups that produced amorphous polymers (MDTE and MDTO).[84,85]

The initial studies on semi-crystalline CAS7 and CAS8 were limited to thermal polymerization using AIBN showing 100% conversion of the monomers of both 7- and 8-

membered versions.[83] The successful ring opening of subsequent amorphous CAS monomers was demonstrated with both thermal initiators (AIBN) and photoinitiators (Darocur 1173). The studies on the photopolymerization of amorphous monomers, MDTE and MDTO, showed a dependence on ring size. Seven-membered CAS monomer, MDTE, only reached 80% conversion compared to 100% conversion of 8-membered rings with 1 or 2 methyl groups and 6-membered rings showed 0 or near 0 conversion.[84] While 1 hybrid methacrylate 7-membered CAS monomer did reach complete conversion, but 7-membered CAS rings with -$CH_2OH$ and -$CH_2OCH_3CO$ side groups had limiting photopolymerization conversions of 60-70%.[85] The small relative entropy and enthalpy of polymerization of six- and seven-membered rings leads to lower conversions and more sensitivity to substituents in the ring.[86]

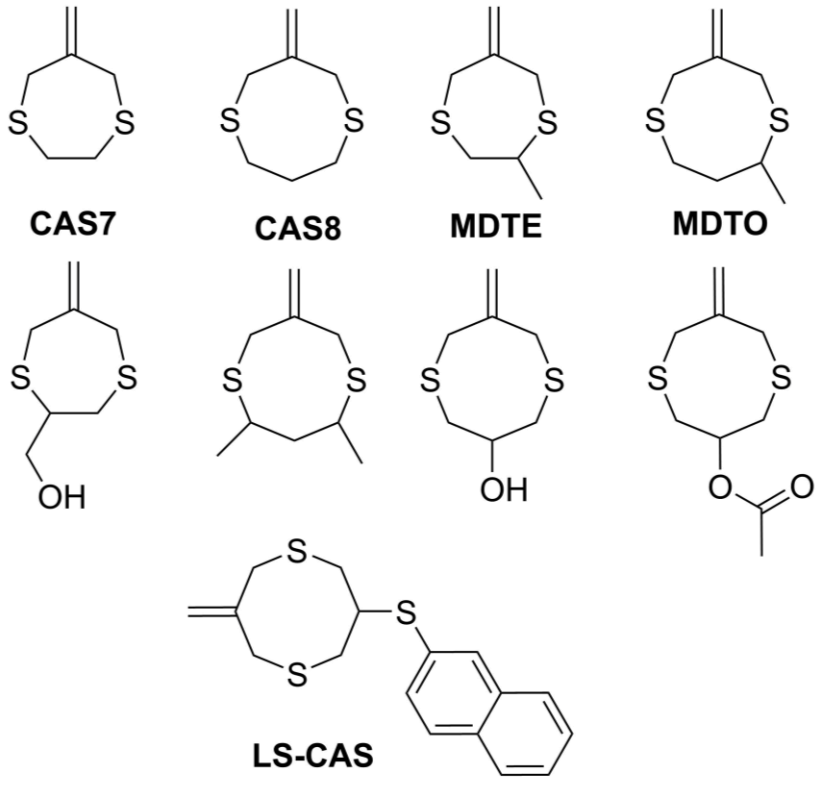


***Figure 1.5 CAS monomers reported in literature.***

CAS monomers have a significant amount of chain transfer to monomer, more than with other typical monomers. Due to addition-fragmentation the chain transfer to polymer is significant at higher conversions. The copolymerization behavior of MDTO CAS monomers with methyl methacrylate (MMA) and styrene (STY) wasn't too different from copolymerization of cyclic ketene acetals with MMA and STY. Similar to proposed electron donor-acceptor pairs formed in polyMMA formation, it appears that MMA copolymerization with MDTO is accelerated due to the electron donating potential of CAS monomers and forming complexes with polyMMA radicals rather than polystyryl radicals.[87,88]

An additional benefit to using CAS monomers is the apparent lack of inhibition from oxygen. Reported by Yamada *et al*., the photopolymerization of a CAS monomer under air and nitrogen conditions differ by a much smaller margin than the polymerization of 2-ethylhexyl methacrylate.[89] The polymerization of CAS under oxygen led to a greater molecular weight than polymerization under nitrogen but with a wider polydispersity leading to the proposed idea that oxygen may lead to inhibition of the termination mechanism that would control the polydispersity. Thus, the polymerization is not inhibited by oxygen but appears to affect the polydispersity.

The low shrinkage of CAS monomers is advantageous in many applications but has found most application in holographic media. Ring-opening polymerization have low shrinkage since no net bonds are formed and the low shrinkage reduces distortion in holographic media. CAS monomers like LS-CAS (Figure 1.5) have been developed as low distortion holographic recording media.[90] The compatibility of CAS with thiols allowed for various modifications to make crosslinked polymers or non-crosslinked. These

photopolymer formulations were used to create resins with high refractive index modulation of an acetate-functionalized 8-membered CAS monomer.[91] The low shrinkage, photocurable CAS monomers have found numerous uses as photopolymers due to their unique set of properties and chemistry.

### *1.3.4 Polymerization Inhibition for Stereolithography*

Controlling radical polymerizations is important to stop or curtail unwanted polymerizations. For example, phenol inhibitors are typically added to monomers to reduce premature radical polymerization and increase the shelf life. Beyond phenol inhibitors, controlling radical polymerizations through inhibition and chain-transfer is essential to controlling molecular mass and distribution. Controlled radical polymerizations including atom-transfer radical polymerization (ATRP), reversible addition-fragmentation chain transfer polymerization (RAFT), and nitroxide-mediated polymerization (NMP) use inhibition through a series of chain transfer or activation-deactivation cycles to control the molecular weight and produce polymers with a narrower range of molecular weights to produce more reliable and higher quality products.

Stereolithography can implement similar radical control mechanisms to control the spatiotemporal resolution of the polymerization. Until recently, stereolithographic approaches have been exclusively layer-by-layer and require considerable time in between layer exposures to detach the cured layer from the transparent window, allow for resin reflow, and reposition for the next layer exposure. This time between exposures, rather than the irradiation exposure time itself, fundamentally limited the printing speed that was capable in stereolithography. The first implementation of inhibition to stereolithography,

continuous liquid interface production (CLIP), used an oxygen-permeable transparent window to allow dissolved oxygen to inhibit the radical (meth)acrylate polymerizations of the thin layer of resin directly next to the window.[92,93] The inhibition allowed for removal of the time intensive steps between exposures affording the first successful continuous stereolithographic printing method and attaining rapid vertical print speeds. Since the inhibition is accomplished through dissolved oxygen, it is limited by the diffusion of oxygen into the resin from the environment which limits the control over the depth of inhibition and the viable monomer viscosities.

Controlling the radical inhibition actively is more desirable than passive oxygen inhibition. Photo-controlled inhibition provides an additional element of spatiotemporal control over the termination. Some of the first photoinhibitors used UV lasers to activate radical terminators to limit polymerization. Inhibition of radical-mediated polystyrene was achieved using a laser-initiated 2-napthylmethyl 1-napthylacetate.[94] Similarly, a 308 nm laser was used to terminate radical polymerizations using arylmethyl sulfone photoinhibitors.[95,96] However, these photoinhibition approaches don't afford photoorthogonality with common photoinitiators that would make possible the independent control over the photoinitiation and photoinhibition using separate wavelengths of light. Scott *et al.* described a photoorthogonal approach for direct-write lithography using two-color photoinitiation/photoinhibition. The blue light photoinitator, Camphorquinone (CQ), allowed for complete polymerization in areas exclusively irradiated with blue light while irradiation of any area with UV light, with or without blue light, inhibits the polymerization.[97] The UV-active photoinhibitor, tetraethylthiuram disulfide (TED), inhibited the polymerization under UV irradiation thereby confining

polymerization to areas irradiated with only blue light, however TED also participates in chain transfer under exclusive initiating wavelengths leading to reduced polymerization rates without activating the inhibiting radicals.

Improvement on this concept sought to eliminate the reliance on chain transfer which limits the scope and ability of this method. Using a new photoinhibitor, hexaarylbimidazole (HABI), De Beer *et al.* was able to generate three-dimensional objects using dual wavelength additive manufacturing. By using photoorthogonal initiators and inhibitors they control the inhibition thickness by varying the intensity of UV and blue wavelength independently affording greater control in SLA printing (Figure 1.6). The main detraction of using HABI as a photoinhibitor is the slow radical recombination rate of lophyl radicals causing inhibition for several seconds after irradiation ends.

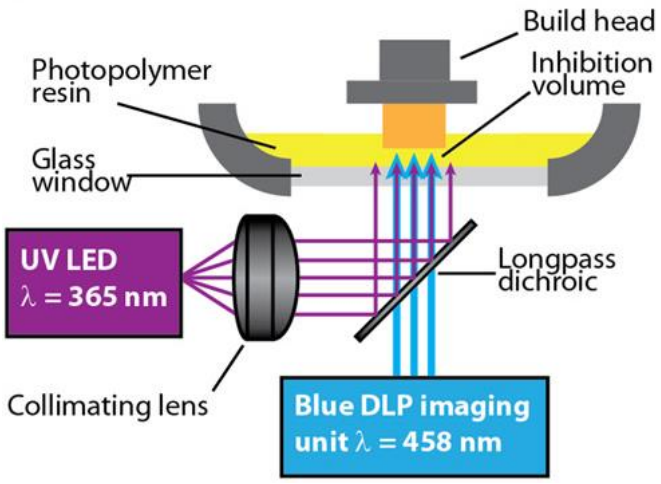


***Figure 1.6 Dual wavelength stereolithography using simultaneous polymerization initiation and inhibition[98]***

An increased rate of elimination of inhibiting species allows for faster cycling of polymerization with greater control. An improvement on the elimination rate of inhibiting

species in the dark was described by Van der Laan *et al.* by using an alkyl nitrite photoinhibitor instead of HABI. Butyl nitrite inhibit by producing 1 initiating radical and 3 inhibiting radicals for every activation event resulting in net radical inhibition. Butyl nitrite was found to be more advantageous for rapid cycling of irradiation with faster consumption of inhibiting radicals in the dark. When combined with camphorquinone as a photoorthogonal blue-light initiator, the spatial confinement of polymerization capable under concurrent blue and near-UV light is ideal for producing three-dimensional volumetric tomographic projections as demonstrated by the complex three dimensional shapes produced using dual-wavelength photopatterning.[99] The photoinhibition for dual wavelength affords rapid production rate of 3D printed materials providing a method for expanding the applications of stereolithography to producing high volume parts.

### 1.4 Overview of Subsequent Chapters

Chapter 2 describes the synthesis of tetraacrylate-functionalized hexaarylbimidazole and its incorporation into two-stage thiol-ene films. The photoinitiated reinforcing is evaluated and use to tune mechanical properties of the polymer. Finally, the self-reinforcing nature of the film is evaluated using ultrasonic welding to activate the mechanophoric hexaarylbimidazole.

Chapter 3 demonstrated the ability of cyclic allylic sulfides as a capable radical ring-opening monomer in thermoplastic stereolithographic resins. 7- and 8-membered cyclic allylic sulfides are synthesized and evaluated for their photopolymerization kinetics and mechanical properties as bulk materials and as 3D printed thermoplastics.

Chapter 4 describes the further of cyclic allylic sulfide based resins. The synthesis of 11- and 15- membered rings is described. The new monomers are evaluated for their photopolymerization kinetics and mechanical properties. The properties of copolymers from combinations of 11- and 15-membered rings with previously described 7- and 8-membered rings are assessed.

Chapter 5 describes the use of cyclic allylic sulfides in a two color photoinitiation/photoinhibition system. The photopolymerization kinetics of visible light photoinitiators are assesed. Common photoinhibitors are examined for their ability to inhibit the ring opening polymerization of CAS monomers.

Chapter 6 is a summary of the work and the future directions of the work.

## 1.5 References


(1) Blaiszik, B. J.; Kramer, S. L. B.; Olugebefola, S. C.; Moore, J. S.; Sottos, N. R.; White, S. R. Self-Healing Polymers and Composites. *Annu. Rev. Mater. Res.* **2010**, *40*, 179–211.

(2) Dry, C.; McMillan, W. A Novel Method to Detect Crack Location and Volume in Opaque and Semi-Opaque Brittle Materials. *Smart Mater. Struct.* **1997**, *6* (1), 35–39.

(3) Burattini, S.; Greenland, B. W.; Chappell, D.; Colquhoun, H. M.; Hayes, W. Healable Polymeric Materials: A Tutorial Review. *Chem. Soc. Rev.* **2010**, *39* (6), 1973–1985.

(4) Shchukin, D. G. Container-Based Multifunctional Self-Healing Polymer Coatings. *Polym. Chem.* **2013**, *4* (18), 4871.

(5) Zhao, Z.; Arruda, E. M. An Internal Cure for Damaged Polymers. *Science (80-. ).* **2014**, *344* (6184), 591–592.

(6) Garcia, S. J. Effect of Polymer Architecture on the Intrinsic Self-Healing Character of Polymers. *Eur. Polym. J.* **2014**, *53* (1), 118–125.

(7) Wei, Z.; Yang, J. H.; Zhou, J.; Xu, F.; Zrínyi, M.; Dussault, P. H.; Osada, Y.; Chen, Y. M. Self-Healing Gels Based on Constitutional Dynamic Chemistry and Their Potential Applications. *Chem. Soc. Rev.* **2014**, *43* (23), 8114–8131.

(8) Hart, L. R.; Harries, J. L.; Greenland, B. W.; Colquhoun, H. M.; Hayes, W. Healable Supramolecular Polymers. *Polym. Chem.* **2013**, *4* (18), 4860–4870.

(9) White, S. R.; Sottos, N., R.; Geubelle, P., H.; Moore, Jeffrey, S.; Kessler, M., R.; Sriram, S., R.; Brown, E., N.; Viswanathan, S. Autonomic Healing of Polymer Composites. *Nature* **2001**, *409* (6822), 794.

(10) An, S. Y.; Arunbabu, D.; Noh, S. M.; Song, Y. K.; Oh, J. K. Recent Strategies to

Develop Self-Healable Crosslinked Polymeric Networks. *Chem. Commun.* **2015**, *51* (66), 13058–13070.

(11) Maizatul, S.; Salehuddin, F.; Hafiz, M.; Shafinaz, A.; Khan, B.; Hajjar, S.; Man, C.; Khairuddin, W.; Ali, W. A Review of Recent Developments : Self-Healing Approaches for Polymeric Materials. *Chem. Eng. Trans.* **2019**, *7* (April 2018), 433–438.

(12) Bergman, S. D.; Wudl, F. Mendable Polymers. *J. Mater. Chem.* **2008**, *18* (1), 41–62.

(13) Adzima, B. J.; Aguirre, H. A.; Kloxin, C. J.; Scott, T. F.; Bowman, C. N. Rheological and Chemical Analysis of Reverse Gelation in a Covalently Cross-Linked Diels−Alder Polymer Network. *Macromolecules* **2008**, *41* (23), 9112–9117.

(14) Reutenauer, P.; Buhler, E.; Boul, P. J.; Candau, S. J.; Lehn, J. M. Room Temperature Dynamic Polymers Based on Diels-Alder Chemistry. *Chem. - A Eur. J.* **2009**, *15* (8), 1893–1900.

(15) Telitel, S.; Amamoto, Y.; Poly, J.; Morlet-Savary, F.; Soppera, O.; Lalevée, J.; Matyjaszewski, K. Introduction of Self-Healing Properties into Covalent Polymer Networks via the Photodissociation of Alkoxyamine Junctions. *Polym. Chem.* **2014**, *5* (3), 921–930.

(16) Habault, D.; Zhang, H.; Zhao, Y. Light-Triggered Self-Healing and Shape-Memory Polymers. *Chem. Soc. Rev.* **2013**, *42* (17), 7244–7256.

(17) Fiore, G. L.; Rowan, S. J.; Weder, C. Optically Healable Polymers. *Chem. Soc. Rev.* **2013**, *42* (17), 7278.

(18) Coqueret, X. Photoreactivity of Polymers with Dimerizable Side-Groups: Kinetic Analysis for Probing Morphology and Molecular Organization. *Macromol. Chem. Phys.* **1999**, *200* (7), 1567–1579.

(19) Schreier, W. J.; Schrader, T. E.; Koller, F. O.; Gilch, P.; Crespo-Hernández, C. E.;

Swaminathan, V. N.; Carell, T.; Zinth, W.; Kohler, B. Thymine Dimerization in DNA Is an Ultrafast Photoreaction. *Science* **2007**, *315* (5812), 625–629.

(20) Amamoto, Y.; Kamada, J.; Otsuka, H.; Takahara, A.; Matyjaszewski, K. Repeatable Photoinduced Self-Healing of Covalently Cross-Linked Polymers through Reshuffling of Trithiocarbonate Units. *Angew. Chemie* **2011**, *123* (7), 1698–1701.

(21) Amamoto, Y.; Otsuka, H.; Takahara, A.; Matyjaszewski, K. Self-Healing of Covalently Cross-Linked Polymers by Reshuffling Thiuram Disulfide Moieties in Air under Visible Light. *Adv. Mater.* **2012**, *24* (29), 3975–3980.

(22) Patrick, J. F.; Robb, M. J.; Sottos, N. R.; Moore, J. S.; White, S. R. Polymers with Autonomous Life-Cycle Control. *Nature* **2016**, *540* (7633), 363–370.

(23) Boldyreva, E. Mechanochemistry of Inorganic and Organic Systems: What Is Similar, What Is Different? *Chem. Soc. Rev.* **2013**, *42* (18), 7719–7738.

(24) James, S. L.; Adams, C. J.; Bolm, C.; Braga, D.; Collier, P.; Friščić, T.; Grepioni, F.; Harris, K. D. M.; Hyett, G.; Jones, W.; Krebs, A.; Mack, J.; Maini, L.; Orpen, A. G.; Parkin, I. P.; Shearouse, W. C.; Steed, J. W.; Waddell, D. C. Mechanochemistry: Opportunities for New and Cleaner Synthesis. *Chem. Soc. Rev.* **2012**, *41* (1), 413–447.

(25) Boulatov, R. The Challenges and Opportunities of Contemporary Polymer Mechanochemistry. *ChemPhysChem* **2017**, *18* (11), 1419–1421.

(26) Hickenboth, C. R.; Moore, J. S.; White, S. R.; Sottos, N. R.; Baudry, J.; Wilson, S. R. Biasing Reaction Pathways with Mechanical Force. *Nature* **2007**, *446* (7134), 423–427.

(27) Encina, M. V.; Lissi, E.; Sarasúa, M.; Gargallo, L.; Radic, D. Ultrasonic Degradation of Polyvinylpyrrolidone: Effect of Peroxide Linkages. *J. Polym. Sci. Polym. Lett. Ed.* **1980**, *18* (12), 757–760.

(28) Berkowski, K. L.; Potisek, S. L.; Hickenboth, C. R.; Moore, J. S. Ultrasound-

Induced Site-Specific Cleavage of Azo-Functionalized Poly(Ethylene Glycol). *Macromolecules* **2005**, *38* (22), 8975–8978.

(29) Brantley, J. N.; Wiggins, K. M.; Bielawski, C. W. Polymer Mechanochemistry: The Design and Study of Mechanophores. *Polym. Int.* **2013**, *62* (1), 2–12.

(30) Paulusse, J. M. J.; Sijbesma, R. P. Selectivity of Mechanochemical Chain Scission in Mixed Palladium(II) and Platinum(II) Coordination Polymers. *Chem. Commun.* **2008**, No. 37, 4416–4418.

(31) Karthikeyan, S.; Potisek, S. L.; Piermattei, A.; Sijbesma, R. P. Highly Efficient Mechanochemical Scission of Silver-Carbene Coordination Polymers. *J. Am. Chem. Soc.* **2008**, *130* (45), 14968–14969.

(32) Piermattei, A.; Karthikeyan, S.; Sijbesma, R. P. Activating Catalysts with Mechanical Force. *Nat. Chem.* **2009**, *1* (2), 133–137.

(33) Larsen, M. B.; Boydston, A. J. Successive Mechanochemical Activation and Small Molecule Release in an Elastomeric Material. *J. Am. Chem. Soc.* **2014**, *136* (4), 1276–1279.

(34) Diesendruck, C. E.; Steinberg, B. D.; Sugai, N.; Silberstein, M. N.; Sottos, N. R.; White, S. R.; Braun, P. V.; Moore, J. S. Proton-Coupled Mechanochemical Transduction: A Mechanogenerated Acid. *J. Am. Chem. Soc.* **2012**, *134* (30), 12446–12449.

(35) Davis, D. A.; Hamilton, A.; Yang, J.; Cremar, L. D.; Van Gough, D.; Potisek, S. L.; Ong, M. T.; Braun, P. V.; Martínez, T. J.; White, S. R.; Moore, J. S.; Sottos, N. R. Force-Induced Activation of Covalent Bonds in Mechanoresponsive Polymeric Materials. *Nature* **2009**, *459* (7243), 68–72.

(36) Chen, Y.; Spiering, A. J. H.; Karthikeyan, S.; Peters, G. W. M.; Meijer, E. W.; Sijbesma, R. P. Mechanically Induced Chemiluminescence from Polymers Incorporating a 1,2-Dioxetane Unit in the Main Chain. *Nat. Chem.* **2012**, *4* (7), 559–562.

(37) Peterson, G. I.; Yurtoglu, M.; Larsen, M. B.; Craig, S. L.; Ganter, M. A.; Storti, D. W.; Boydston, A. J. Additive Manufacturing of Mechanochromic Polycaprolactone on Entry-Level Systems. *Rapid Prototyp. J.* **2015**, *21* (5), 520–527.

(38) Imato, K.; Irie, A.; Kosuge, T.; Ohishi, T.; Nishihara, M.; Takahara, A.; Otsuka, H. Mechanophores with a Reversible Radical System and Freezing-Induced Mechanochemistry in Polymer Solutions and Gels. *Angew. Chemie* **2015**, *127* (21), 6266–6270.

(39) Robb, M. J.; Kim, T. A.; Halmes, A. J.; White, S. R.; Sottos, N. R.; Moore, J. S. Regioisomer-Specific Mechanochromism of Naphthopyran in Polymeric Materials. *J. Am. Chem. Soc.* **2016**, *138* (38), 12328–12331.

(40) Li, J.; Nagamani, C.; Moore, J. S. Polymer Mechanochemistry: From Destructive to Productive. *Acc. Chem. Res.* **2015**, *48* (8), 2181–2190. h

(41) Black, A. L.; Orlicki, J. A.; Craig, S. L. Mechanochemically Triggered Bond Formation in Solid-State Polymers. *J. Mater. Chem.* **2011**, *21* (23), 8460–8465.

(42) Ramirez, A. L. B.; Kean, Z. S.; Orlicki, J. A.; Champhekar, M.; Elsakr, S. M.; Krause, W. E.; Craig, S. L. Mechanochemical Strengthening of a Synthetic Polymer in Response to Typically Destructive Shear Forces. *Nat. Chem.* **2013**, *5* (9), 757–761.

(43) Gordon, M. B.; Wang, S.; Knappe, G. A.; Wagner, N. J.; Epps, T.; Kloxin, C. Force-Induced Cleavage of a Labile Bond for Enhanced Mechanochemical Crosslinking. *Polym. Chem.* **2017**, 6485–6489.

(44) Matsuda, A. T.; Kawakami, R.; Namba, R.; Nakajima, T.; Ping, J. Mechanoresponsive Self-Growing Hydrogels Inspired by Muscle Training. *Science* **2019**, *363* (February), 504–508.

(45) Hayashi, T.; Maeda, K. Preparation of a New Phototropic Substance. *Bull. Chem. Soc. Jpn.* **1960**, *33* (4), 565–566.

(46) Dessauer, R. *Photochemistry, History and Commercial Appciations of Hexaarylbimidazoles: All about HABIs*; Elvesier: Amsterdam, 2006.

(47) Tanaseichuk, B. S. Triarylimidazole Radicals and Their Dimers (Review). *Chem. Heterocycl. Compd.* **1974**, *8* (10), 1173–1180.

(48) Berdzinski, S.; Horst, J.; Straßburg, P.; Strehmel, V. Recombination of Lophyl Radicals in Pyrrolidinium-Based Ionic Liquids. *ChemPhysChem* **2013**, *14* (9), 1899–1908.

(49) Kawano, M.; Sano, T.; Abe, J.; Ohashi, Y. The First in Situ Direct Observation of the Light-Induced Radical Pair from a Hexaarylbiimidazolyl Derivative by x-Ray Crystallography [2]. *J. Am. Chem. Soc.* **1999**, *121* (35), 8106–8107.

(50) Kishimoto, Y.; Abe, J. A Fast Photochromic Molecule That Colors Only under UV Light. *J. Am. Chem. Soc.* **2009**, *4876* (15), 4227–4229.

(51) Ahn, D.; Sathe, S. S.; Clarkson, B. H.; Scott, T. F. Hexaarylbiimidazoles as Visible Light Thiol-Ene Photoinitiators. *Dent. Mater.* **2015**, *31* (9), 1075–1089.

(52) Igarashi, H.; Igarashi, T.; Sagawa, M.; Mori, T.; Kotani, Y.; Muroya, Y.; Katsumura, Y.; Yamashita, T. Preparation and Photoractivity of a Novel Lophine Dimer Containing a Hydrophillic Group. *J. Photopolym. Sci. Technol.* **2007**, *20* (5), 757–762.

(53) Verstraeten, F.; Göstl, R.; Sijbesma, R. P. Stress-Induced Colouration and Crosslinking of Polymeric Materials by Mechanochemical Formation of Triphenylimidazolyl Radicals. *Chem. Commun.* **2016**, *52* (55), 8608–8611.

(54) Ahn, D.; Zavada, S. R.; Scottt, T. F. Rapid, Photomediated Healing of Hexaarylbiimidazole-Based Covalently Cross-Linked Gels. *Chem. Mater.* **2017**, *29* (16), 7023–7031.

(55) Eaton, D. F.; Horgan, A. G.; Horgan, J. P. Mechanism of Coinitiation of Photopolymerization of Methyl Methacrylate by Hexaarylbiimidazole-Hydrogen-Atom Donor Combinations . The Role of Electron Transfer Us . Direct Hydrogen-Atom Abstraction. *J. Photochem. Photobiol. AChemistry* **1991**, *58* (3), 373–391.

(56) Hoyle, C. E.; Bowman, C. N. Thiol-Ene Click Chemistry. *Angew. Chemie Int. Ed.* **2010**, *49* (9), 1540–1573.

(57) Roper, T. M.; Lee, T. Y.; Guymon, C. A.; Hoyle, C. E. In Situ Characterization of Photopolymerizable Systems Using a Thin-Film Calorimeter. *Macromolecules* **2005**, *38* (24), 10109–10116.

(58) Bowman, C. N.; Peppas, N. A. Coupling of Kinetics and Volume Relaxation during Polymerizations of Multiacrylates and Multimethacrylates. *Macromolecules* **1991**, *24* (8), 1914–1920.

(59) Kannurpatti, A. R.; Anseth, J. W.; Bowman, C. N. A Study of the Evolution of Mechanical Properties and Structural Heterogeneity of Polymer Networks Formed by Photopolymerizations of Multifunctional (Meth)Acrylates. *Polymer* **1998**, *39* (12), 2507–2513.

(60) Stolz, R. M.; Northrop, B. H. Experimental and Theoretical Studies of Selective Thiol-Ene and Thiol-Yne Click Reactions Involving N -Substituted Maleimides. *J. Org. Chem.* **2013**, *78* (16), 8105–8116.

(61) Chan, J. W.; Hoyle, C. E.; Lowe, A. B. Sequential Phosphine-Catalyzed, Nucleophilic Thiol Ene/Radical-Mediated Thiol-Yne Reactions and the Facile Orthogonal Synthesis of Polyfunctional Materials. *J. Am. Chem. Soc.* **2009**, *131* (16), 5751–5753.

(62) Nair, D. P.; Cramer, N. B.; McBride, M. K.; Gaipa, J. C.; Shandas, R.; Bowman, C. N. Enhanced Two-Stage Reactive Polymer Network Forming Systems. *Polymer* **2012**, *53* (12), 2429–2434.

(63) Hull, C. W. Apparatus for Production of Three-Dimensional Objects by

Stereolithography. 4575330, 1984.

(64) Ligon, S. C.; Liska, R.; Stampfl, J.; Gurr, M.; Mülhaupt, R. Polymers for 3D Printing and Customized Additive Manufacturing. *Chem. Rev.* **2017**, *117* (15), 10212–10290.

(65) Tesavibul, P.; Felzmann, R.; Gruber, S.; Liska, R.; Thompson, I.; Boccaccini, A. R.; Stampfl, J. Processing of 45S5 Bioglass® by Lithography-Based Additive Manufacturing. *Mater. Lett.* **2012**, *74*, 81–84.

(66) Zhang, J.; Xiao, P. 3D Printing of Photopolymers. *Polym. Chem.* **2018**, *9* (13), 1530–1540.

(67) Murphy, E. J.; Ansel, R. E.; Krajewski, J. J. Method Of Forming A Three-Dimiensional Object By Stereolthography And Compostion Therefore. *US Pat.* **1990**, No. 19, 1–5.

(68) Ligon, S. C.; Husár, B.; Wutzel, H.; Holman, R.; Liska, R. Strategies to Reduce Oxygen Inhibition in Photoinduced Polymerization. *Chem. Rev.* **2014**, *114* (1), 577–589.

(69) O'Brien, A. K.; Bowman, C. N. Impact of Oxygen on Photopolymerization Kinetics and Polyme Structure. *Macromolecules* **2006**, *39* (7), 2501–2506.

(70) Lapin, S. C.; Snyder, J. R.; Sitzmann, E. V.; Barnes, D. K.; Green, G. D. Stereolithography Using Vinyl Ether-Epoxide Polymers. 5,437,964, 1995.

(71) Kloxin, J. C.; Scott, F. T.; Bowman, N. C. Stress Relaxation via Addition Fragmentation Chain Transfer in a Thiol-Ene Photopolymerization. *Macromolecules* **2009**, *42* (7), 2551–2556.

(72) Lu, H.; Carioscia, J. A.; Stansbury, J. W.; Bowman, C. N. Investigations of Step-Growth Thiol-Ene Polymerizations for Novel Dental Restoratives. *Dent. Mater.* **2005**, *21* (12), 1129–1136.

(73) Ligon-Auer, S. C.; Schwentenwein, M.; Gorsche, C.; Stampfl, J.; Liska, R. Toughening of Photo-Curable Polymer Networks: A Review. *Polym. Chem.* **2016**, 257–286.

(74) Gorsche, C.; Koch, T.; Moszner, N.; Liska, R. Exploring the Benefits of β-Allyl Sulfones for More Homogeneous Dimethacrylate Photopolymer Networks. *Polym. Chem.* **2015**, *6* (11), 2038–2047.

(75) Hegde, M.; Meenakshisundaram, V.; Chartrain, N.; Sekhar, S.; Tafti, D.; Williams, C. B.; Long, T. E. 3D Printing All-Aromatic Polyimides Using Mask-Projection Stereolithography: Processing the Nonprocessable. *Adv. Mater.* **2017**, *29* (31), 1701240.

(76) Herzberger, J.; Meenakshisundaram, V.; Williams, C. B.; Long, T. E. 3D Printing All-Aromatic Polyimides Using Stereolithographic 3D Printing of Polyamic Acid Salts. *ACS Macro Lett.* **2018**, *7* (4), 493–497.

(77) Deng, S.; Wu, J.; Dickey, M. D.; Zhao, Q.; Xie, T. Rapid Open-Air Digital Light 3D Printing of Thermoplastic Polymer. *Adv. Mater.* **2019**, *31* (39), 1903970.

(78) Sycks, D. G.; Safranski, D. L.; Reddy, N. B.; Sun, E.; Gall, K. Tough Semicrystalline Thiol–Ene Photopolymers Incorporating Spiroacetal Alkenes. *Macromolecules* **2017**, *50* (11), 4281–4291.

(79) Sycks, D. G.; Wu, T.; Park, H. S.; Gall, K. Tough, Stable Spiroacetal Thiol-ene Resin for 3D Printing. *J. Appl. Polym. Sci.* **2018**, *135* (22), 46259.

(80) Alim, M. D.; Childress, K. K.; Baugh, N. J.; Martinez, A. M.; Davenport, A.; Fairbanks, B. D.; McBride, M. K.; Worrell, B. T.; Stansbury, J. W.; McLeod, R. R.; Bowman, C. N. A Photopolymerizable Thermoplastic with Tunable Mechanical Performance. *Mater. Horizons* **2020**, *7* (3), 835–842.

(81) Childress, K. K.; Alim, M. D.; Hernandez, J. J.; Stansbury, J. W.; Bowman, C. N. Additive Manufacture of Lightly Crosslinked Semicrystalline Thiol–Enes for

Enhanced Mechanical Performance. *Polym. Chem.* **2020**, *11* (1), 39–46.

(82) Huang, R. L.; Goh, S. H.; Ong, S. H. A. *The Chemistry of Free Radicals*; Hodder Education, 1974.

(83) Evans, R. A.; Rizzardo, E. Free-Radical Ring-Opening Polymerization of Cyclic Allylic Sulfides. *Macromolecules* **1996**, *29* (22), 6983–6989.

(84) Evans, R. A.; Rizzardo, E. Free Radical Ring-Opening Polymerization of Cyclic Allylic Sulfides: Liquid Monomers with Low Polymerization Volume Shrinkage. *J. Polym. Sci. Part A Polym. Chem.* **2001**, *39* (1), 202–215.

(85) Evans, R. A.; Rizzardo, E. Free-Radical Ring-Opening Polymerization of Cyclic Allylic Sulfides. 2. Effect of Substituents on Seven- and Eight-Membered Ring Low Shrink Monomers. *Macromolecules* **2000**, *33* (18), 6722–6731.

(86) Ivin, K. J. Thermodynamics of Addition Polymerization. **2000**, *38* (March), 2137–2146.

(87) Harrisson, S.; Davis, T. P.; Evans, R. A.; Rizzardo, E. Chain Transfer in the Sulfur-Centered Free Radical Ring-Opening Polymerization of 3-Methylene-6-Methyl-1,5-Dithiacyclooctane. *Macromolecules* **2000**, *33* (26), 9553–9560.

(88) Harrisson, S.; Davis, T. P.; Evans, R. A.; Rizzardo, E. Pulsed Laser Copolymerization of Ring-Opening Cyclic Allylic Sulfide Monomers with Methyl Methacrylate and Styrene. *Macromolecules* **2002**, *35* (7), 2474–2480.

(89) Yamada, S.; Goto, Y. Reduction of Oxygen Inhibition in Photopolymerization of Cyclic Allylic Sulfide Monomers. *J. Photopolym. Sci. Technol.* **2010**, *23* (1), 109–114.

(90) Choi, K.; Chon, J. W. M.; Gu, M.; Malic, N.; Evans, R. A. Low-Distortion Holographic Data Storage Media Using Free-Radical Ring-Opening Polymerization. *Adv. Funct. Mater.* **2009**, *19* (22), 3560–3566.

(91) Galli, P.; Evans, R. A.; Bertarelli, C.; Bianco, A. Cyclic Allylic Sulfide Based Photopolymer for Holographic Recording Showing High Refractive Index Modulation. *J. Polym. Sci.* **2021**, No. March, 1399–1413.

(92) Tumbleston, J. R.; Shirvanyants, D.; Ermoshkin, N.; Janusziewicz, R.; Johnson, A. R.; Kelly, D.; Chen, K.; Pinschmidt, R.; Rolland, J. P.; Ermoshkin, A.; Samulski, E. T.; DeSimone, J. M. Continuous Liquid Interface Production of 3D Objects. *Science* **2015**, *347* (6228), 1349–1352.

(93) Janusziewicz, R.; Tumbleston, J. R.; Quintanilla, A. L.; Mecham, S. J.; DeSimone, J. M. Layerless Fabrication with Continuous Liquid Interface Production. *Proceedings of the National Academy of Sciences of the United States of America*. 2016, pp 11703–11708.

(94) Holdcroft, S.; Guillet, J. E. Studies of Photoinitiation and Phototermination of Free Radical Polymerization Using Dual Pulsed Laser Techniques. *J. Polym. Sci. Part A Polym. Chem.* **1991**, *29* (5), 729–737.

(95) Karatekin, E.; Landis, M.; Lem, G.; O'Shaughnessy, B.; Turro, N. J. Photocopying Living Chains. 1. Steady-State. *Macromolecules* **2001**, *34* (23), 8187–8201.

(96) Karatekin, E.; Landis, M.; Lem, G.; O'Shaughnessy, B.; Turro, N. J. Photocopying Living Chains. 2. Time-Dependent Measurements. *Macromolecules* **2001**, *34* (23), 8202–8215.

(97) Scott, T. F.; Kowalski, B. A.; Sullivan, A. C.; Bowman, C. N.; McLeod, R. R. Two-Color Single-Photon Photoinitiation and Photoinhibition for Subdiffraction Photolithography. *Science* **2009**, *324* (5929), 913–917.

(98) de Beer, M. P.; van der Laan, H. L.; Cole, M. A.; Whelan, R. J.; Burns, M. A.; Scott, T. F. Rapid, Continuous Additive Manufacturing by Volumetric Polymerization Inhibition Patterning. *Sci. Adv.* **2019**, *5*.

(99) Van Der Laan, H. L.; Burns, M. A.; Scott, T. F. Volumetric Photopolymerization

Confinement through Dual-Wavelength Photoinitiation and Photoinhibition. *ACS Macro Lett.* **2019**, *8* (8), 899–904.

# Chapter 2 Hexaarylbimidazoles in Two-Stage Self-Reinforcing Thiol-ene Films

## 2.1 Abstract

Synthetic polymer materials are widely produced worldwide but the ability to heal and reinforce like biological systems remains elusive. Moreover, polymeric materials have finite lifetimes exacerbated by wear and tear that accumulates causing irreversible damage. Polymers that display healing or reinforcing often require an external stimulus, we describe the use of mechanophoric hexaarylbimidazole (HABI) in a two-stage force-initiated reinforcing polymer. In this work, we describe the design of a two-stage polymer network using the orthogonality of thiol-Michael addition between thiols and acrylates and radial thiol-ene between thiols and allyls that can be self-initiated by mechanical perturbations that cause cleavage of a polymer-bound HABI mechanophore. The two-stage network was evaluated using both light and force as a stimulus and demonstrated the range of properties attainable through simple modifications in the monomers and stoichiometric ratios between them.

## 2.2 Introduction

The ability to both self-repair and self-reinforce are key biological processes found in both bone and muscle; nevertheless, these key biological processes have not been well replicated in synthetic materials. Typical solid-state elastomeric materials suffer from progressive microcrack propagation during stress-induced bond scission events. These

microcracks formed by repetitive mechanical loading lead to macroscopic damage and failure.[1] Moreover, damaged solid-state material is often non-recyclable leading to a growing amount of plastic waste.[2] Autonomous stimuli-responsive materials aim to reduce plastic waste by extending the lifetime of polymeric materials and increasing the safety and reliability of these products.[3]

Self-healing materials are one of the most common stimuli-responsive materials and have been studied for more than a few decades.[4] While self-healing polymers repair a percentage of damaged bonds, the healing efficiencies are often less than 100%.[3] Hickenboth *et al.* described a method of using mechanical stress to bias a reaction in 2007, demonstrating the conversion of typically destructive mechanical stress to chemical potential energy.[5] Further research into mechanochemistry discovered various mechanophores which can utilize mechanical stress as a stimulus for mechanoluminescence,[6,7] releasing small molecules,[8] and activating or generating catalysts.[9]

More recently, mechanochemistry has been used in polymer networks to initiate secondary reactions *in situ*. First, in a polymer solution where the ultrasonically-generated radicals initiated cross-linking and subsequent gelation,[10] in a rapidly frozen gel using thiol-ene chemistry,[11] and finally in a double network hydrogel where the mechanically-initiated cross-linking reactions reinforced the hydrogel in a self-reinforcing reaction.[12] Nevertheless, the use of mechanophores in stress-initiated self-reinforcing solid-state polymers still remains a challenge.

Hexaarylbimidazoles (HABIs) are unique dimers with a weak carbon-nitrogen bond that can be easily cleaved with light, heat, and mechanical stress. Owing to these

properties, they have been investigated as photoinitiators for thiol-ene polymerizations,[13] dynamic bonds in self-healing gels,[14] photoinhibitors in stereolithography,[15] and recently been studied for their mechanophore properties.[11] Additionally, HABIs have previously been functionalized and incorporated into polymer networks with documented pathways to functionalization.[11,14]

Utilizing HABI's unique combination of mechanophoric nature and ability to initiate thiol-ene polymerizations, we examine the incorporation of acrylate-functionalized HABIs into a thiol-ene film through base-catalyzed thiol-Michael addition.[16] We examine the selectivity of base-catalyzed thiol-Michael addition with the addition of triallyl-1,3,5-triazine-2,4,6-trione (TATATO) as a non-reactive diluent during thiol-Michael addition to create a lightly cross-linked film. Then the HABI-initiated thiol-ene cross-linking between the triallyl and residual thiol function groups in the network is demonstrated, and mechanical properties analyzed using UV light as a stimulus. Finally, the ultrasonically initiated self-reinforcing is examined using FTIR and mechanical analysis and discussed.

## 2.3 Experimental

### *2.3.1 Materials*

The tetraacrylate-HABI was synthesized as described below in a series of 6 steps and provided the acrylate groups in the system. Triallyl-1,3,5-triazine-2,4,6-trione (TATATO) was sourced from Sigma-Aldrich and was added as a source of allyls for secondary polymerization. A nitrosamine radical inhibitor, Q1301 N-nitroso-N-phenylhydroxylamine Aluminum salt, was used to limit premature radical polymerization and sourced from Wako Chemicals. Triethylamine (TEA) was used as a catalyst for

Michael addition and was sourced from Sigma-Aldrich. A combination of thiols was used for the films, the di-functional ethylene glycol bis(mercaptopropionate) (EGMP) was purchased from TCI Americas, the tetra-functional tetra(2-mercaptoethyl)silane (TMES) was synthesized in 2 steps as described below.

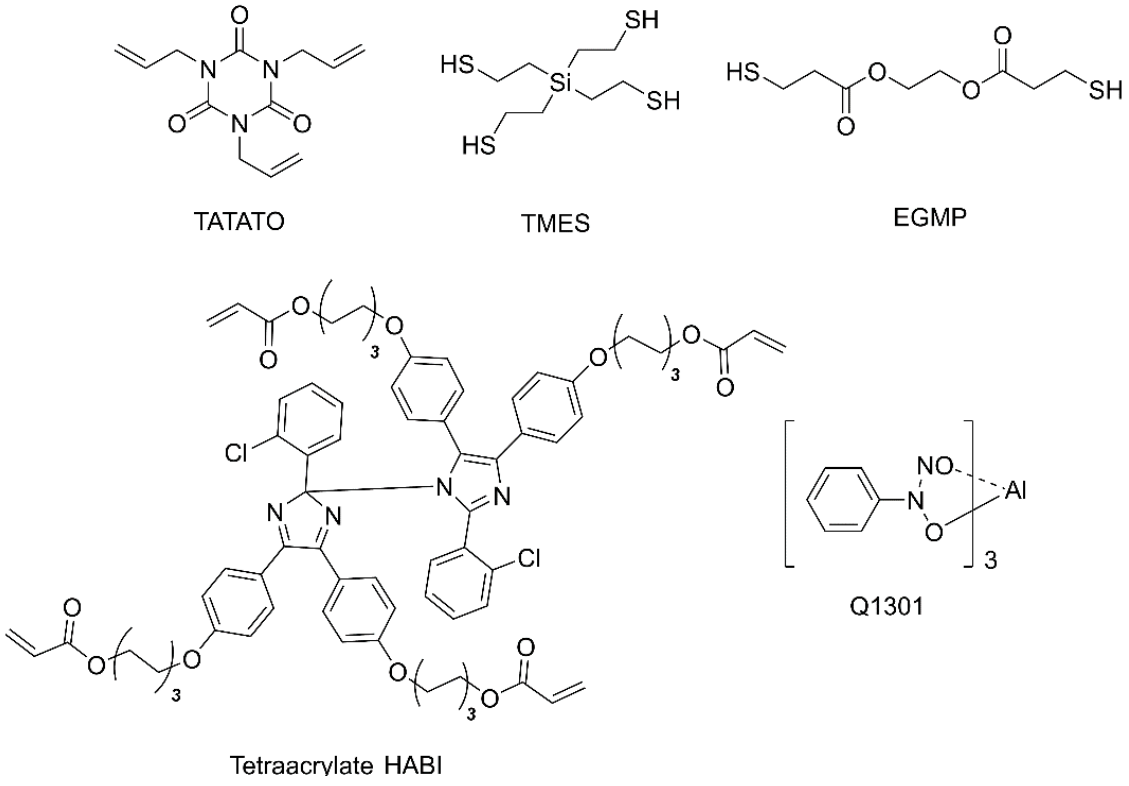


***Figure 2.1 Acrylate-functionalized hexaarylbimidazole (Tetraacrylate HABI), Thiol monomers (TMES and EGMP), allyl monomer (TATATO), and radical inhibitor (Q1301) used in this study.***

### *2.3.2 Methods*

#### *2.3.2.1 Resin formulation and film preparation*

The resin was prepared by dissolving the tetacry-HABI in a minimum amount of dichloromethane. The ratio of thiols consumed in the first reaction to thiols consumed in the second reaction can be changed by varying the amount of secondary monomer, triallyl-1,3,5-triazine-2,4,6-trione (TATATO), and then added to the HABI solution. The thiol molar amount is determined by a 1:1 ratio of double bonds (acrylate + allyl) to thiols. The molar amount of the individual thiols is determined by the molar ratio of TMES:EGMP which was then multiplied by the total molar amount of thiols to determine the mole fraction of thiol from TMES and EGMP. A nitrosamine radical inhibitor (Q1301) was added at 0.01 wt% to limit any premature radical polymerization. Nitrogen was blown over the sample in the dark for ~15 minutes to remove excess dichloromethane before injecting. Lastly, triethylamine (TEA) was added as a basic catalyst at ~5 wt%. After adding TEA and mixing, the samples were immediately cast between glass slides separated by 0.25 mm spacers and coated in a release agent, rain-x, and allowed to polymerize overnight in the dark.

#### *2.3.2.2 Photocuring and intensity measurement*

Violet light was provided by a collimated, LED-based illumination source (Thorlabs M405L2-C) with an emittance centered at 405 nm (FWHM 13 nm), used in combination with a current-adjustable LED driver (Thorlabs LEDD1B) for intensity control. Irradiation intensities were measured with an International Light IL1400A

radiometer equipped with a broadband silicon detector (model SEL033), a 10x attenuation neutral density filter (model QNDS1), and a quartz diffuser (model W). Light exposed samples were exposed to 405 nm light at 60 mW/cm$^2$ for 5 minutes on both sides.

#### *2.3.2.3 Dynamic mechanical analysis (DMA)*

Using the method described above, cross-linked films were prepared. Samples of approximately 20 mm × 3 mm × 0.25 mm were cut from the cured films and mounted in a TA Instruments DMA Q800 dynamic mechanical analyzer (DMA) equipped with a tension clamp. Experiments were performed at a strain of 0.1% and frequency of 1 Hz, scanning over a temperature range of -45°C to 100°C at 2°C/min., and the storage moduli (E′) and tan δ curves were recorded.

#### *2.3.2.4 Fourier transform infrared spectroscopy (FTIR)*

Each sample was placed in a Thermo Scientific Nicolet 6700 FTIR spectrometer equipped with a horizontal transmission accessory, as described elsewhere, and spectra were collected from 2000 to 6500 cm$^{-1}$. The functional group conversion was determined from the peak area centered at 2560 cm$^{-1}$ corresponding to the thiol group stretch, 6130 cm$^{-1}$ corresponding to allyl C=C stretch from TATATO, and 6160 cm$^{-1}$ corresponding to the acrylate C=C stretch from the acrylate functionalized HABI. All samples were 0.25 mm thick and tested after initial curing in the glass slides and subsequently after photo- or mechano- curing. Control samples were evaluated similarly but were kept in the dark and away from external stimuli for the same duration.

#### *2.3.2.5 Fatigue testing*

Samples of approximately 20 mm × 5 mm × 0.25 mm were cut from the cured films and mounted in a TA Instruments DMA Q800 dynamic mechanical analyzer (DMA) equipped with a tension clamp. Samples were exposed to higher strains and frequencies than DMA testing for a period of hours. The frequency used was 5 hz and the strain was varied from 0.25% to about 1% which was around the point where fracture was common for most samples. A gas cooling accessory maintained the temperature of 25℃ in the chamber during cyclic loadings while storage modulus (E′) was recorded.

#### *2.3.2.6 Ultrasonic bath on film samples*

Samples of approximately 15mm × 2.5 mm × 0.13 mm were cut from a cured polymer film and placed in a glass vial wrapped in foil. The samples were placed in the metal wire basket and placed in the ultrasonic water bath (Branson CPX3800 Ultrasonic bath) with the lid on to bath remaining on to keep the samples dark. Additionally, the temperature of the bath was monitored regularly and when the water heated up above 30-35℃ (a mild temperature that the HABIs are often exposed to) then the water was replaced with room temperature water.

#### *2.3.2.7 Ultrasonic welding on film samples*

Mechanical stress was imparted using an ultrasonic welder (Dukane IQ Series) operating at 20 kHz, 20% amplitude and 24 lb trigger force. The energy of the weld was varied from 50 J up to 800 J. The samples were wrapped lightly in aluminum foil and

placed between Teflon supports which removed them from direct contact with the horn. For a single weld the sample was taken out and examined after the 400 J weld was completed (~20 secs). For multiple welds, the time between welds is just the minimum time that it takes the horn to return to the home position and then manually initiate a new weld sequence (~5 secs). To measure the internal temperature of the films, a thermocouple was cured within a thiol-ene film and connected to LabView software to capture the internal temperature (~1 hz) of the film upon exposure to repeated ultrasonic welds as described further in the discussion.

### *2.3.3 Synthesis*

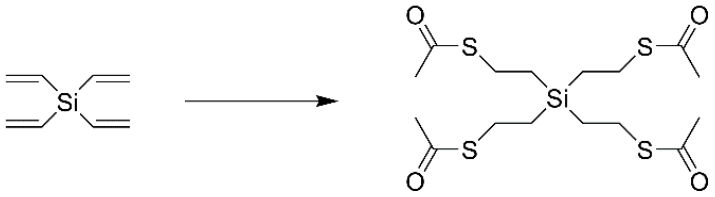


***Scheme 2.1 Synthesis of tetra(S-ehtylethanethioate)silane***

#### *2.3.3.1 Tetra(S-ethylethanethioate)silane*

Tetravinylsilane (50g), thioacetic acid (120mL), and azobisisobutyronitrile (8g) were dissolved in 500 mL tetrahydrofuran. The solution was heated to 70℃ and stirred overnight. The solution was allowed to cool to room temperature, and the solvent was removed under reduced pressure to afford a yellow oil which was used without further purification. $^{1}$H NMR (400 MHz, $CDCl_3$): δ = 1.01-1.07 (m, 8H), 2.32 (s, 12H), 2.90-2.96 (m, 8H).

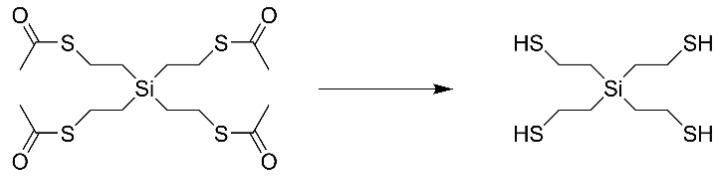


***Scheme 2.2 Synthesis of tetra(2-mercaptothyl)silane***

### *2.3.3.2 Tetra(2-mercaptoethyl)silane*

The product from the previous step, tetra(S-ethylethanethioate)silane, was dissolved in methanol (200 mL) and 1,4-dioxane (300 mL). 100 mL of concentrated hydrochloric acid was added and the solution heated to 65℃ and stirred for 24 hours. The solution was allowed to cool to room temperature and then solvent was removed under reduced pressure. 200 mL of water was added and the mixture was extracted with 100 mL of dichloromethane 3 times. The organic fractions were combined and dried with sodium sulfate before removing the solvent under reduced pressure. $^{1}$H NMR (400 MHz, $CDCl_3$): δ = 1.03-1.16 (m, 8H), 1.56-1.62 (m, 4H), 2.57-2.70 (m, 8H).

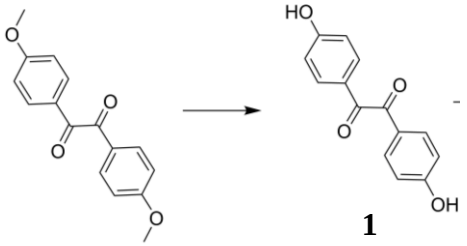


**1**

***Scheme 2.3 Synthesis of 1,2-bis(4-hyrdoxyphenyl)ethane-1,2-dione (1)***

### *2.3.3.3 1,2-bis(4-hyrdoxyphenyl)ethane-1,2-dione (1)*

4,4′-dimethoxy benzil (10.0 g, 37.0 mmol) was mixed with 30 mL acetic acid and heated to 85°C for 30 minutes. Hydrobromic acid (40%, 20.0 mL, 0.10 mol) was added into the

mixture and the mixture was refluxed at 120°C for 5 days. After cooling to room temperature, the solution was distilled to remove acetic acid and excessive hydrobromic acid. The residue was dissolved in ethyl acetate and washed with water. The solution was dried with sodium sulfate and solvent was removed under reduced pressure. The crude product was further purified by silica gel chromatography eluting with hexane/ethyl acetate (1/1, v/v) to afford 7.06 g of **1** (78.8% yield).

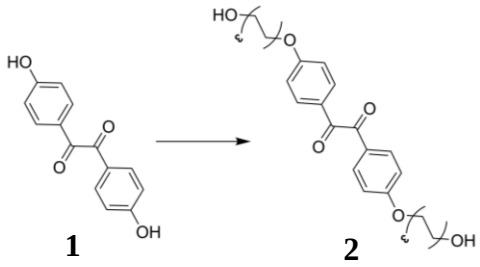


***Scheme 2.4 Synthesis of 1,2-bis(4-((6-hydroxyhexyl)oxy)phenyl)ethane-1,2-dione (2)***

***2.3.3.4 1,2-bis(4-((6-hydroxyhexyl)oxy)phenyl)ethane-1,2-dione (2)***

**1** (7.50 g, 31.0 mmol) and potassium carbonate (12.8 g, 92.9 mmol) were added to 100 mL of dimethylformamide (DMF) and the mixture magnetically stirred. 6-Chlorohexanol (11.0 g, 80.5 mmol) was added to the mixture and heated at 120°C for 16 hours under nitrogen. After cooling to room temperature, the mixture was filtered, DMF was evaporated, and the residue was purified by silica gel chromatography eluting with hexane/ethyl acetate (1/3, v/v), yielding 11.7 g of **2** (85.4% yield).

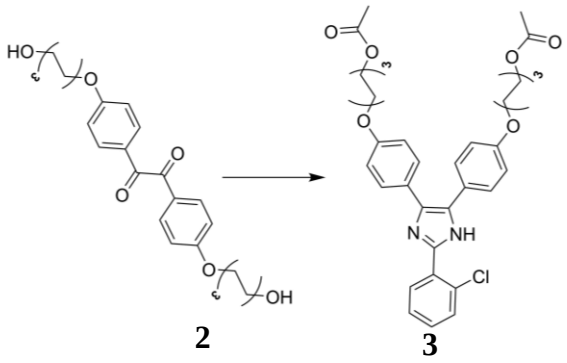


**2** **3**

***Scheme 2.5 Synthesis of (((2-(2-chlorophenyl)-1H-imidazole-4,5-diyl_bis(4,1-phenylene))bis(oxy))bis(hexane-6,1-diyl)diacetate (3)***

***2.3.3.5 (((2-(2-chlorophenyl)-1H-imidazole-4,5-diyl_bis(4,1-phenylene))bis(oxy))bis(hexane-6,1-diyl)diacetate (3)***

A mixture of **2** (10.0 g, 22.6 mmol), 2-chlorobenzaldehyde (3.18 g, 22.6 mmol), ammonium acetate (14.8 g, 192 mmol), and 150 mL of acetic acid was purged for five minutes with nitrogen and then refluxed at 120℃ overnight. After cooling to room temperature, the solvent was partially removed and poured into excess water. After allowing the mixture to precipitate for 24 hours, there was a thick, waxy gel that is highly immiscible with water and primarily stuck to the side of the flask and doesn't pour through the Buchner funnel at all. The wastewater was filtered first and precipitate collected on the filter paper. Then, the walls of the flask were sprayed with DCM to dissolve precipitate on the walls using a pipette. The dissolved DCM mixture was poured through the filter paper into a clean flask to dissolve the precipitate left on the paper to get a DCM solution of the crude product. The product was washed with water, dried, and excess DCM removed.. The precipitate was purified by silica gel chromatography eluting with hexane/ethyl acetate (1/2, v/v) to afford 12.32 g of **3** (84.1% yield).

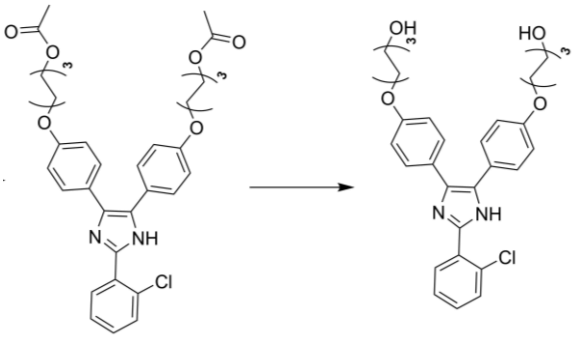


**3** **4**

***Scheme 2.6 Synthesis of 6,6'-(((2-(2-chlorophenyl)-1H-imidazole-4,5-diyl(bis(4,1-phenylene))bis(oxy))bishexan-1-ol) (4)***

### *2.3.3.6 6,6'-(((2-(2-chlorophenyl)-1H-imidazole-4,5-diyl(bis(4,1-phenylene))bis(oxy))bishexan-1-ol) (4)*

A solution of **3** (10.0 g, 15.5 mmol) in 100 mL of tetrahydrofuran was mixed with 100 mL of 3 M NaOH aqueous solution and refluxed at 68°C for 12 hours. After cooling to room temperature, solvent was removed under reduced pressure and extracted with dichloromethane. The organic layer was collected, washed with brine, and dried over sodium sulfate. The solvents were removed under reduced pressure to afford a yellow powder, yielding 7.6 g of **5** (87.4% yield).

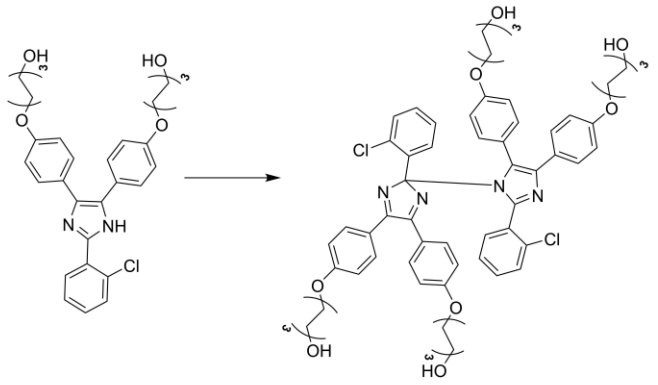


**4** **5**

***Scheme 2.7 Synthesis of tetra-OH HABI (5)***

***2.3.3.7 tetra-OH HABI (5)***

To a stirred solution of potassium ferricyanide (13.2 g, 40.0 mmol) and potassium hydroxide (24.0 g, 428 mmol) in 200 mL of water, a solution of **4** (7.50 g, 13.3 mmol) in 100 mL of dichloromethane was added dropwise. The mixture was refluxed at 45°C overnight. After cooling to room temperature, the organic layer was collected, washed with water, dried over anhydrous magnesium sulfate, filtered, and the solvent removed under reduced pressure. The residue was purified by silica gel chromatography eluting with hexane/ethyl acetate (1/2, v/v) to afford 11.5 g of **5** (75.7% yield).

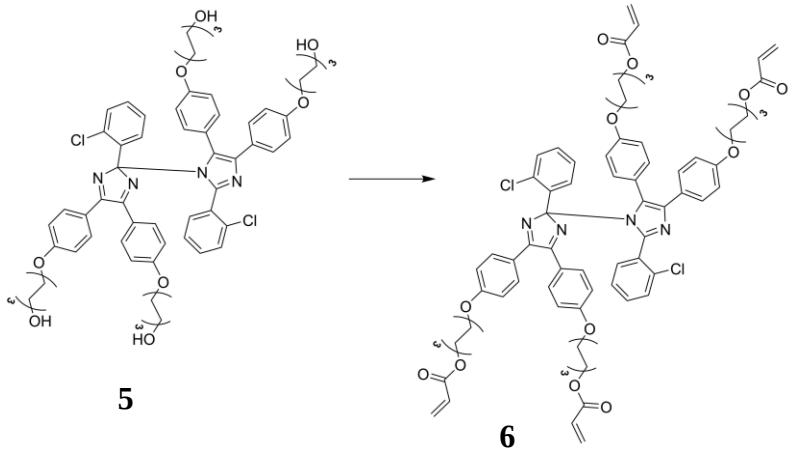


***Scheme 2.8 Synthesis of tetra-acrylate HABI (6)***

***2.3.3.8 tetra-acrylate HABI (6)***

A solution of **5** (1.50 g, 1.34 mmol) was dissolved in 20 mL dichloromethane and 1.3 mL triethylamine (9.4 mmol). The solution was stirred over ice until it was cooled to 0℃. Acryloyl chloride (0.58 g, 5.37 mmol) was added dropwise at 0℃ until fully added. The solution was allowed to warm and up and stir at room temperature overnight. The solvent was removed under reduced pressure and redissolved in THF and vacuum filtered to remove salts. The solvent was removed under reduced pressure to afford a light brown oil. The residue was purified by silica gel chromatography eluting with hexane/ethyl acetate (3/2, v/v) to afford 1.17g of **6** (70% yield).

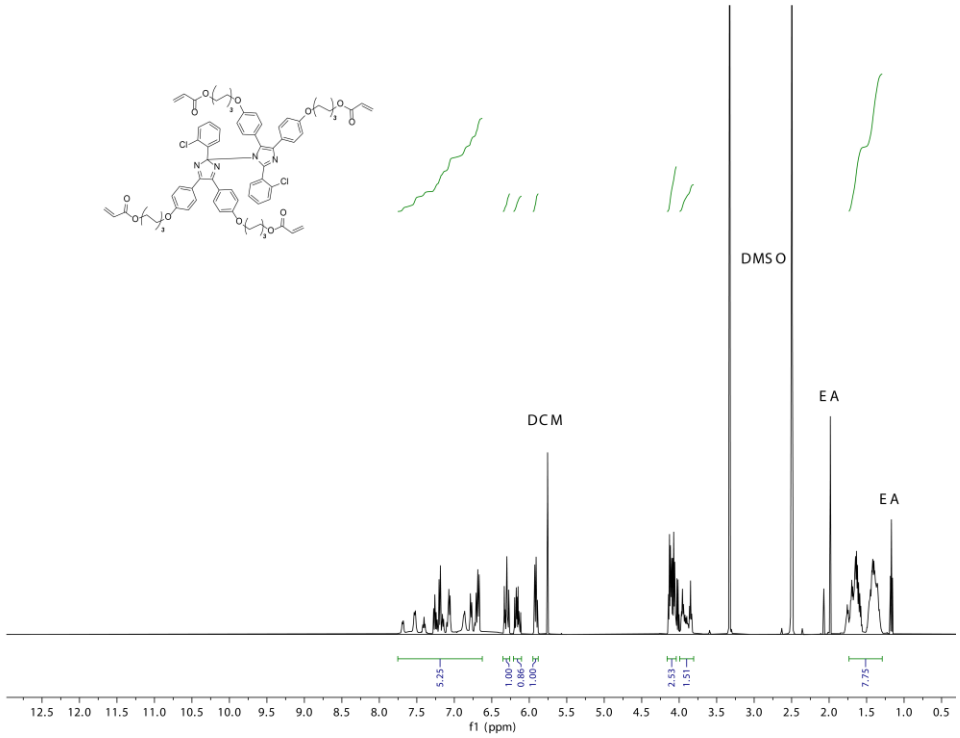


***Figure 2.2 $^{1}$H-NMR spectrum of tetra-acrylate HABI***

## 2.4 Results and Discussion

Hexaarylbimidazoles (HABI) are uniquely suited for application in autonomous self-reinforcing films. HABI are known thiol-ene initiators upon cleavage of their weak carbon-nitrogen bond whereby the generated lophyl radical abstract a hydrogen from thiol to form highly reactive thiyl radicals. Moreover, the widely documented functionalization of HABI affords many attainable options for HABI synthesis to incorporate HABI into polymers. Acrylate-functionalized HABI was synthesized from previously documented tetra-OH HABI[17] in a single-step esterification. Electron-deficient acrylates react rapidly in thiol-ene reactions, both thiol-Michael addition and radical thiol-ene reactions. Thus, the initial polymerization of thiol-acylates proceeds via thiol-Michael addition, a base-catalyzed thiol-ene reaction that proceeds only in the presence of sufficiently electron-deficient double bonds. The selectivity of thiol-Michael addition allows for polymerization of electron-deficient double bonds over electron-rich ones. Furthermore, this orthogonality lends itself to the development of two-stage networks by incorporating both types of double bonds, whereby the electron-deficient acrylates are consumed in the thiol-Michael addition to form the preliminary first stage network and leaves the unreacted electron-rich double bonds available for stimuli-responsive local polymerization.

Thiol-ene polymerizations are easily characterized by FTIR to measure conversions of the thiol and double bond functional group and confirm the orthogonality of the thiol-ene chemistries to produce two-stage films. HABI is a documented thiol-ene photoinitiator[13] so UV light was used as the initiation method to test the validity of the first stage to second stage *in situ* thiol-ene reaction of the residual thiol and -ene (allyl) functional groups. In Figure 2.3a, the IR peaks of the allylic and acrylate double bonds

show the functional group conversion through the multiple stages. Before the thiol-Michael addition, the double peaks centered at 6130 and 6160 $cm^{-1}$ represent the slightly different frequencies of the allylic and acrylic double bonds, respectively. The allylic double bond peak at 6130 $cm^{-1}$ exactly matches the allylic peak seen in the pure TATATO monomer and further confirms the identity of each double bond peak. The base-catalyzed thiol-Michael addition is confirmed by the complete consumption of the acrylate peak while the allylic peak remains intact, thereby also confirming the orthogonality of the thiol-ene chemistries. Figure 2.3b shows the thiol stretch peak at 2560 $cm^{-1}$ which is severely reduced after a substantial portion is consumed after stage 1. The conversion of thiol after stage 1 is going to be determined by the stoichiometric ratio of acrylate to allyl functional groups since the stoichiometric ratio of thiol to carbon-carbon double bonds is 1:1.

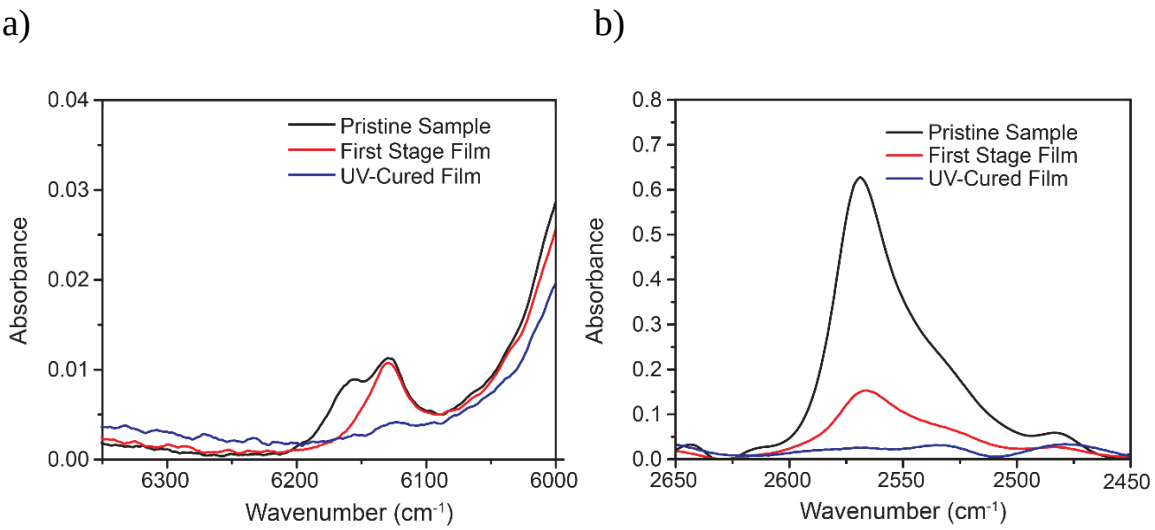


***Figure 2.3 FTIR spectra of monomer resin (black), first stage film (red), and second stage film (blue) looking at the a) allyl (6130 $cm^{-1}$) and acrylate (6160 $cm^{-1}$) double bond peaks and b) thiol peak (2560 $cm^{-1}$).***

There are many advantages for developing materials able to locally change mechanical properties and have multiple stages of mechanical properties such as orthopedic shape-memory polymers[18] and holographic data storage.[19] Photoresponsive polymers allow for localized reinforcement to create complex films and coatings that can exhibit locally increased mechanical properties in specific areas on the film. The ability to tune the mechanical properties of the stages individually also allows for the adaptation to a variety of applications. HABI thiol-ene films can be tuned by the modification of the acrylate:allyl ratio which determines the proportion of thiols that are covalently bonded in the stage 1 film compared to the stage 2 film. The choice of thiol and allyl can also be changed to result in different mechanical properties. Here, only a single allyl, TATATO, is demonstrated and the network is modified by changing the stoichiometric ratio of thiols between the tetra-functional TMES and the difunctional EGMP. These changes influence the properties of both stages of polymer and the mechanical properties can be characterized by their changes in their storage modulus and glass transition temperature.

The acrylate:allyl ratio of the pristine thiol-Michael polymerized film has a large effect on the change in glass transition temperature ($T_g$) from stage 1 to stage 2. When more acrylate groups are used than allyl groups in sample $acry_{57}$-$TMES_{33}$ (57% of total double bonds are acrylates with the balance being allyl double bonds in $acry_{57}$-$TMES_{33}$) the initial glass transition is slightly higher and the change in $T_g$ after photocuring is smaller compared to sample $acry_{40}$-$TMES_{33}$ with 40% acrylate (See Figure 2.3a and b). However, the thiols are participants in both thiol-ene reactions and thus the thiol ratio effects both stages. When the acrylate:allyl ratio is held constant but the amount of thiol changed from 33% moles of thiol from TMES and 66% moles of thiol from EGMP to 75% moles of thiol

from TMES, both the initial and the final glass transition temperature increase along with the room temperature storage modulus, resulting in a more rigid polymer at room temperature (See Fig 2.3b and c). The change in glass transition temperature is also greater with higher TMES and the glass transition temperatures are summarized in table 2.2. This demonstration of the tunability of a two-stage thiol-ene network using simple formulation changes not only shows the potential of HABI in photoresponsive two-stage polymers but also serves to provide a benchmark for mechanical initiation of HABI.

The *in situ* crosslinking response using light allows for spatial manipulation of the cross-link density of a single initially-uniform polymer film. However, the response requires additional stimuli that may cost additional time and energy. Every polymeric material experiences fatigue over time due to regular use that causes macroscopic damage over longer timescales. Since HABI is both a photoinitiator and a potential mechanophore,[11] the two-stage polymer film should respond to local stresses in a similar manner to the demonstrated photoresponse. Photocuring is a simpler method of breaking the HABI bond whereas mechanical breaking of HABI bonds requires a sufficient transfer of mechanical energy to the weak HABI bond while not breaking other covalent bonds in the process.

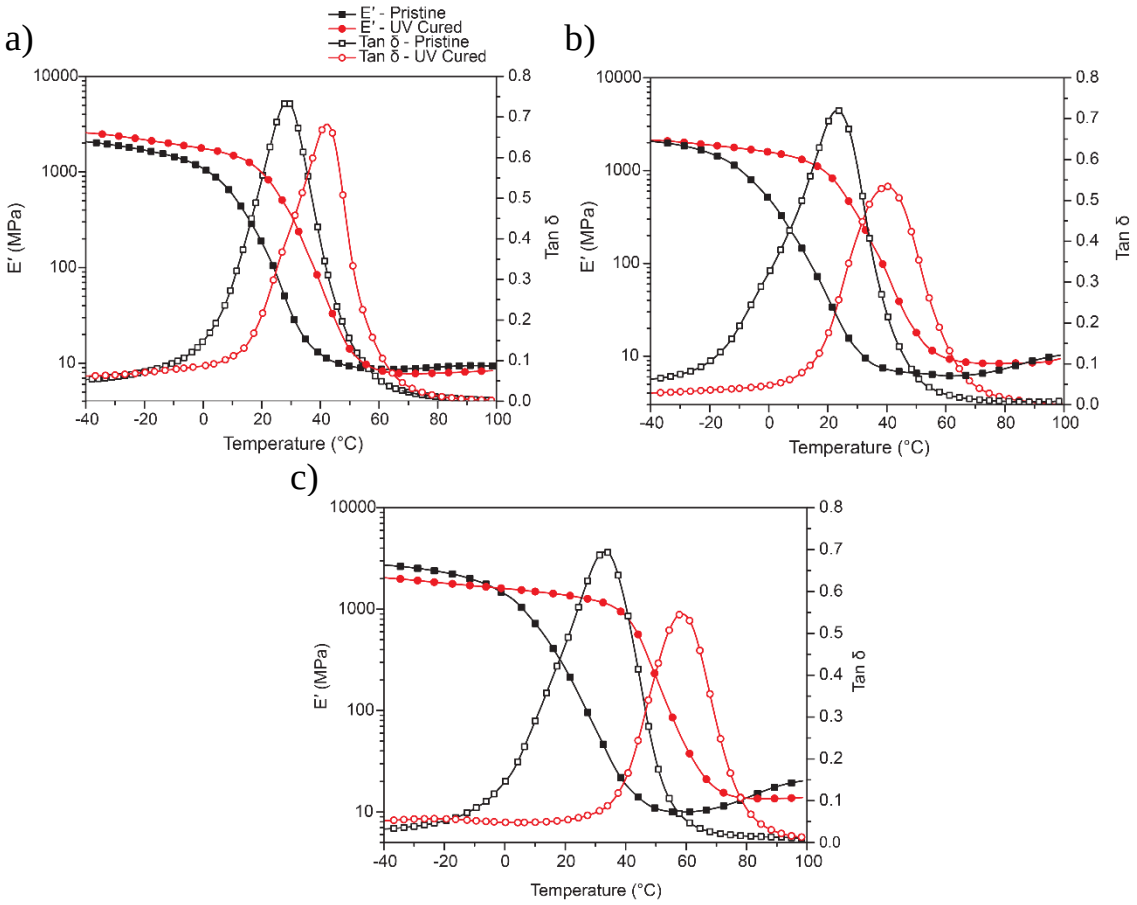


***Figure 2.4 Dynamic Mechanical Analysis traces of storage modulus (E', solid points) and tan δ (open points) as a function of temperature of polymerized first stage films (black) and 405 nm cured second stage films (red) for a) acry$_{57}$-TMES$_{33}$, b) acry$_{40}$-TMES$_{33}$, and c) acry$_{40}$-TMES$_{75}$.***

***Table 2.1 Summary of glass transition temperature changes in two-stage films.***

| Thiol-ene formulation | Pristine $T_g$ (°C) (first stage) | UV Cured $T_g$ (°C) (second stage) | $\Delta T_g$ (°C) |
|---|---|---|---|
| Acry$_{57}$-TMES$_{33}$ | 28 | 42 | 14 |
| Acry$_{40}$-TMES$_{33}$ | 24 | 41 | 17 |
| Acry$_{40}$-TMES$_{75}$ | 33 | 59 | 26 |
| Acry$_{21}$-TMES$_{70}$ | 29 | 69 | 40 |

Fatigue manifests in all materials as a result of repetitive loads that initiate microcrack formation and propagate until complete material failure. The objective of the mechanically induced two-stage polymer is using the mechanical energy from the repetitive loading to drive the thiol-ene reaction. First, we examine the polymer response to tensile cyclic loading by monitoring the storage modulus. Thermal effects cause thermal softening in polymers and potentially cleave the HABI C-N bond resulting in thermal initiation of HABI. Thermal effects are undesirable so during cyclic loading the chamber was kept under isothermal conditions using a gas cooling accessory on a DMA. This reduces any thermal initiation effects and thermal effects on the mechanical properties to isolate the response to mechanical fatigue. Applying strain without fracturing the material turned out to be difficult and it took many trials to tailor the settings to fatigue the material for many minutes without abrupt fracture. The $acry_{28}$-$TMES_{75}$ polymer samples were exposed to constant strains of 0.35% and 0.50% at a frequency of 5 hz while the atmosphere was kept at a constant 25℃ (Figure 2.5). When exposed to repeated loadings at constant temperature, the storage modulus increases from a starting value of 360 MPa until it reaches a plateau around 450 MPa. Being kept at constant temperature, the increase in storage modulus must be a result of a change in connectivity of the network from polymerization induced by HABI. Without thermal or light effects, its reasonable to suggest that the increase is due to mechanical strengthening, completely opposite to what typically happens to stressed materials. The plateau is thought to be explained by the depletion of easily activated HABI remaining intact in the film. Some HABI are activated, but the complex connectivity of the network may result in many bonds just not

experiencing the force needed to break them before too many covalent bonds break to cause macroscopic fracture.[20]

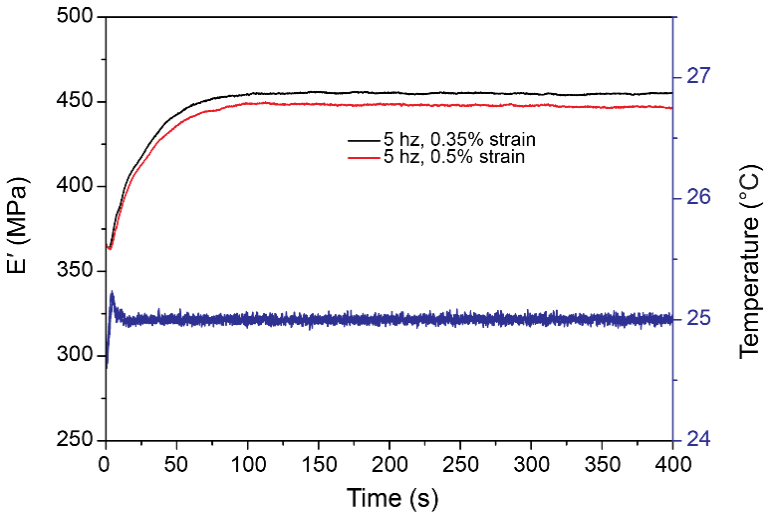


***Figure 2.5 Storage modulus evolution during cyclic loading at 5 hz frequency and 0.35% or 0.5% strain.***

The increase in storage modulus as a response to cyclic loading suggests a transfer of mechanical energy to chemical energy in the form of crosslinking. During cyclic loading the storage modulus would be expected to decrease as typically bonds are broken or decreased from internal heating. However, the uniaxial loading only provides small increases in modulus when compared to the modulus increases seen in the photocured two-stage polymers descried earlier (see Fig. 2.4). This suggests a small number of HABIs are actually being initiated and thus the properties are only minutely changed in response to uniaxial loading.

Ultrasonic acoustic waves are often used as a source of mechanical energy such as demonstrations in activating mechanophores.[5] Often mechanophores are activated on polymers in dilute solutions that don't need to consider solid-state fracture. As opposed to

applying a uniaxial force, the acoustic waves allow for vibrations to propagate through the film in all directions instead of in a single axis which should allow for more activation of HABI. To test this, an ultrasonic bath was used to apply mechanical energy to the sample. The goal was to isolate the mechanical initiation from thermal or photoinitiation so the samples were covered in foil with the top of the bath remaining on to keep the samples dark. Additionally, the temperature of the bath was monitored regularly and when the water heated up above 30-35°C (a mild temperature that the HABIs are often exposed to) then the water was replaced with room temperature water. The thin films were initially either just wrapped in foil and plastic wrap. However, the changes in the films were mostly minimal, if any, due to the ultrasonic bath and the results were mostly inconclusive, but one factor may have been the method of exposing the sample to ultrasound. New samples were cut and placed inside a vial wrapped in foil and placed inside the ultrasonic bath. Some of the samples did show moderate conversions of thiol and allyl with a modest shift in the $T_g$ and storage modulus (Figure 2.6). This suggested a limited amount of HABI-initiated thiol-ene had taken place but repeated attempts to generate similar results yielded inconsistent and miniscule changes to the network.

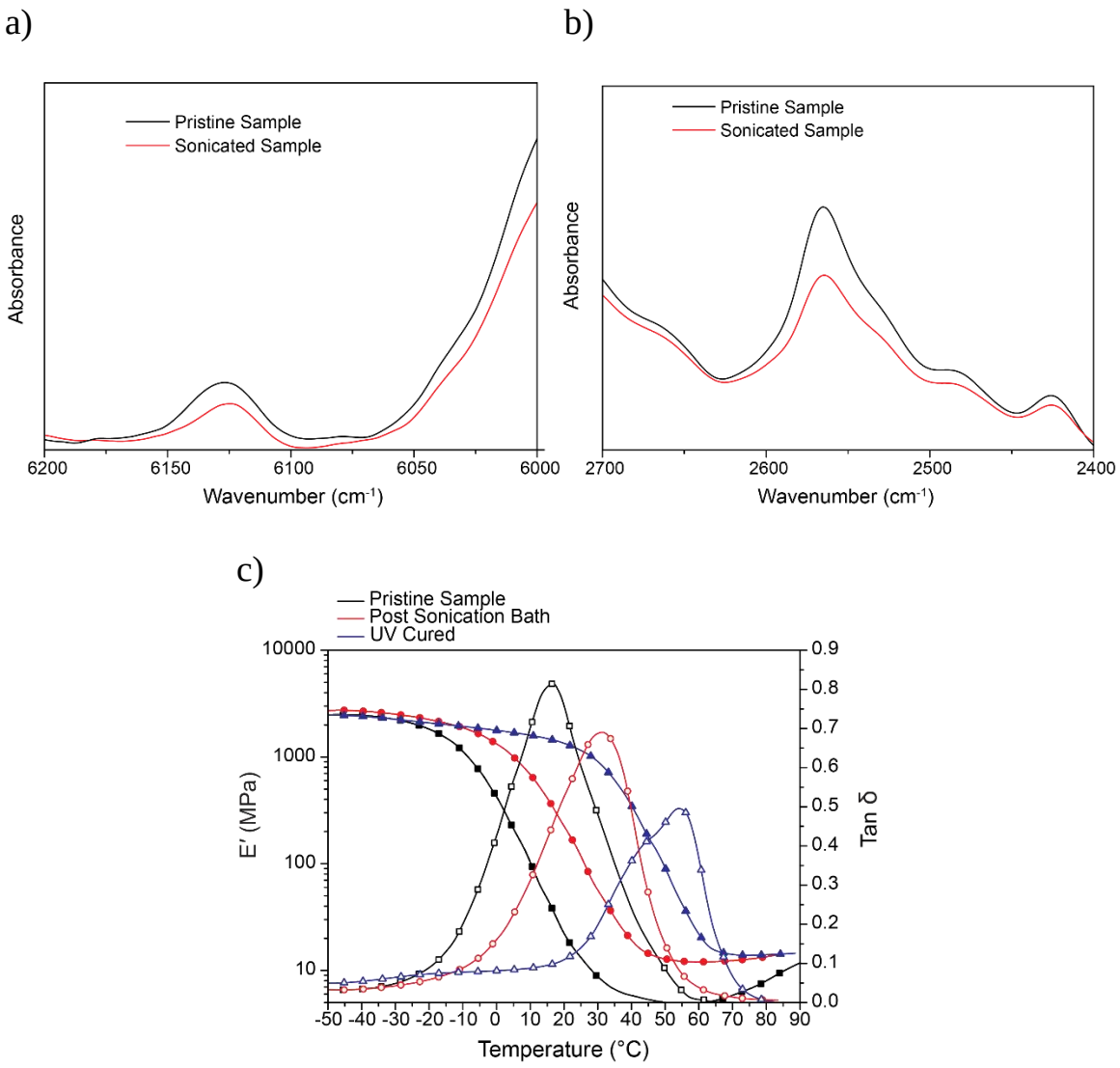


***Figure 2.6 a) 6130 cm$^{-1}$ allyl FTIR peak, and b) 2560 cm$^{-1}$ thiol FTIR peak before and after sonication bath. c)Dynamic Mechanical Analysis traces of storage modulus (E', solid points) and tan δ (open points) as a function of temperature before and after sonication bath.***

The modest mechanical changes in the network were promising but didn't yield a conclusive result that mechanical force can repeatably trigger HABI *in situ* and impart significant change in the network. It was hypothesized that the difficulty of transferring the ultrasonic energy through many different media and to the film may result in miniscule

bond breaking and thus limited conversion of the network and a more direct way of transferring force through the sample was desired.

Ultrasonic welding (USW) is a technique used with thermoplastics where 2 pieces of a thermoplastic can be welded together by the application of compression force and high frequency acoustic waves which trigger localized melting at the point of contact between two thermoplastics.[21] USW is typically used with thermoplastics but the mechanism of applying compressive force and high frequency acoustics may be a more direct method of applying mechanical force through the network than an ultrasonic bath or uniaxial tension. This will determine whether it's possible to trigger the HABI-initiated reinforcement reaction without macroscopic damage. To reduce the heat generated, the amplitude of the USW was reduced to 20% of its typical capacity and the energy of the weld could be controlled to reduce the total time that the welder would contact the sample.

Owing to the welder's ability to generate heat and the possibility of thermal initiation of HABI, it's necessary to understand the temperature effects on the film from the ultrasonic welder. Using a thermocouple embedded within a test film, the temperature was recorded while welding the polymer. The ultrasonic welder was set to various energy levels from 400 J to 600 J to measure the effect of changing the energy of the welder (Figure 2.7). After hitting the sample with two 400 Joule welds, the temperature increase is less than 2°C and recovers within seconds of the completion of the weld. Similar results are seen at higher energy welds where 600 J welds impart a little more thermal energy but even after 4 welds in repeated fashion, the temperature never spikes above 26°C. Importantly, the temperatures seem to decrease rapidly after completion which allows for multiple welds in a row without much of an effect on temperature.

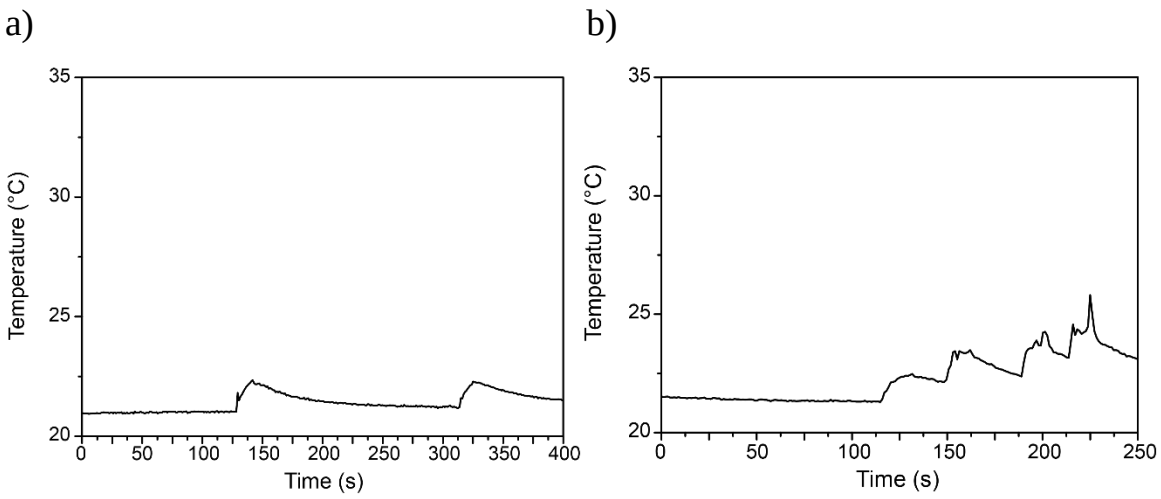


***Figure 2.7 Internal temperature over time during ultrasonic welding at a) 400 J and b) 600 J. The spikes in the temperature are the individual welds with 2 welds at 400J in a and 4 welds at 600 J in b.***

To investigate the effects of mechanical force of ultrasonic welding on the stimuli-responsiveness of the polymer film, the focus was on 3 main variables; the network connectivity, the energy of a weld, and the amount of total weld events imparted on the sample. The network structure was varied by changing the double bond ratios from 14% acrylate to 25% of the double bonds being acrylates. The ratio of dithiol (EGMP) to tetrathiol (TMES) monomers was varied with the acrylate ratio so that the film was stiff enough to manipulate, with lower acrylate ratios being paired with more TMES and higher acrylate ratio with less TMES and more EGMP. This resulted in most samples having moderate initial $T_g$ values around room temperature (~ 15-30℃).

Changing the energy of a weld affects the total length of the ultrasonic weld and the lower amplitude provided the energy slower over a longer period of time instead of an instant burst of energy. Comparing the properties of a mild 250 J weld (~20s) to a weld of 550 J (~35s) didn't affect a substantial change on the network (Figure 2.8). However, both

the samples that were exposed to the welder-induced mechanical perturbations display a shift in both storage modulus and tan δ with respect to the control sample. The peak in tan δ represents an approximation of the $T_g$ and the small shift in this peak suggests a cross-linking response to the mechanical stress in both welded samples that was different from the pristine sample. However, the shift of 3°C and 5°C in $T_g$ of the 250 J and 550 J samples, respectively, is significantly smaller than the changes seen in photocured two-stage films described earlier (see Figure 2.4). Unlike photocured networks, the HABI activation is dependent on mechanical energy transfer through the network which depends on the crosslink density and the connectivity of the HABI. It is possible that only a small number of HABI bonds could reach their force threshold to cleave without disrupting other covalent bonds and damaging the film and could explain the lack of additional crosslinking at higher energies.

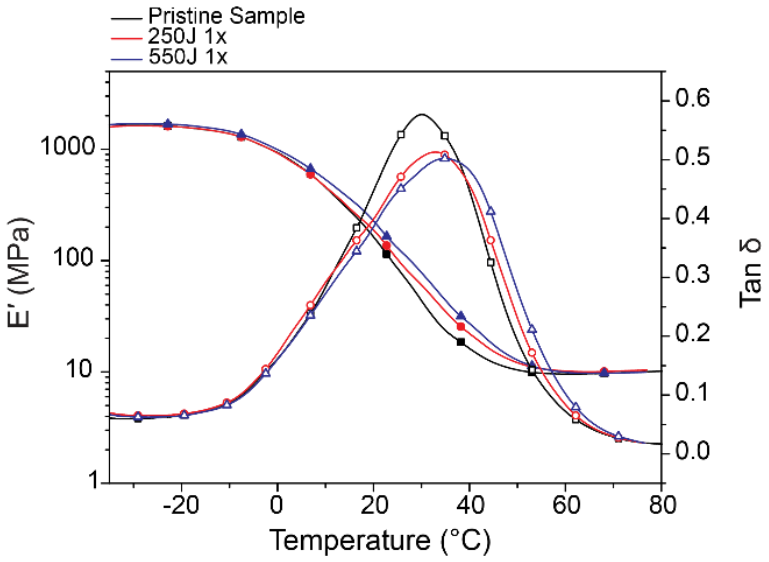


***Figure 2.8 Dynamic Mechanical Analysis traces of storage modulus (E', solid points) and tan δ (open points) as a function of temperature before and after ultrasonic welding of acry$_{25}$-TMES$_{60}$.***

Instead of increasing the energy, the welder energy can be lowered and applied multiple times to simulate non-catastrophic level mechanical stress events that create the typical wear and tear on a polymer. Separate welding events allows for dissipation of heat and avoid any heat buildup that may trigger HABI activation while also affording extra time for the network to complete all the reinforcing bond formation reactions caused by the first event.

The influence of multiple welds on the mechanical properties was assessed by applying different numbers of welds to the same formulation and comparing them to each other and non-welded control samples. Using $acry_{21}$-$TMES_{70}$ formulation, the $T_g$ increase of 14℃ after just 1 400 J weld is comparable to changes seen in the ultrasonic bath sample but an even greater $T_g$ increase is seen in the sample exposed to 3 welds of 400 J (Figure 2.9a). The increase in $T_g$ was also accompanied by an increase in the storage modulus at room temperature, the first stage polymer was a rubbery polymer under 100 MPa while the stressed samples became more glassy with a storage modulus at 25℃ greater than 1 GPa. This automatic reinforcing response to stress to modify the polymer from rubbery to glassy allows for local reinforcement of areas that may experience more wear and tear.

The sensitivity of the reinforcing response due to complex force transfer is highlighted when the experiment is repeated with the softer, $acry_{18}$-$TMES_{100}$, formulation (Figure 2.9b). The rubbery initial polymer with a $T_g$ of 20℃ and a storage modulus around 20 MPa sustained significant damage in the welder compared to the $acry_{21}$-$TMES_{70}$ formulation. This necessitated lowering the weld energy to generate a reinforcing effect without rupturing the polymer film. The weld energy of 125 J was significantly lower and may play a role in the smaller effects displayed. The largest change in properties was

between the non-welded and welded samples, highlighting the effect even a small mechanical perturbation can have on activating the self-reinforcing film. The thrice welded sample does show the greatest change in $T_g$ and modulus from the control, but the $T_g$ difference between the welded samples is no more than a few degrees. As new covalent bonds are formed, the force is spread out over more bonds and the lower weld energy may not transfer enough energy to cleave the remaining intact HABI.

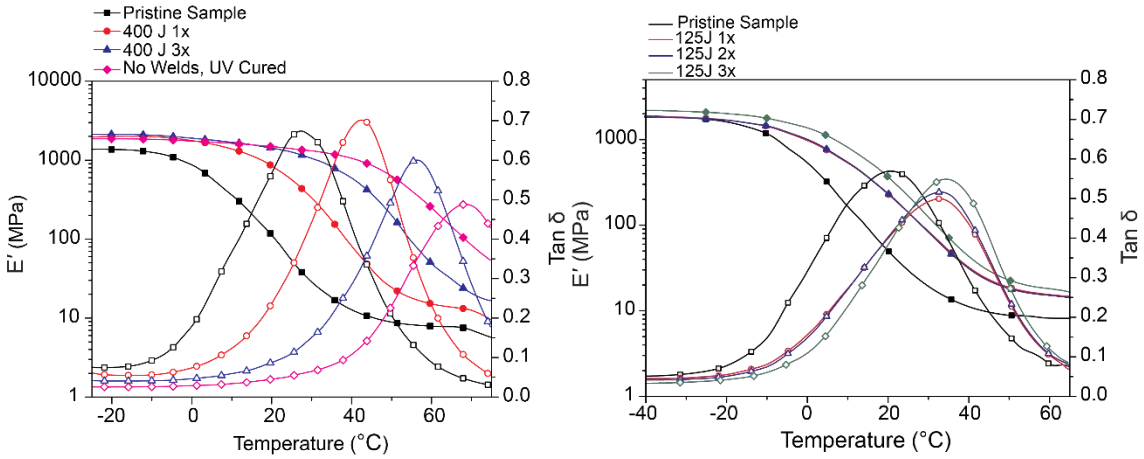


***Figure 2.9 Dynamic Mechanical Analysis traces of storage modulus (E', solid points) and tan δ (open points) as a function of temperature before and after ultrasonic welding of a) 400J welds of acry$_{21}$-TMES$_{70}$ and b) 125 J welds of acry$_{18}$-TMES$_{100}$.***

The disappearance of the thiol and allyl functional groups in FTIR confirms that a reaction took place to generate the crosslinks and change the mechanical properties. After repeating the 400 J welds multiple times on different acry$_{21}$-TMES$_{70}$ films the average conversion of thiol and allyl functional groups can be compared against the number of welds and normalized for the control samples (Figure 2.10, Table 2.2).

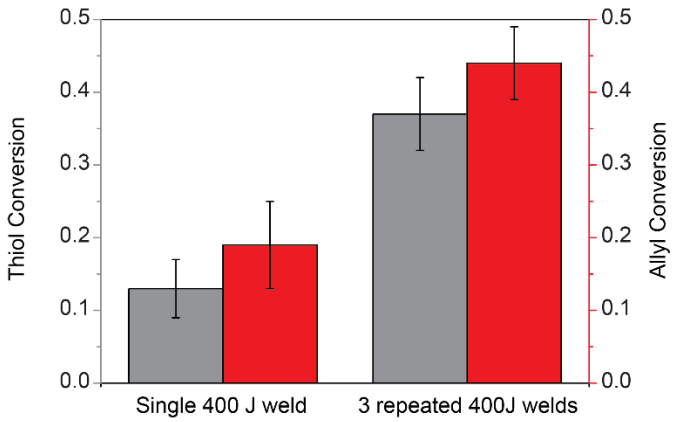


***Figure 2.10 Allyl (red bar) and thiol (gray bar) conversion difference between single welds and triple welds.***

***Table 2.2 Summary of allyl and thiol conversion determined by FTIR after 400J welding events.***

| $Acry_{21}$-$TMES_{70}$ | Allyl Conversion | Thiol Conversion |
|---|---|---|
| Single 400 J Weld | 0.19 ± 0.06 | 0.13 ± 0.04 |
| Three 400 J Welds | 0.44 ± 0.05 | 0.37 ± 0.05 |

While the conversions are low compared to almost 100% conversion of photocured two-stage networks, the correlation of the conversion of the functional groups and the mechanical property change show the potential of using HABI in thiol-ene two-stage films. Initiating the tetraacrylate HABI using mechanical stress is more challenging because of the destructive nature of the stress. Nonetheless, the ability to autonomously reinforce without application of external stimulus is advantageous to produce synthetic materials that respond and adapt to environmental conditions.

## 2.5 Conclusions

In this work, we demonstrated the ability to use orthogonal thiol-ene chemistry to produce two-stage polymers. By synthesizing HABI with acrylate functional groups, the first stage network can be formed with backbone HABI moieties. Utilizing the thiol-ene initiating capabilities of HABI, the radical-initiated second stage reaction was demonstrated with UV light. Varying the choice of thiol, acrylate, and allyl monomers or stoichiometric ratios between them allows for boundless possible properties of first and second stage networks. Here, simple changes in the ratio of acrylate:allyl or thiol monomers afford first and second stage polymers that can range from soft elastomers to rigid, glassy polymers. Using the developed two-stage networks under mechanical stress led to small changes in the mechanical properties of the network from activation of mechanophoric HABI. The networks achieved limited self-reinforcing behavior under tensile strain, in a sonication bath, and under compressive ultrasonic welds without significant optimization of the network. The monomer conversions from force-initiated reinforcement are typically only 20-40% compared to almost 100% conversion in photocured networks but the changes in the modulus and glass transition temperature after mechanical perturbation demonstrate the potential of HABI in this type of two-stage thiol-ene network.

## 2.6 References


(1) Anderson, T. L. *Fracture Mechanics: Fundamentals and Applications*, 4th ed.; CRC Press, 2017.

(2) Rebitzer, G.; Ekvall, T.; Frischknecht, R.; Norris, G.; Rydberg, T.; Schmidt, W.-P.; Suh, S.; Weidema, B. P.; Pennington, D. W. Life Cycle Assessment: Part 1: Framework, Goal and Scope Definition, Inventory Analysis, and Applications. *Environ. Int.* **2004**, No. 30, 701–720.

(3) Patrick, J. F.; Robb, M. J.; Sottos, N. R.; Moore, J. S.; White, S. R. Polymers with Autonomous Life-Cycle Control. *Nature* **2016**, *540* (7633), 363–370.

(4) Wool, R. P. Self-Healing Materials: A Review. *Soft Matter* **2008**, *4* (3), 400–418.

(5) Hickenboth, C. R.; Moore, J. S.; White, S. R.; Sottos, N. R.; Baudry, J.; Wilson, S. R. Biasing Reaction Pathways with Mechanical Force. *Nature* **2007**, *446* (7134), 423–427.

(6) Chen, Y.; Spiering, A. J. H.; Karthikeyan, S.; Peters, G. W. M.; Meijer, E. W.; Sijbesma, R. P. Mechanically Induced Chemiluminescence from Polymers Incorporating a 1,2-Dioxetane Unit in the Main Chain. *Nat. Chem.* **2012**, *4* (7), 559–562.

(7) Davis, D. A.; Hamilton, A.; Yang, J.; Cremar, L. D.; Van Gough, D.; Potisek, S. L.; Ong, M. T.; Braun, P. V.; Martínez, T. J.; White, S. R.; Moore, J. S.; Sottos, N. R. Force-Induced Activation of Covalent Bonds in Mechanoresponsive Polymeric Materials. *Nature* **2009**, *459* (7243), 68–72.

(8) Larsen, M. B.; Boydston, A. J. Successive Mechanochemical Activation and Small Molecule Release in an Elastomeric Material. *J. Am. Chem. Soc.* **2014**, *136* (4), 1276–1279.

(9) Piermattei, A.; Karthikeyan, S.; Sijbesma, R. P. Activating Catalysts with Mechanical Force. *Nat. Chem.* **2009**, *1* (2), 133–137.

(10) Ramirez, A. L. B.; Kean, Z. S.; Orlicki, J. A.; Champhekar, M.; Elsakr, S. M.; Krause, W. E.; Craig, S. L. Mechanochemical Strengthening of a Synthetic Polymer in Response to Typically Destructive Shear Forces. *Nat. Chem.* **2013**, *5* (9), 757–761.

(11) Verstraeten, F.; Göstl, R.; Sijbesma, R. P. Stress-Induced Colouration and Crosslinking of Polymeric Materials by Mechanochemical Formation of Triphenylimidazolyl Radicals. *Chem. Commun.* **2016**, *52* (55), 8608–8611.

(12) Matsuda, A. T.; Kawakami, R.; Namba, R.; Nakajima, T.; Ping, J. Mechanoresponsive Self-Growing Hydrogels Inspired by Muscle Training. *Science* **2019**, *363* (February), 504–508.

(13) Ahn, D.; Sathe, S. S.; Clarkson, B. H.; Scott, T. F. Hexaarylbiimidazoles as Visible Light Thiol-Ene Photoinitiators. *Dent. Mater.* **2015**, *31* (9), 1075–1089.

(14) Ahn, D.; Zavada, S. R.; Scottt, T. F. Rapid, Photomediated Healing of Hexaarylbiimidazole-Based Covalently Cross-Linked Gels. *Chem. Mater.* **2017**, *29* (16), 7023–7031.

(15) de Beer, M. P.; van der Laan, H. L.; Cole, M. A.; Whelan, R. J.; Burns, M. A.; Scott, T. F. Rapid, Continuous Additive Manufacturing by Volumetric Polymerization Inhibition Patterning. *Sci. Adv.* **2019**, *5*.

(16) Li, G.; Randev, R. K.; Soeriyadi, A. H.; Rees, G.; Boyer, C.; Tong, Z.; Davis, T. P.; Remzi, C.; Haddleton, D. M. Investigation into Thiol-(Meth)Acrylate Michael Addition Reactions Using Amine and Phosphine Catalysts †. **2010**, 1196–1204.

(17) Dowon Ahn ORCID ID : 0000-0003-4837-0038 © Dowon Ahn 2017. **2017**.

(18) Yakacki, C. M.; Shandas, R.; Safranski, D.; Ortega, A. M.; Sassaman, K.; Gall, K. Strong, Tailored, Biocompatible Shape-Memory Polymer Networks. *Adv. Funct. Mater.* **2008**, *18* (16), 2428–2435.

(19) Curtis, K.; Dhar, L.; Hill, A.; Wilson, W.; Ayres, M. *Holographic Data Storage: From Theory to Practical Systems*; 2010.

(20) Imato, K.; Irie, A.; Kosuge, T.; Ohishi, T.; Nishihara, M.; Takahara, A.; Otsuka, H. Mechanophores with a Reversible Radical System and Freezing-Induced Mechanochemistry in Polymer Solutions and Gels. *Angew. Chemie* **2015**, *127* (21), 6266–6270.

(21) Zhang, Z.; Wang, X.; Luo, Y.; Zhang, Z.; Wang, L. Study on Heating Process of Ultrasonic Welding for Thermoplastics. *J. Thermoplast. Compos. Mater.* **2010**, *23* (5), 647–664.

# Chapter 3 Radical-Mediated Ring Opening Photopolymerization for Semi-crystalline Thermoplastic Additive Manufacturing

## 3.1 Abstract

Conventional approaches to stereolithographic additive manufacturing (SLA) employ liquid resin formulations based on multifunctional (meth)acrylates and epoxides that afford cross-linked polymeric networks upon polymerization. Nevertheless, the utilization of resins that yield semi-crystalline thermoplastics provides facile access to physical and mechanical properties that are otherwise difficult to attain, such as high toughness and resistance to solvent swelling as well as additional post-fabrication processing options that can be used to extend the life cycle of 3D printed polymers. Here, we report the SLA-based additive manufacturing of semi-crystalline thermoplastics utilizing the radical-mediated ring-opening photopolymerization of seven- and eight-membered cyclic allylic sulfides. Photopolymerization of resins formulations incorporating seven- and eight-membered cyclic allylic sulfides and crystallization of the resultant (co)polymers were examined using Fourier transform infrared (FTIR) spectroscopy, photorheology, and isothermal photo-differential scanning calorimetry (photoDSC). The formulated resins were found to polymerize and subsequently crystallize rapidly upon irradiation at ambient conditions. The mechanical properties of stereolithographically-printed copolymers approached the bulk copolymer mechanical properties, demonstrating unusually strong interlayer adhesion atypical of layerwise, stereolithographic printing of semi-crystalline polymers. Finally, high-quality, recyclable,

semi-crystalline thermoplastic parts were printed and melted down, demonstrating the potential for these semi-crystalline materials to provide a path for improved sustainability of polymeric parts produced via SLA.

## 3.2 Introduction

Polymer processing approaches that employ *in situ* polymerization, such as the fabrication of fiber-reinforced polymer composites,[1,2] the photocure of dental restorative materials,[3,4] and the application of spray foam insulation,[5,6] predominantly utilize thermosetting resins which, upon polymerization, afford cross-linked polymer networks. Nevertheless, *in situ* thermoplastic polymerization has become well-accepted in several areas, including the anionic ring opening polymerization of caprolactam in thermoplastic resin transfer molding[7–9] and the free radical polymerization of methyl methacrylate in bone cements.[10,11] One area where *in situ* thermoplastic polymerization holds significant promise is in stereolithographic additive manufacturing (SLA, also known as vat photopolymerization), a common approach for the three-dimensional (3D) printing of polymers based on the patterned photopolymerization of liquid resins, owing to the particular set of physical properties offered by these uncross-linked materials.

In comparison to other additive manufacturing techniques involving extrusion- or powder-based processing techniques, SLA is often regarded as having a superior combination of print quality, print speed, and cost.[12] Utilizing a patterned light source in combination with photopolymerizable resin formulations that strongly absorb at the irradiation wavelength, SLA generates cross-linked, thermoset parts in a layerwise fashion through patterned photocuring of cross-sectional slices. Recent developments in continuous additive manufacturing,[13,14] and volumetric 3D printing[15–17] bypass the

conventional, periodic SLA process to greatly increase print speeds and expand 3D printing applications.[18] Thermoset polymers used in SLA printing are typically limited to resins formulated with multifunctional (meth)acrylates and epoxides which are relatively inexpensive and exhibit high polymerization rates and long shelf lives. Importantly, the rapid mechanical integrity development provided by cross-linking[19] ensures an abrupt distinction between the solidified part and the liquid resin and thus enables prompt repositioning of the stage upon photopolymerization without build failure. Nevertheless, the resultant polymer networks are often brittle[20] and are incapable of being remolded, reprocessed, or recycled, whereas thermoplastics offer the potential for superior mechanical properties and post-fabrication reprocessing.

Several recent studies have examined SLA-based additive manufacturing to afford thermoplastic parts. Long and coworkers demonstrated the ability the use SLA to produce thermoplastic polyimides through the post-print thermal imidization of covalently- or ionically-cross-linked precursor parts, introducing large volumetric shrinkage.[21,22] Deng et. al employed SLA to directly fabricate thermoplastic parts *via* the radical-mediated chain growth photopolymerization of 4-acryloylmorpholine, an acrylate monomer that yields an amorphous polymer with a high glass transition temperature ($T_g$) above the print temperature.[19] As noted by the authors, this process necessitated control over the polymerization and polymer dissolution rates owing to the solubility of the amorphous, uncross-linked polymer in the liquid monomer. This requirement could be precluded by employing a reaction system that affords a semi-crystalline thermoplastic upon photopolymerization, as has been realized with radical-mediated step-growth thiol–ene systems.

Thiol-ene chemistry has many advantages for the *in situ* processing of SLA additive manufacturing including rapid polymerization rates and high reaction specificity and yield.[23] Sycks *et al.* described semicrystalline thiol–ene polymers from photopolymerizable formulations incorporating alkyl dithiol and spiroacetal-based divinyl monomers, and demonstrated the suitability of these formulations for SLA.[24,25] Bowman and coworkers similarly employed photopolymerizable resins formulated from stoichiometric mixtures of dithiol- and diene-based monomers to produce linear semi-crystalline thiol–ene polymers modeled after poly(ethylene terephthalate) and 3D print a variety of geometries.[26,27] Although these systems did rapidly yield tough, semicrystalline thermoplastics via photopolymerization, a large discrepancy in the mechanical properties between bulk samples those printed by SLA was observed, attributable to poor interlayer adhesion in the printed parts. Consequently, the printing of structures with sufficient inter-layer integrity necessitated the incorporation of multi-functional, cross-linking thiols in the resin for mechanical enhancement. Whereas inter-layer adhesion can be readily attained with thermosetting resins owing to the presence of reactive, network-bound functional groups at the solid surface that remain available for reaction with the next photopolymerized layer,[28] thermoplastics lack reactive similar polymer-bound functional groups, and establishing interlayer polymer entanglements is particularly challenging for semi-crystalline polymers that neither dissolve nor swell in their monomeric precursors.

Chain transfer agents are commonly used to control the molecular weight of uncross-linked polymers and provide access to complex polymer architectures.[29] Additionally, addition-fragmentation chain transfer has been employed in cross-linked polymers to provide a mechanism for network connectivity rearrangement and stress

relaxation.[30] Cyclic allylic sulfide monomers, first described and examined by Evans et al., undergo rapid, radical-mediated ring-opening polymerization to afford, when unsubstituted, semi-crystalline thermoplastic polymers (see Scheme 1).[31–33] The chain growth polymerization mechanism of cyclic allylic sulfide monomers proceeds *via* an allyl sulfide-based addition-fragmentation reaction, retaining allyl sulfide groups throughout the polymer backbone which are then available to participate in further addition-fragmentation chain transfer events.[30] These cyclic allylic sulfides thus offer potential for the layerwise, stereolithographic fabrication of semi-crystalline thermoplastic parts with enhanced interlayer adhesion by enabling further addition-fragmentation chain transfer between polymer chains in adjacent layers. Here, using seven- and eight-membered cyclic monomers, we examine the photopolymerization of ring-opening, cyclic allylic sulfides and their utility for rapid, stereolithographic additive manufacturing of semi-crystalline thermoplastic parts.

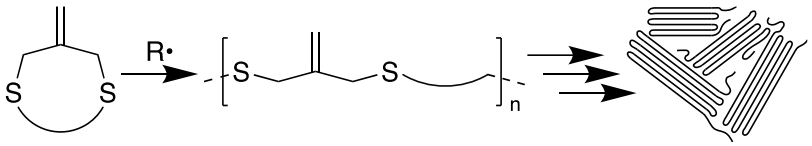


***Scheme 3.1 The radical-mediated ring opening polymerization of unsubstituted cyclic allyl sulfide monomers yields semicrystalline polymers.***

## 3.3 Experimental

### *3.3.1 Materials*

Photopolymerizable resins were formulated using a mixture of synthesized cyclic allylic sulfide monomers and 0.5 wt% bis(2,4,6-trimethylbenzoyl)-phenylphosphineoxide (Irgacure 819, Ciba Specialty Chemicals Inc., Basel, Switzerland) as a violet-active photoinitiator. For stereolithographic printing, 0.1 wt% of Sudan I (Sigma-Aldrich, St. Louis, MO) was also added to the resin formulation as a violet-active photoabsorber to curtail cure-through.[34] All cyclic allylic sulfides were synthesized as described below *via* a single step ring-closing reaction between 3-chloro-2-(chloromethyl)-1-propene (Aaron Chemicals, San Diego, CA) and an alkyl dithiol. 1,2-Ethanedithiol (Sigma Aldrich) and 1,3-propanedithiol (Oakwood Chemical, Estill, SC) were sourced commercially and used as received while 1,2-propanedithiol and 1,3-butanedithiol were synthesized as described below. Carbon disulfide, sodium hydroxide, and potassium hydroxide were obtained from Merck (Bayswater, Australia) and all other reagents were obtained from Sigma Aldrich.

### *3.3.2 Methods*

#### *3.3.2.1 Calorimetry*

Temperature-ramping differential scanning calorimetry (DSC) was performed using a Perkin Elmer DSC 8500 equipped with an intracooler. Polymer samples (approximately 3 mg) were cut from sheets photopolymerized between glass microscope slides using 405 nm light at 10 mW/cm$^2$ for 10 minutes. Samples were subject to a temperature ramp from -50°C to 150°C at 10°C/min under flowing nitrogen gas.

Isothermal photocalorimetry was performed by using the Perkin Elmer DSC 8500 equipped with a photocalorimeter accessory. Light from a Lumen Dynamics Omnicure

2000 mercury arc lamp equipped with a 400-500 nm band pass filter was directed through a bifurcated liquid light guide to irradiate both sample and reference pans *via* quartz windows. The thermal imbalance between the sample and reference pans was corrected by repeating the irradiation of the cured pans in a second run and subtracting the data from the first run. The irradiation intensity was measured by measuring the heat flow increase under irradiation of a graphite disk and dividing the heat flow by the known surface area of the disk. Resin samples were irradiated *in situ* with 405 nm light at 10 mW/cm$^2$ and at 25°C under flowing nitrogen.

#### *3.3.2.2 Fourier tranfrom infrared (FTIR) spectroscopy*

Resin formulations were placed between polished NaCl windows without spacers. Samples were placed in a Thermo Scientific Nicolet 6700 FTIR spectrometer equipped with a horizontal transmission accessory.[35] Samples were irradiated using a 405 nm collimated, light-emitting diode source (Thorlabs M405LP1-C1) with a current-adjustable LED driver (Thorlabs LEDD1B) to control light intensity. Intensities were measured using an International Light IL1400A radiometer equipped with a GaAsP detector (model SEL005), a 10× attenuation neutral density filter (model QNDS1), and a quartz diffuser (model W). Spectra were collected from 650 to 4000 cm$^{-1}$ at a rate of approximately 2 per second.

#### *3.3.2.3 Rheometry*

Rheometry data was collected using an Anton Paar Physica rheometer equipped with a parallel plate photocuring accessory. The top plate was 15 mm diameter and the bottom plate was made of quartz. A liquid light guide below the quartz plate allowed for light from an Omnicure 2000 lamp with a 400-500 nm wavelength filter which was calibrated to emit 10 mW/cm$^2$ irradiation intensity using an International Light IL 1400A radiometer. Resin was pipetted onto the bottom plate and the top plate moved down to a gap of 0.100 mm. Tests were conducted by applying a 1% strain and 1 Hz frequency. After 30 seconds collecting data in dark conditions, the shutter was opened to allow resin irradiation.

#### *3.3.2.4 Stereolithography*

Stereolithographic 3D printing of samples was performed with a Flashforge Hunter DLP printer using a 25 wt% CAS7/75 wt% CAS8 resin formulated with both Irgacure 819 photoinitiator and Sudan I photoabsorber. Layers were irradiated using 405 nm light at 3.5 mW/cm$^2$ for 50 seconds to produce mechanically robust 50 µm layers.

#### *3.3.2.5 Mechanical Testing*

Molds for bulk samples were prepared using 0.50 mm thick silicone sheet cut with an ASTM D1708 dog bone cutting die (38 mm × 15 mm overall, 22 mm grip length, 12 mm × 5 mm in the gauge region). To fabricate bulk dog bone samples, silicone molds were sandwiched between glass microscope slides and injected with formulated resin which was

then cured under 3.5 mW/cm$^2$ LED light (405 nm) for 10 minutes. Printed ASTM D1708 dog bone samples were designed in SolidWorks 2019 (Dassault Systèmes) and imported to Chitubox (CBD-Tech) as an .STL file. All printed objects were arranged and sliced and sent to FlashDLPrint (Flashforge) as an .SVGX file to be printed on a Flashforge Hunter DLP Printer. Printed samples were removed from the build head, lightly wiped with a paper towel to remove excess monomer on the surface, and support structures were removed using a razor blade. Finally, printed samples were post cured with 405 nm light for 40 minutes on both sides concurrently (20 mW/cm$^2$). All samples were stored in the dark overnight before loading them into a uniaxial tensile tester (Instron ElectroPuls E3000) equipped with a 3 kN load cell. Tensile tests were performed at a rate of 1 mm/min under ambient conditions.

#### *3.3.2.6 X-ray Diffraction*

X-ray samples were produced by photopolymerization of resin between glass slides cut to a size of approximately 20 mm × 20 mm with 500 µm silicone spacers. X-ray diffractograms were collected on a Bruker D8 Advance A25 X-ray diffractometer with Cu Kα radiation (1.54056λ, 40 kV, 40 mA) equipped with a Lynx Eye XE-T detector. 2θ scans were collected from 5° - 40° at a step size of 0.05° and 1.5 s per time step.

#### *3.3.2.7 Polarized Microscopy*

Polarized microscopy was conducted using an Olympus PMG-3 optical microscope during the photopolymerization of CAS7 formulated with 0.5 wt% Irgacure 819,

sandwiched between glass slides separated by 19 µm shims, and irradiated with 405 nm LED at 3 mW/cm$^2$.

### *3.3.3 Synthesis*

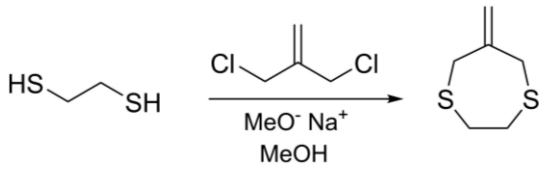


CAS7

***Scheme 3.2 Synthesis of 6-methylene-1,4-dithiepane (CAS7)***

#### *3.3.3.1 6-methylene-1,4-dithiepane (CAS7)*

Using a modified literature procedure[34], 3-chloro-2-(chloromethyl)-1-propene (3.94 g, 31.5 mmol) and 1,2-ethanedithiol (2.97 g, 31.5 mmol) were each made up into separate 60 mL solutions with methanol. These two solutions were then added simultaneously and separately by syringe pump at a rate of 4 mL/h to a refluxing solution of sodium metal (1.52 g, 66.2 mmol) in methanol (200 mL) under argon protection. Upon the completion of the addition, the reaction mixture remained under reflux for 4 hours, then the mixture was filtered to remove the precipitate formed during the reaction. The solvent was then evaporated, 200 mL water was added, and the mix extracted twice with 50 mL diethyl ether. The ether extracts were pooled, dried with sodium sulfate and the ether evaporated, affording 3.5 g of pale amber liquid. This material was then bulb-to-bulb distilled (55°C, 0.2 mmHg) to yield a clear oil (2.4 g, 16.4 mmol, 52%). $^1$H NMR (400 MHz, $CDCl_3$, 25°C) δ 3.01 (s, 4H, SC**H**$_2$C**H**$_2$S), 3.64 (s, 4H, =CC**H**$_2$S), 4.84 ( pent., *J* = 1.1 Hz, 2H, =C**H**$_2$) ppm.

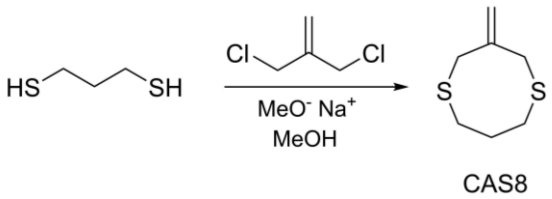


***Scheme 3.3 Synthesis of 3-methylene,1-4-dithiacyclooctane (CAS8)***

***3.3.3.2 3-methylene,1-4-dithiacyclooctane (CAS8)***

Using the same synthetic procedure employed for CAS7, methanolic solutions of 3-chloro-2-(chloromethyl)-1-propene (3.94 g 31.5 mmol) and 1,3-propanedithiol (3.40 g, 31.5 mmol) were added to a refluxing solution of sodium metal (1.52 g, 66.2 mmol) in methanol (200 mL) under argon protection. After addition and an additional 4 hours under reflux, the mixture was filtered, solvent evaporated, water added, and extracted with ether. The ether extracts were pooled, dried and the ether evaporated, affording 4.02 g of pale amber liquid. A final bulb-to-bulb distillation (65°C, 0.2 mmHg) yielded a clear oil (3.0 g, 18.7 mmol, 59%). $^{1}$H NMR (400 MHz, $CDCl_3$, 25°C) δ 1.79 (m, *J* = 6.2 Hz, 2H, $SCH_2C\mathbf{H}_2CH_2S$), 2.88 (t, *J* = 6 Hz, 4H, $SC\mathbf{H}_2CH_2C\mathbf{H}_2S$), 3.25 (s, 4H, $=CC\mathbf{H}_2S$), 5.19 (s, 2H, $=C\mathbf{H}_2$) ppm.

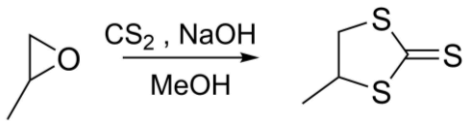


***Scheme 3.4 Synthesis of 4-methyl-1,3-dithiacyclopentan-2-thione***

### *3.3.3.3 4-methyl-1,3-dithiacyclopentan-2-thione*

Propylene oxide (10 g, 172 mmol) was added dropwise to a solution of potassium hydroxide (20 g, 356 mmol) and carbon disulfide (36 g, 473 mmol) in 70 mL ethanol while the temperature was maintained below ~ 40℃. The reaction was stirred for four hours and subsequently extracted with chloroform. Solvent was removed by under reduced pressure, producing a yellow oil which was further bulb-to-bulb distilled to yield a very pale yellow oil (7.7 g, 51 mmol, 30%). $^{1}$H NMR (400 MHz, $CDCl_3$, 25℃) δ 1.63 (d, *J* = 6.8 Hz, 3H, C**H**$_3$), 3.67 (dd, *J* = 11.9 Hz, *J* = 7.6 Hz, 1H, C**H**H ), 4.0 (dd, *J* = 11.9 Hz, *J* = 5.4 Hz, 1H, CH**H**), 4.45 – 4.6 (m, 1H, C**H**$CH_3$) ppm.

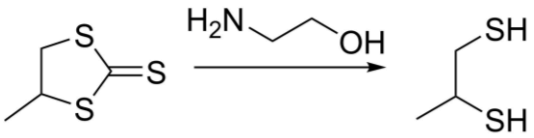


***Scheme 3.5 Synthesis of 1,2-propanedithiol***

### *3.3.3.4 1,2-propanedithiol*

4-Methyl-1,3-dithiacyclopentan-2-thione (4 g, 26.7 mmol) and ethanolamine (1.63 g, 26.7 mmol) were added together in a round-bottomed flask set up for vacuum distillation. The mixture was stirred at 100°C for 15 min with the reaction open to the atmosphere. A

vacuum was then applied and a pale yellow distillate was obtained. The oil was redistilled to give a clear oil (1.1 g, 10.2 mmol, 38%). $^{1}$H NMR (400 MHz, $CDCl_3$, 25°C) δ 1.37 (d, *J* = 6.7 Hz, 3H, C**H**$_3$) 1.75 – 1.95 (m, 2H, $CH_2$S**H**, CHS**H**), 2.6 – 2.7 (m, 2H, C**H**$_2$SH), 3.0 – 3.15 (m, 1H, C**H**SH) ppm.

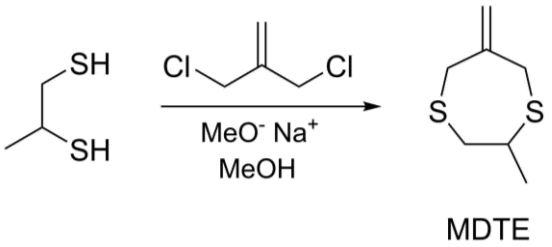


MDTE

***Scheme 3.6 Synthesis of 2-methyl-6-methylene-1,4-dithiepane (MDTE)***

***3.3.3.5 2-methyl-6-methylene-1,4-dithiepane (MDTE)***

Using the same synthetic procedure employed previously, methanolic solutions of 3-chloro-2-(chloromethyl)-1-propene (3.28 g, 26.2 mmol) and 1,2-propandithiol (2.84 g, 26.2 mmol) were added to a refluxing solution of sodium metal (1.52 g, 66.2 mmol) in methanol (200 mL) under argon protection. After addition and an additional 4 hours under reflux, the mixture was filtered, solvent evaporated, water added, and extracted with ether. The ether extracts were pooled, dried and the ether evaporated. This material was then bulb-to-bulb distilled (50°C, 0.2 mmHg) to yield a clear oil (2.2 g, 13.7 mmol, 52%). $^{1}$H NMR (400 MHz, $CDCl_3$, 25°C) δ 1.33 (d, *J* = 7.0 Hz, 3H, C**H**$_3$), 2.79 (dd, *J* = 14.5 Hz, *J* = 9.3 Hz, 1H, C**H**H), 2.97 – 3.28 (m, 2H, CH**H** and C**H**), 3.49 (dd, *J* = 15.7 Hz, *J* = 10.2 Hz, 2H, allylic C**H**$_2$), 3.79 (d, *J* = 15.1 Hz, 2H, allylic C**H**$_2$), 4.83 (d, *J* = 8.9 Hz, 2H, =C**H**$_2$) ppm.

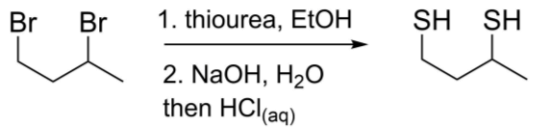


***Scheme 3.7 Synthesis of 1,3-butanedithiol***

***3.3.3.6 1,3-butanedithiol***

1,3-Dibromobutane (10 g, 46.5 mmol) and thiourea (7.4 g, 97 mmol) were added together into 60 mL of ethanol and refluxed for 6 hours. During this time the mixture became a clear homogenous solution. The solvent was then rotary evaporated to give a clear sticky residue. To this residue was added a solution of aqueous sodium hydroxide (23 g in 120 mL) and the mixture refluxed for a further 6 hours, cooled, and slowly acidified with concentrated HCl (ca. 50 mL). The solution was extracted with ether, the extracts dried and evaporated to give a light yellow oil which was further bulb-to-bulb distilled to give a clear, malodorous oil (2.02 g, 16.5 mmol, 35%). $^{1}$H NMR (400 MHz, $CDCl_3$, 25°C) δ 1.37 (d, *J* = 6.8 Hz, 3H, C**H**$_3$), 1.45 (d, *J* = 7.0 Hz, 1H, $CH_2S$**H**), 1.72 – 1.94 (m, 2H, $CH(CH_3)C$**H**$_2CH_2SH$), 2.60 – 2.72 (m, 2H, C**H**$_2$SH), 3.09 (m, 1H, SHC**H**($CH_3$)) ppm.

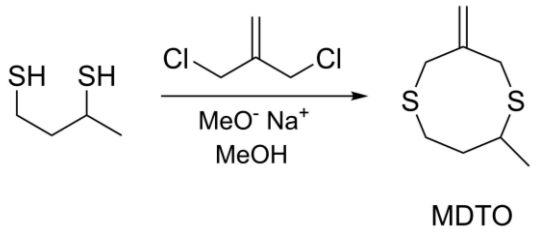


***Scheme 3.8 Synthesis of 6-methyl-3- methylene-1,5-dithiacyclooctane (MDTO)***

***3.3.3.7 6-methyl-3-methylene-1,5-dithiacyclooctane (MDTO)***

Using the same synthetic procedure employed previously, methanolic solutions of 3-chloro-2-(chloromethyl)-1-propene (2.07 g 16.6 mmol) and 1,3-butanedithiol (2.02 g, 16.6 mmol) were added to a refluxing solution of sodium metal (1.0 g, 44.2 mmol) in methanol (200 mL) under argon protection. After addition and an additional 4 hours under reflux, the mixture was filtered, solvent evaporated, water added, and extracted with ether. The ether extracts were pooled, dried with sodium sulfate and the ether evaporated. This material was then bulb-to-bulb distilled (50°C, 0.2 mmHg) to yield a clear oil (1.34 g, 7.7 mmol, 46%). $^{1}$H NMR (400 MHz, $CDCl_3$, 25°C) δ 1.33 (d, *J* = 7.1 Hz, 3H, C**H**$_3$), 1.55 – 1.9 (m, 2H, C**H**$_2$), 2.8 – 3.4 (m, 7H, C**H**$_2$ S, C**H**S), 5.16 (d, *J* = 6.5 Hz, *J* = 1.2 Hz, 2H, =C**H**$_2$) ppm.

## 3.4 Results and Discussion

Ring opening polymerization kinetics depend on the ring strain of the monomer to promote ring cleavage, the stability of the propagating species, and the rate of the accompanying isomerization process to produce the more energetically favored product and a propagating center. Cyclic allylic sulfide monomers contain C-S bonds that readily fragment upon radical addition to the allylic C=C bond, resulting in ring opening and

yielding a newly formed allyl sulfide functional group and a sulfur-centered propagating radical. In this study, seven- and eight-membered cyclic allylic sulfide monomers, 6-methylene-1,4-dithiepane (CAS7, Figure 3.1) and 3-methylene-1,4-dithiacyclooctane (CAS8, Figure 3.1), respectively, were utilized in resin formulations. Whereas both monomers afford semi-crystalline thermoplastics upon polymerization[31], the differing monomer ring sizes should yield distinct ring strains.[36]

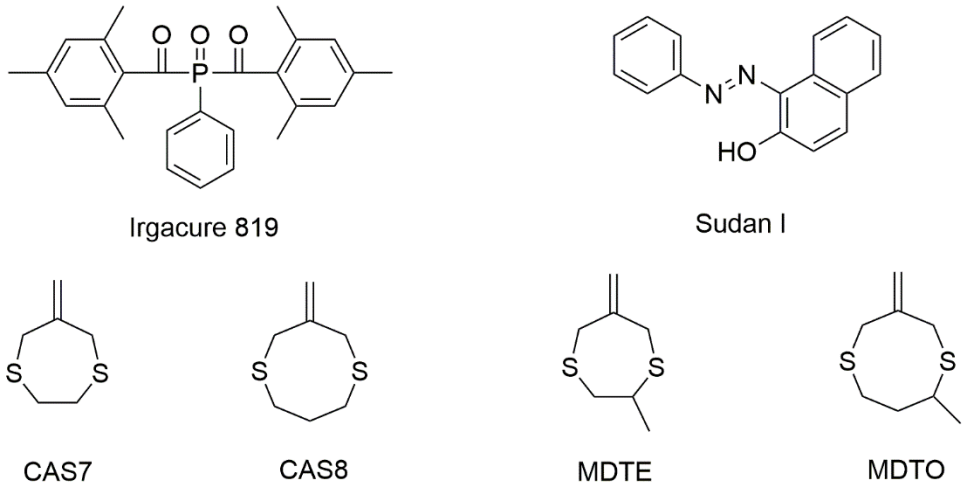


***Figure 3.1 Chemical structures of the photoinitiator (Irgacure 819), photoabsorber (Sudan I) and monomers used in this study.***

The photopolymerization kinetics of CAS7, CAS8, and their blends were initially examined by isothermal photoDSC. Importantly, and in distinct contrast to most polymer systems, the chemical bonds found in the cyclic allylic sulfide precursor monomers are conserved upon ring opening. Polymerization instead proceeds via a bond connectivity rearrangement from a cyclic to a linear structure; thus, any observed exotherm must be in part attributable to the strain release by the ring opening. As shown in Figure 3.2a, heat was rapidly evolved upon sample irradiation; however, rather than the generation of a single exothermic peak, either a shoulder or two distinct peaks were observed in the

isotherm traces for these resin formulations. Shoulders in isothermal photoDSC traces, while not ubiquitous, are not uncommon and have been observed in the of chain growth photopolymerization of resins formulated exclusively using a single vinyl monomer[37] and vinyl monomer blends.[38] For reactions yielding amorphous polymers, the occurrence of photopolymerization exotherm shoulders has been interpreted in several ways,[39–43] including that they are a consequence of initiation efficiency and the rate constants for propagation and termination changing throughout the course of the reaction to afford complex, conversion-dependent reaction kinetics. Interpretation of the photoDSC traces generated upon irradiation of unsubstituted cyclic allyl sulfide monomer formulations has an additional complexity where both the exothermic ring opening polymerization reaction and the enthalpy of fusion attributable to the crystallization of the generated polymer must be considered. As polymerization of CAS7, CAS8, and their blends is presumed to afford semicrystalline polymers,[31] the shoulders or double peaks observed in the photoDSC traces of these resins (Figure 3.2a) is consistent with initial exothermic polymerization and subsequent crystallization processes. Notably, all resins formulated from CAS7 and CAS8 became translucent upon polymerization. The occurrence of the shoulder or second peak in the photoDSC traces in Figure 3.2a depends upon the monomer ratio used in each resin formulation; whereas the shoulders in the traces for CAS 7 and CAS8 are relatively subtle, suggesting rapid post-polymerization crystallization, each of the isothermal traces yielded by monomer blend photopolymerization display distinct a clear second peak that, for the 50:50 monomer blend, occurs several minutes after the first peak, indicative of an initial, rapid photopolymerization followed by a relatively slow polymer crystallization.

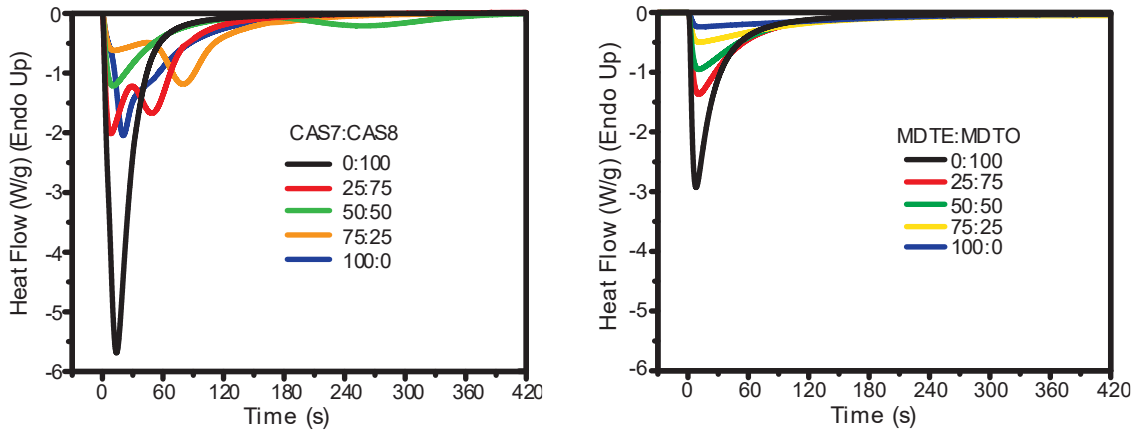


a) b)

***Figure 3.2 Isothermal photoDSC traces for cyclic allyl sulfide resins (as shown) formulated with 0.5 wt% Irgacure 819 and irradiated with 405 nm light at 10 mW/cm2 and at 25°C. a) Heat flow versus time for the photopolymerization of resins formulated from CAS7 and CAS8 upon 405 nm irradiation at t=0. b) Heat flow versus time for the photopolymerization of resins formulated from MDTE and MDTO upon 405 nm irradiation at t=0.***

To estimate the contributions of polymerization and crystallization to the isothermal photoDSC traces for resins formulated from CAS7 and CAS8, equivalent isothermal photoDSC experiments were performed using the methyl-substituted, seven- and eight- membered cyclic allyl sulfide monomers MDTE and MDTO, respectively, that yield amorphous polymers. Thus, although the heat evolved by the ring opening polymerization reaction of these monomers should closely match that of their unsubstituted analogues, their use circumvents the complicating factor of post-polymerization crystallization. As shown in Figure 3.2b, no shoulder or second peak is observed in the isothermal photoDSC traces of MDTE, MDTO, and their blends for the compositions examined, indicating that the additional features and increased maximum heat evolution rate observed in the photoDSC traces for CAS7/CAS8-based resins were indeed a result of post-polymerization crystallization. Upon irradiation, the maximum heat flow for MDTO is several times that for MDTE, attributable to the greater ring strain of the eight-membered

cyclic allyl sulfide relative to that of the seven-membered cyclic monomer,[36] while resins formulated from blends of the two monomers yielded intermediate heat flows that approximately scale with the expected contribution from each monomer in the resin formulation.

The total heats released upon irradiation for both the semicrystalline polymer yielding CAS7/CAS8 resin formulations and the MDTE/MDTO resins that afford amorphous polymers are tabulated in Table 3.1. In addition to its rapid reaction rate, the photopolymerization of MDTO evolves approximately three times the heat released during the photopolymerization of MDTE owing to the greater ring strain of the eight-membered cyclic monomer relative to the seven-membered one. Table 3.1 also illustrates that the heats evolved upon photopolymerization of the methyl-substituted MDTE/MDTO-based resins are substantially lower than those released during the photopolymerization of equivalent, unsubstituted CAS7/CAS8-based formulations. Assuming that the ring strains for unsubstituted and methyl-substituted cyclic allyl sulfide monomers with equivalent ring sizes are essentially equal and that all polymerizations examined proceeded to completion, the differences in the apparent heats of polymerization between the semi-crystalline, CAS7/CAS8 resins and their amorphous MDTE/MDTO-based equivalents represent the enthalpies of fusion for the polymerized CAS7/CAS8 formulations. As shown in Table 3.1, the calculated enthalpies of fusion are highest for the two homopolymers and lowest for the 50:50 copolymer, attributable to an expected reduced crystallinity for the copolymers relative to the homopolymers.

***Table 3.1 Summary of CAS7:CAS8 resin photocalorimetry.***

| Semi-crystalline resin formulation | | Amorphous resin formulation | | Enthalpy of fusion ($\Delta H_{p,\ semicryst.}$ - $\Delta H_{p,\ amorph.}$) (J/g) |
|---|---|---|---|---|
| CAS7:CAS8 (wt%) | $\Delta H_{p,\ semicryst.}$ (J/g) | MDTE:MDTO (wt%) | $\Delta H_{p,\ amorph.}$ (J/g) | |
| 100:0 | 135 ± 5 | 100:0 | 33 ± 3 | 102 ± 6 |
| 75:25 | 113 ± 4 | 75:25 | 54.1 ± 1.7 | 59 ± 5 |
| 50:50 | 93.3 ± 1.1 | 50:50 | 68.6 ± 1.6 | 24.7 ± 1.9 |
| 25:75 | 146 ± 5 | 25:75 | 78.7 ± 1.8 | 68 ± 5 |
| 0:100 | 175 ± 3 | 0:100 | 100.1 ± 0.7 | 75 ± 3 |

Crystallization upon photopolymerization of unsubstituted cyclic allyl sulfide monomers was confirmed directly through observation of crystallite formation by polarized optical microscopy. In semicrystalline materials, formed spherulites display birefringence giving them a characteristic, Maltese cross appearance under polarized light. In Figure 3.3a, micrographs taken at representative time points demonstrate spherulite-like crystallite growth during the irradiation of a CAS7 resin with 405 nm light at 3 mW/cm$^2$. Upon irradiation, crystallites become apparent within fifteen seconds and which subsequently coalesce after approximately 30 seconds, again consistent with initial photopolymerization and subsequent crystallization processes.

To directly determine the contribution of polymer crystallization to the photoDSC exotherms observed for the unsubstituted cyclic allyl sulfide-based resin formulations, temperature-ramping DSC was performed on photopolymerized samples. An endothermic

melting peak was observed for all samples of photopolymerized CAS7, CAS8, and their blends in the single heating DSC temperature scans (see Figure 3.3b), further demonstrating the semicrystallinity of these materials. In contrast, no melting peak was observed for photopolymerized samples of the methyl-substituted MDTE and MDTO formulations, confirming their amorphous nature. Whereas the homopolymers of CAS7 and CAS8 exhibit the highest melting points and enthalpies of fusion (see Table 3.2), the 50:50 CAS7:CAS8 copolymer displayed the lowest melting point and enthalpy of fusion, indicative of relatively low crystallinity as commonly seen in statistical copolymers.[44] Notably, the enthalpies of fusion obtained directly by scanning DSC (Table 3.2) and those derived from the difference in the apparent heats of polymerization for semicrystalline systems and their amorphous analogues (Table 3.1) demonstrate the same trend, where the enthalpy of fusion is greatest for the semicrystalline homopolymers and, for the compositions examined, reaches a minimum for the 50:50 CAS7:CAS8 copolymer. The minor discrepancies in the enthalpy of fusion values obtained via these two approaches may arise from small differences in ring strain between the unsubstituted cyclic allyl sulfide monomers and their methyl-substituted analogues.

***Table 3.2 Thermal Properties of CAS7:CAS8 copolymers.***

| CAS7:CAS8 (wt%) | Melting point (°C) | Enthalpy of Fusion (J/g) |
|---|---|---|
| 100:0 | 116.4 ± 0.3 | 75.2 ± 1.4 |
| 75:25 | 78.9 ± 0.3 | 57 ± 2 |
| 50:50 | 59.9 ± 1.1 | 30.4 ± 1.3 |
| 25:75 | 71.9 ± 0.7 | 58 ± 1 |
| 0:100 | 90.8 ± 0.4 | 82.5 ± 1.7 |

The crystallinity of the cyclic allyl sulfide-based polymers was qualitatively examined by X-ray diffractometry (see Figure 3.3c). Supporting the results obtained by temperature-ramping DSC, the degree of crystallinity appears highest in the homopolymers and lowest in the 50:50 CAS7:CAS8 copolymer. Whereas the homopolymers display distinct diffractograms, exhibiting sharp peaks that remain apparent in the 25:75 and 75:25 CAS7:CAS8 copolymers, the peaks shown in the 50:50 copolymer diffractogram are broader and resemble those for the CAS7 homopolymer. No peaks were observed in the diffractograms for the methyl-substituted MDTE- and MDTO-based homopolymers, again confirming the amorphous character of these materials.

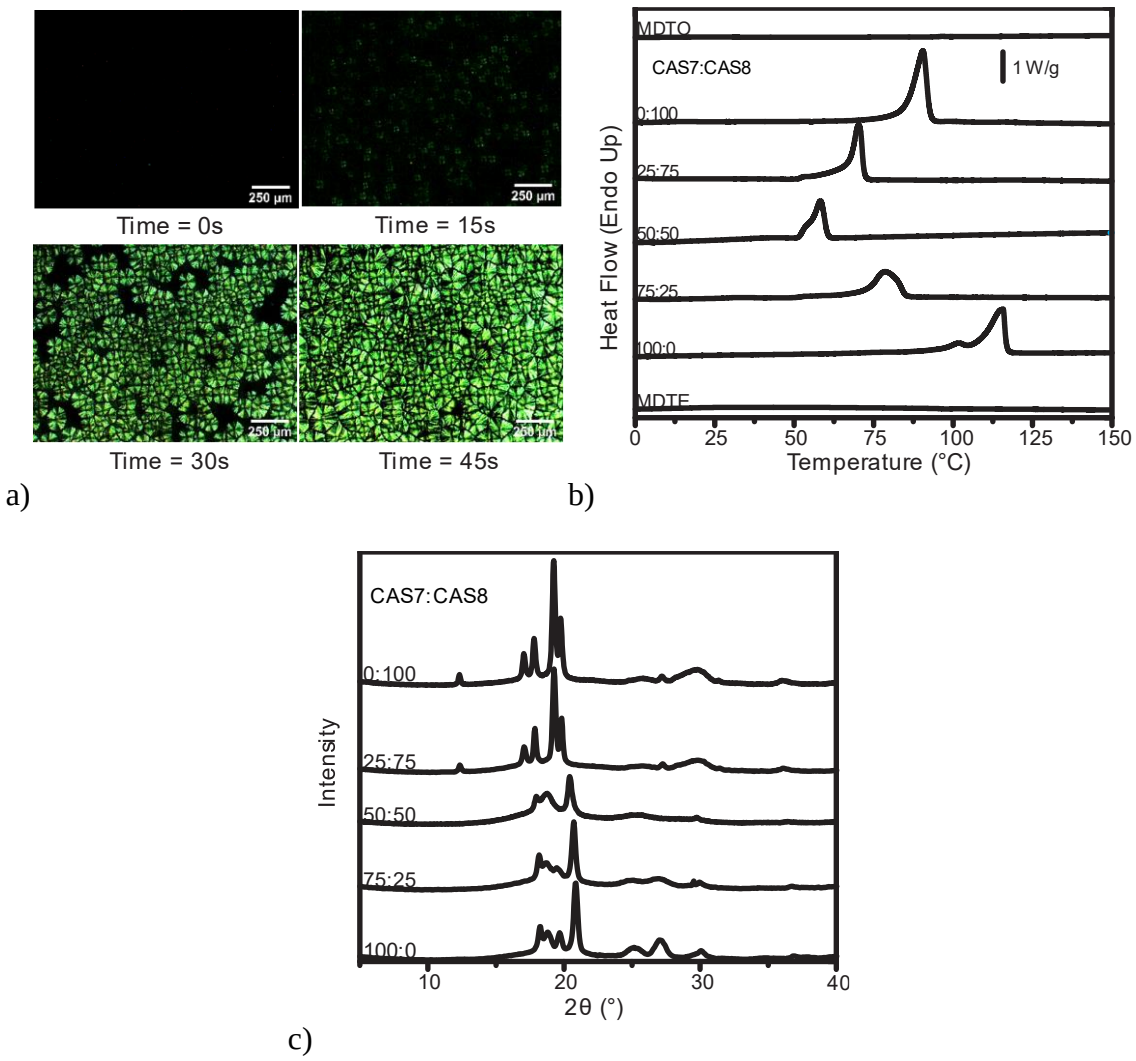


***Figure 3.3 Characterization of poly(cyclic allyl sulfide) crystallization. a) Representative time points of CAS7 crystallization under polarized optical microscopy. b) Temperature-ramping DSC traces for photopolymerized cyclic allyl sulfide (co)polymers (as shown). c) Qualitative X-ray diffractograms of photopolymerized cyclic allyl sulfide (co)polymers (as shown).***

The solubility of the CAS7- and CAS8-based semicrystalline polymers was limited in organic solvents at moderate temperatures. Whereas dissolution of these materials was not achieved using any common organic solvents at temperatures below the respective (co)polymer melting points, dissolution was achieved using high boiling point solvents such as *N*-methyl-2-pyrrolidone (NMP) and dimethylacetamide (DMAc) at raised temperatures (> 100°C). With the exception of the CAS7 (100:0) homopolymer, all

(co)polymers showed some degree of swelling above their melting point before full dissolution at temperatures 20-30℃ higher than their respective melting temperatures.

As the convolution of heat-evolving polymerization and crystallization processes complicates the monitoring the photopolymerization kinetics of these systems by photoDSC, the photopolymerization of cyclic allylic sulfide monomers and their blends was also monitored by Fourier transform infrared (FTIR) spectroscopy. Without the confounding crystallization and polymerization exotherms, photopolymerization conversion trajectories might be directly accessed from time-resolved FTIR spectra collected during irradiation. Nevertheless, characterizing the ring-opening polymerization of these monomers by FTIR spectroscopy presents a particular challenge owing to the bond conservation upon ring opening as noted above. Consequently, many of the infrared absorbance peaks for cyclic allylic sulfide monomers are similar to those of the resultant polymers. For example, peak area centered at 3074 $cm^{-1}$, attributable to the vinyl-CH stretch and often used to monitor functional group conversion during the polymerization of vinyl monomers by FTIR spectroscopy,[45] exhibits only a very small change upon polymerization for both CAS7 and CAS8. Nevertheless, several peaks either diminish or emerge in the FTIR spectra for both CAS7 and CAS8 upon photopolymerization. For example, an isolated peak in the CAS7 spectrum centered at 677 $cm^{-1}$ disappears as polymerization proceeds, enabling monomer conversion during photopolymerization to be readily monitored for the CAS7 homopolymer resin (Figure 3.4a). The CAS8 spectra do not present a similarly isolated peak; rather, the peaks centered at 839 and 1314 $cm^{-1}$ that disappear during photopolymerization are partially overlapped by emergent peaks centered at 830 and 1291 $cm^{-1}$, respectively (Figure 3.4b), necessitating peak deconvolution to

obtain monomer conversion. Notably, the extent of peak overlap in the spectra obtained for resins formulated from CAS7 and CAS8 blends precluded obtaining monomer conversion trajectories by deconvolution during the photopolymerization these mixed systems. The conversion trajectories shown in Figure 3.4c reveal that the photopolymerization of CAS8 proceeds more rapidly than that of CAS7, approaching full conversion within 1 and 3 minutes irradiation, respectively, confirming the relative photopolymerization rates observed by isothermal photoDSC.

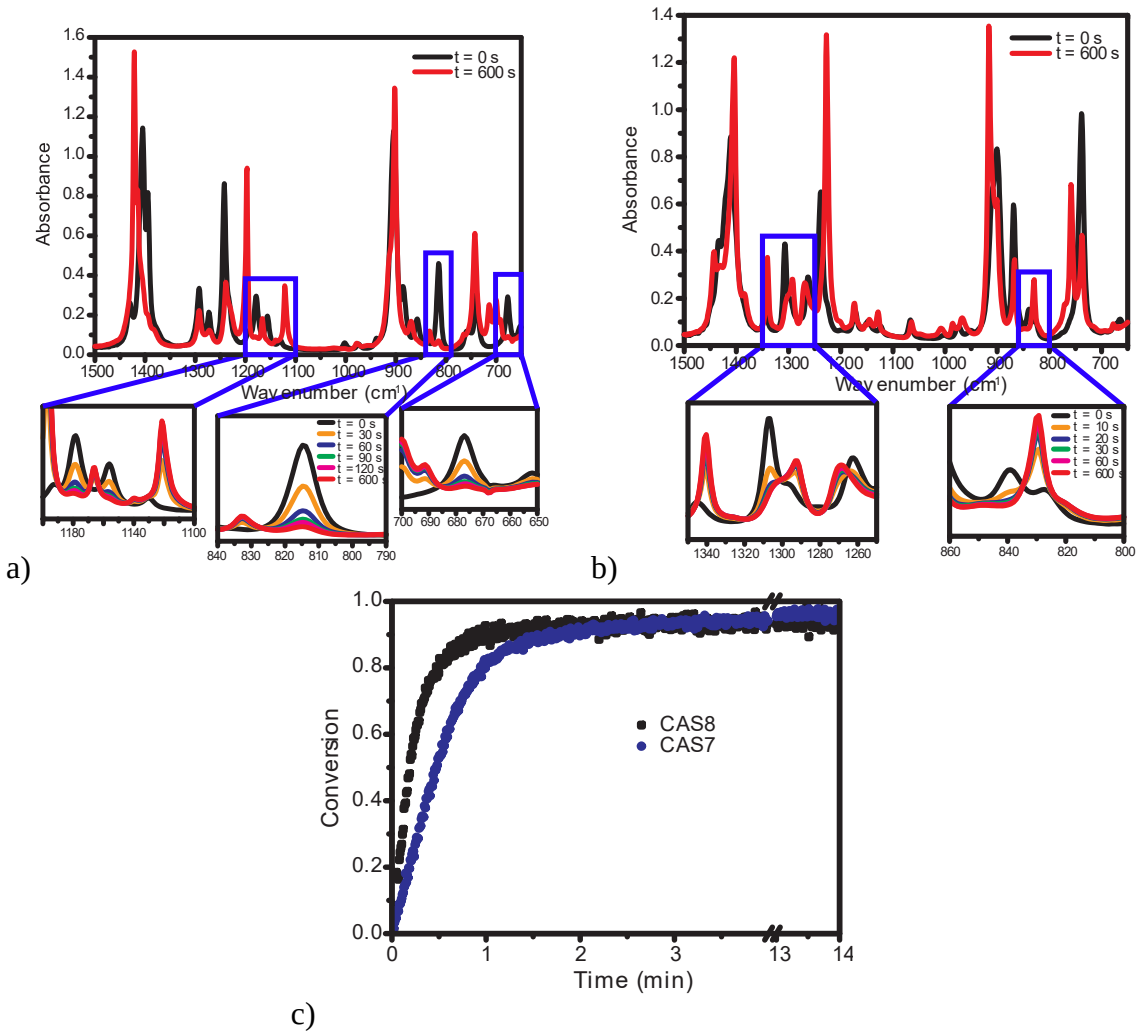


***Figure 3.4 FTIR spectra of a) CAS7 and b) CAS8 resins formulated with 0.5 wt% Irgacure 819 prior to irradiation (black) and after 10 min irradiation with 405 nm light at 10 mW/cm$^2$ (red). Magnified regions highlight peaks diminishing and emerging during irradiation at the time points indicated. c) Conversion trajectories of CAS7 and CAS8 resin formulations upon irradiation using the reaction conditions above.***

Stereolithographic additive manufacturing requires not only the rapid conversion of liquid resin to polymer but also that each layer has sufficiently solidified to ensure its mechanical integrity. The successful printing of non-crosslinked thermoplastics relies upon the polymerization process proceeding faster than the dissolution or diffusion of the polymer chains into the remaining liquid resin.[19] This necessitates rapidly producing sufficiently high molecular weight species or rapid crystallization to overcome the

diffusion rate of the polymer chains.[19] In order to assess the potential of CAS-based resins for stereolithographic printing, the modulus development during photopolymerization was monitored by photorheometry. Upon irradiation, CAS7 and CAS8 homopolymer resins rapidly polymerized and crystallized (see Figure 3.5a), as shown by the shear storage modulus (G′) increase of over 7 orders of magnitude within fifteen seconds. CAS8 demonstrated a more rapid G′ increase than CAS7, correlating well with the photopolymerization kinetics observed by isothermal photoDSC and FTIR spectroscopy. Copolymerization of CAS monomers yielded G′ curves with evident shoulders at an intermediate storage modulus (~$10^4$ Pa), again attributable to delayed polymer crystallization subsequent to the initial photopolymerization. Resin formulations exhibiting short post-polymerization crystallization delays enable facile stereolithographic thermoplastic additive manufacturing where the crystallization process is rate limiting for the part fabrication.

The influence of crystallization on the modulus development was further examined by monitoring G′ during the photopolymerization of methyl-substituted MDTE and MDTO cyclic allyl sulfide monomer resins. In contrast to the semicrystalline materials generated upon CAS7 and CAS8 polymerization, the G′ curves during MDTE and MDTO photopolymerization do not exhibit a shoulder and ultimately achieve moduli several order of magnitude lower than those of their semi-crystalline counterparts, confirming that the second storage modulus increase for CAS7- and CAS8-based formulations is attributable to post-polymerization crystallization rather than continued polymerization in these systems (Figure 3.5b).

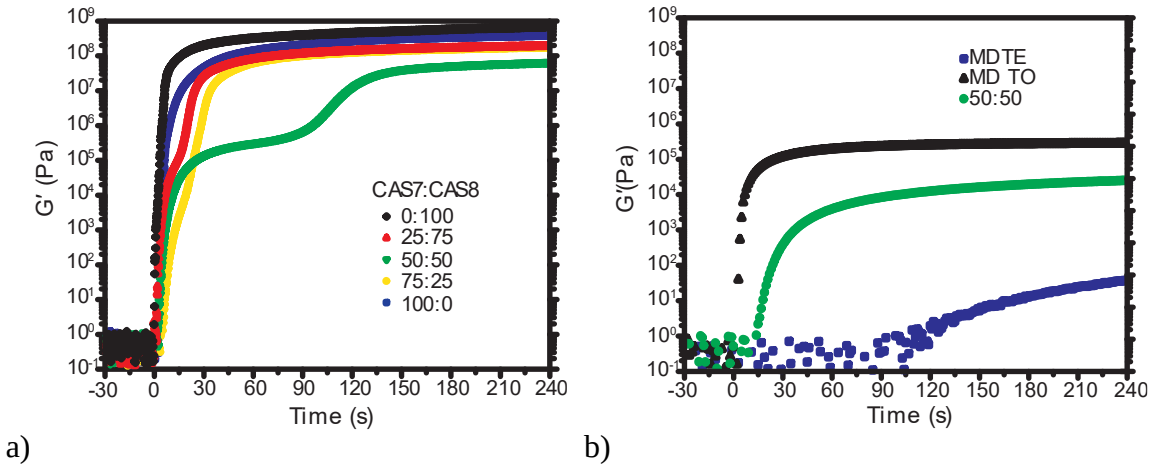


a) b)

***Figure 3.5 Shear storage modulus trajectories for a) unsubstituted CAS7- and CAS8-based resins, and b) methyl-substituted MDTE- and MDTO-based resins, formulated with 0.5 wt% Irgacure 819 and irradiated with 405 nm light at 10 mW/cm$^2$.***

During stereolithography, the exposure time of each layer is minimized to reduce the total print time. After the exposure time has elapsed, the layer is expected to be mechanically robust to continue the printing process without failures. The crystallization of non-crosslinked CAS needs to proceed so the polymers form rigid solid layers before the next layer can begin printing. Using photorheology, the CAS resins are exposed to an array of exposure times to determine the modulus development after irradiation ceases. When the exposure time is reduced to a short pulse of light instead of continuous irradiation, the subsequent crystallization behavior differs. An irradiation time over 90 secs in 25:75 resin leads to modulus evolution with similar behavior to continuous irradiation over 10 minutes. However, at shorter irradiation times of 30 seconds the rate of modulus evolution decreases after irradiation ceases (Figure 3.6a). The 25:75 polymer after 15 secs of irradiation shows a prolonged plateau in modulus before beginning to increase after three minutes in the dark with longer irradiation times like 25 secs displaying a shorter plateau and a quicker increase in modulus in the dark. This dark crystallization likely

results from dark polymerization that slowly increase the molecular weight of the polymer after irradiation slowly causing crystallization to occur. Crystallization is partially driven by molecular weight so a shorter irradiation time causing lower molecular weight polymers and no crystallization is plausible. If the polymers were soluble, they could be measured using gel permeation chromatography and the molecular weights could be tested but the poor solubility didn't allow for reliable molecular weight measurements.

The 50:50 copolymer crystallizes slower than 25:75 so the shorter exposure times were repeated with the slower crystallizing resins. The 50:50 resins display the same pattern with the exposure times being increased to see the desired effect and still the length of the modulus plateau differs with exposure times of 45-60 secs crystallizing after at least four minutes in the dark post-irradiation (see Figure 3.6b). The benefit of dark crystallization is that the resin can be irradiated for shorter periods while still realizing the rigid semi-crystalline polymer at the end. Longer irradiation times lead to poor resolution as light is scattered and transmitted deeper into the resin bath than is warranted. Using shorter exposure times but longer waiting periods after exposure ends may allow for high resolution structures to be printed, albeit at slower printing rates.

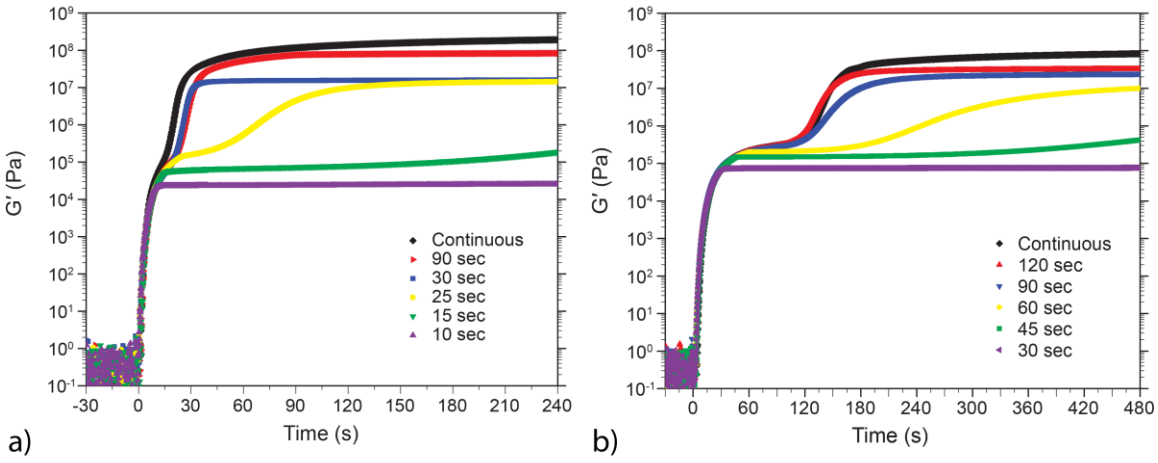


***Figure 3.6 Shear modulus trajectories with varying exposure times for a) 25:75 CAS7:CAS8 copolymerization and b) 50:50 CAS7:CAS8 copolymerization.***

Random copolymers tend to have glass transition temperatures ($T_g$) that are a function of composition with the proposed relationship being based on the additivity of basic thermophysical properties. The Fox equation proposes that the copolymer $T_g$ is simply a function of the $T_g$ of each homopolymer individually and lies in between the two homopolymer $T_g$'s at a ratio dependent on the mass fractions of each. The $T_g$ of CAS polymers can be calculated by finding the peak in Tan δ measured using DMA. The $T_g$ can also be calculated from DSC, but the small glass transitions were difficult to determine in DSC. The $T_g$ of the hompolymers, CAS7 and CAS8, were found to be 0°C and -10°C respectively (Figure 3.7). Interestingly, the copolymer, 25:75, did not display a $T_g$ that was between the $T_g$s of the homopolymers but instead was much lower at around -20°C. This could be due to the crystallites having a large effect on the damping properties as other semi-crystalline polymers have reported such a deviation from the Fox equation.[25]

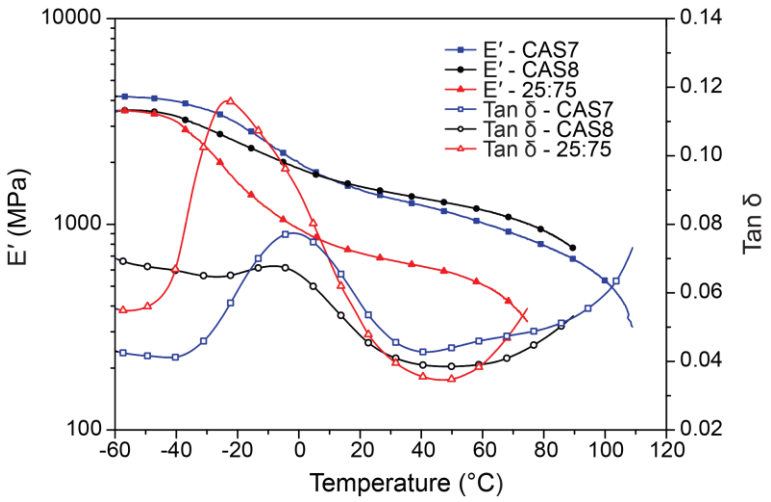


***Figure 3.7 Storage Modulus (E') and Tan δ traces of homopolymers CAS7 (blue) and CAS8 (black) and the 25:75 copolymer (red).***

The mechanical properties of the photopolymerized CAS thermoplastics were evaluated using uniaxial tensile testing with 500 µm thick ASTM D1708 microtensile dog bones tested at 1 mm/min. Representative stress-strain curves (Figure 3.6a) show the stress-strain curves for different photopolymerized CAS7/CAS8 (co)polymers, all of which exhibited brittle behavior. Compared with the copolymers, the CAS7 and CAS8 homopolymers exhibited higher modulus, lower fracture strain, and generally higher ultimate stress (see Table 3.3), consistent with the higher degree crystallinity observed in the homopolymers as determined by DSC melting endotherms (Table 3.2).[46] The low ultimate tensile stress/high fracture strain 50:50 CAS7:CAS8 copolymer is also consistent with its relatively low crystallinity and was the only polymer examined that did not exhibit brittle fracture for every tensile test. Nevertheless, the best combination of stress and strain as determined by the toughness calculated from the area under the stress-strain curves, was the 25:75 CAS7:CAS8 copolymer which retained a good combination of rigidity and ductility.

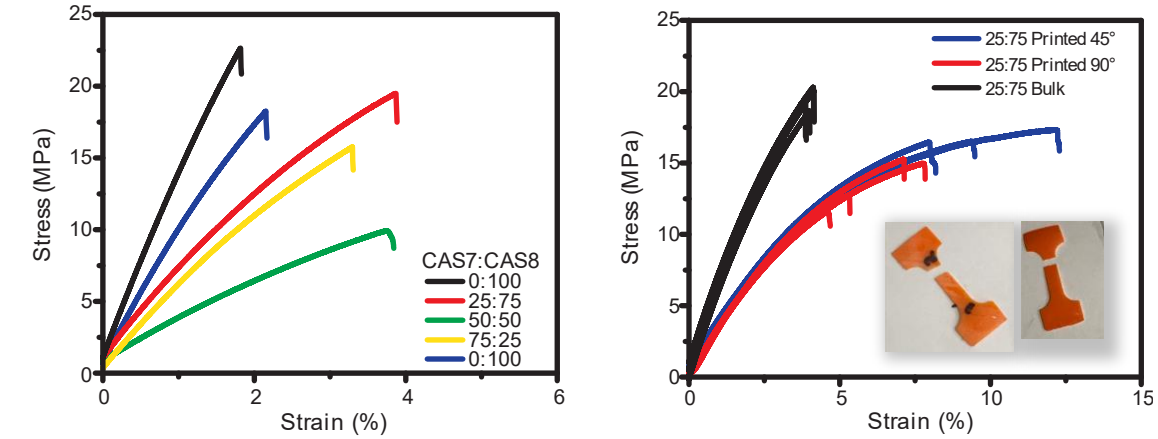


a) b)

***Figure 3.8 Stress-strain curves for a) photopolymerized CAS7:CAS8 (co)polymer samples fabricated in bulk and b) 25:75 CAS7:CAS8 copolymer samples fabricated either in bulk or via stereolithographic 3D printing.***

***Table 3.3 Bulk mechanical properties of photopolymerized CAS7:CAS8 (co)polymers using the ASTM D1708 tensile test.***

| CAS7:CAS8 (wt%) | Young's modulus (MPa) | Ultimate tensile stress (MPa) | Fracture strain (%) | Toughness ($MJ/m^3$) |
|---|---|---|---|---|
| 100:0 | 974 ± 8 | 18.1 ± 0.6 | 2.1 ± 0.1 | 0.25 ± 0.01 |
| 75:25 | 604 ± 7 | 16.1 ± 0.5 | 3.6 ± 0.2 | 0.47 ± 0.07 |
| 50:50 | 318 ± 7 | 9.8 ± 0.4 | 3.8 ± 0.3 | 0.22 ± 0.01 |
| 25:75 | 688 ± 9 | 19.5 ± 0.3 | 4.0 ± 0.1 | 0.52 ± 0.03 |
| 0:100 | 1260 ± 30 | 24 ± 2 | 2.2 ± 0.2 | 0.43 ± 0.03 |

Using a Flashforge Hunter stereolithographic 3D printer, ASTM D1708 dog bone samples were printed such that the layers were oriented 45° and 90° relative to the stress applied during tensile testing. The ASTM D1708 standard was selected over the more conventional ASTM D638 type V as its smaller size would fit in multiple orientations on the 25 mm × 40 mm build plate fitted to the printer. The size of the build plate allowed for seven dog bones to be printed in a single batch, where four 90° and three 45° dog bones were printed simultaneously and subsequently subject to tensile testing. The 25:75 CAS7:CAS8 resin formulation was used for printing as it exhibited rapid polymerization and crystallization rates, enabling short irradiation times for each printed layer, and provided the highest toughness of the resins examined.

As shown in Figure 3.8b and Table 3.4, the stereolithographically printed dog bone samples at both 45° and 90° orientations exhibited lower moduli than those of the dog bones photopolymerized in bulk; however, the printed samples displayed greater fracture strain and toughness than those fabricated in bulk. Moreover, all of the 45° oriented samples fractures along a plane perpendicular to the applied tensile stress (see Figure 3.8b) rather than along a layer interface. The results for the cyclic allyl sulfide-based system studied here are distinct from those obtained for previously described approaches to SLA-based printing of semi-crystalline thermoplastic polymers where the mechanical properties of printed parts were significantly inferior to those of samples fabricated in bulk,[24,26] even after thermal conditioning cycles,[27] owing to weak adhesion between semi-crystalline thermoplastic layers. For these previously described systems, the residual functional groups at the surface of each cured layer available for reaction with successive layers are exclusively restricted to chain ends and necessarily have low concentrations, the inter-layer

adhesion is primarily mechanical rather than covalent. In contrast, the comparable toughness between bulk and printed samples observed for the poly(cyclic allyl sulfide) described here can be attributed to the residual allyl sulfide functionalities in the polymer backbone, allowing for addition-fragmentation chain transfer between a cured layer and its successive layer, allowing for extensive covalent bonding and thus improved adhesion between printed layers.

***Table 3.4 Mechanical properties of photopolymerized 25:75 CAS7:CAS8 copolymer using the ASTM D1708 tensile test.***

| Sample fabrication method | Young's modulus (MPa) | Ultimate tensile stress (MPa) | Fracture strain (%) | Toughness ($MJ/m^3$) | % Toughness of bulk |
|---|---|---|---|---|---|
| Bulk | 688 ± 9 | 19.5 ± 0.3 | 4.0 ± 0.1 | 0.52 ± 0.03 | 100% |
| Printed at 45° | 368 ± 2 | 16.1 ± 0.6 | 10 ± 1.0 | 1.7 ± 0.3 | 327% |
| Printed at 90° | 356 ± 8 | 14.0 ± 0.6 | 6.2 ± 0.5 | 0.77 ± 0.05 | 148% |

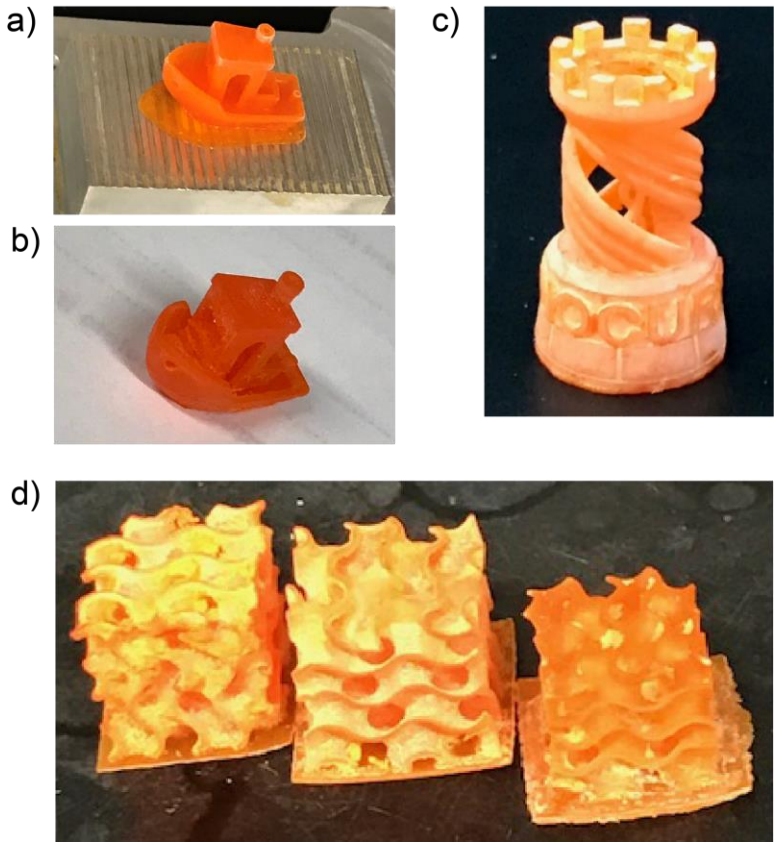


***Figure 3.9 Photographs of stereolithographically printed test geometries using 25:75 CAS7:CAS8 resin formulations. a) 3DBenchy test geometry still attached to build head. b) 3DBenchy test geometry after removal from build head. c) Monocure Rook test geometry. d) Test prints of gyroid geometry using different layer exposure times (left to right:55 sec, 50 sec, 45 sec).***

To illustrate the utility of cyclic allylic sulfide resins in SLA, common printing test specimens, including 3D Benchy[47] and Monocure Rook,[48] were printed using the 25:75 CAS printing resin (see Figure 3.9). Owing to the low irradiation intensity of the printer, the printing rate was relatively low, with an irradiation time of 50 seconds being used for each 50 µm thick layer. The resultant high-quality models demonstrated the potential of CAS-based resins to produce quality thermoplastic SLA printed parts which, akin to conventional thermoplastics, could be melted at raised temperature for reutilization as a moldable polymer (see Figure 3.10), providing a path for end-of-life reprocessing.

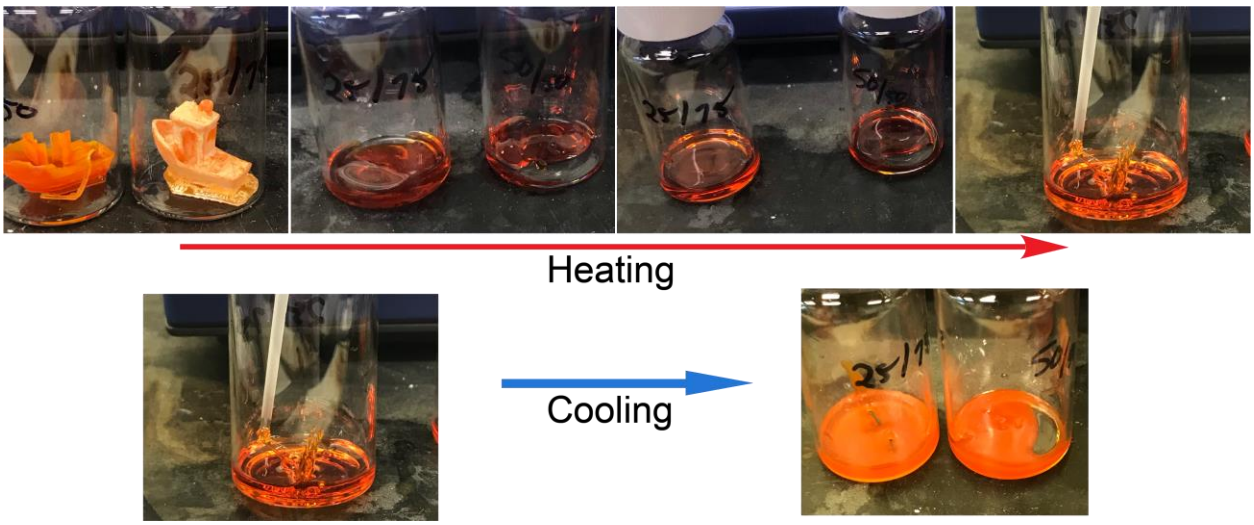


***Figure 3.10 Melting at raised temperature and resolidification at reduced temperature of stereolithographically printed 3DBenchy samples using 25:75 CAS7:CAS8 and 50:50 CAS7:CAS8 resin formulations.***

### 3.5 Conclusions

Radical-mediated ring-opening photopolymerization to yield semi-crystalline thermoplastics described here is well-suited for use in stereolithographic 3D printing. Formulating resins with varying ratios of seven- to eight-membered cyclic allyl sulfide monomers affects photopolymerization and crystallization kinetics, as well as the extent of crystallinity and mechanical properties of the resultant polymers. The polymerization and crystallization kinetics of these materials enables rapid layer-wise printing, while the incorporation of mid-chain allyl sulfide functional groups enhanced inter-layer adhesion in printed parts, yielding mechanical properties in these parts that were comparable to the bulk properties irrespective of the printing orientation. Employing photopolymerizable resins to fabricate semicrystalline thermoplastics provides a path to reprocessing and recycling of parts printed by SLA.

## 3.6 References


(1) Sathishkumar, T.; Satheeshkumar, S.; Naveen, J. Glass Fiber-Reinforced Polymer Composites – a Review. *J. Reinf. Plast. Compos.* **2014**, *33* (13), 1258–1275.

(2) Coleman, J. N.; Khan, U.; Blau, W. J.; Gun'ko, Y. K. Small but Strong: A Review of the Mechanical Properties of Carbon Nanotube–Polymer Composites. *Carbon* **2006**, *44* (9), 1624–1652.

(3) Cramer, N. B.; Stansbury, J. W.; Bowman, C. N. Recent Advances and Developments in Composite Dental Restorative Materials. *J. Dent. Res.* **2011**, *90* (4), 402–416.

(4) Rueggeberg, F. A. State-of-the-Art: Dental Photocuring—A Review. *Dent. Mater.* **2011**, *27* (1), 39–52.

(5) Fesmire, J. E.; Coffman, B. E.; Meneghelli, B. J.; Heckle, K. W. Spray-on Foam Insulations for Launch Vehicle Cryogenic Tanks. *Cryogenics* **2012**, *52* (4–6), 251–261.

(6) Khazabi, M.; Gu, R.; Sain, M. Fiber Reinforced Soy-Based Polyurethane Spray Foam Insulation. Part 1: Cell Morphologies. *BioResources* **2011**, *6* (4), 3757–3774.

(7) Ageyeva, T.; Sibikin, I.; Karger-Kocsis, J. Polymers and Related Composites via Anionic Ring-Opening Polymerization of Lactams: Recent Developments and Future Trends. *Polymers* **2018**, *10*, 357.

(8) Sibikin, I.; Karger-Kocsis, J. Toward Industrial Use of Anionically Activated Lactam Polymers: Past, Present and Future. *Adv. Ind. Eng. Polym. Res.* **2018**, *1*, 48–60.

(9) Gong, Y.; Yang, G. All-Polyamide Composites Prepared by Resin Transfer Molding. *J. Mater. Sci.* **2010**, *45* (19), 5237–5243.

(10) Vaishya, R.; Chauhan, M.; Vaish, A. Bone Cement. *J. Clin. Orthop. Trauma* **2013**, *4* (4), 157–163.

(11) Webb, J. C. J.; Spencer, R. F. The Role of Polymethylmethacrylate Bone Cement in Modern Orthopaedic Surgery. *J. Bone Joint Surg. [Br]* **2007**, *89-B* (7), 851–857.

(12) Layani, M.; Wang, X.; Magdassi, S. Novel Materials for 3D Printing by Photopolymerization. *Adv. Mater.* **2018**, *30* (41), 1706344.

(13) de Beer, M. P.; van der Laan, H. L.; Cole, M. A.; Whelan, R. J.; Burns, M. A.; Scott, T. F. Rapid, Continuous Additive Manufacturing by Volumetric Polymerization Inhibition Patterning. *Sci. Adv.* **2019**, *5*, eaau8723.

(14) Tumbleston, J. R.; Shirvanyants, D.; Ermoshkin, N.; Janusziewicz, R.; Johnson, A. R.; Kelly, D.; Chen, K.; Pinschmidt, R.; Rolland, J. P.; Ermoshkin, A.; Samulski, E. T.; DeSimone, J. M. Continuous Liquid Interface Production of 3D Objects. *Science* **2015**, *347* (6228), 1349–1352.

(15) Shusteff, M.; Browar, A. E. M.; Kelly, B. E.; Henriksson, J.; Weisgraber, T. H.; Panas, R. M.; Fang, N. X.; Spadaccini, C. M. One-Step Volumetric Additive Manufacturing of Complex Polymer Structures. *Sci. Adv.* **2017**, *3*, eaao5496.

(16) Kelly, B. E.; Bhattacharya, I.; Heidari, H.; Shusteff, M.; Spadaccini, C. M.; Taylor, H. K. Volumetric Additive Manufacturing via Tomographic Reconstruction. *Science* **2019**, *363* (6431), 1075–1079.

(17) Regehly, M.; Garmshausen, Y.; Reuter, M.; König, N. F.; Israel, E.; Kelly, D. P.; Chou, C.; Koch, K.; Asfari, B.; Hecht, S. Xolography for Linear Volumetric 3D Printing. *Nature* **2020**, *588* (7839), 620–624.

(18) Ngo, T. D.; Kashani, A.; Imbalzano, G.; Nguyen, K. T. Q.; Hui, D. Additive Manufacturing (3D Printing): A Review of Materials, Methods, Applications and Challenges. *Composites Part B.* **2018**, *143*, 172–196.

(19) Deng, S.; Wu, J.; Dickey, M. D.; Zhao, Q.; Xie, T. Rapid Open-Air Digital Light 3D Printing of Thermoplastic Polymer. *Adv. Mater.* **2019**, *31* (39), 1903970.

(20) Zhang, J.; Xiao, P. 3D Printing of Photopolymers. *Polym. Chem.* **2018**, *9* (13), 1530–1540.

(21) Hegde, M.; Meenakshisundaram, V.; Chartrain, N.; Sekhar, S.; Tafti, D.; Williams, C. B.; Long, T. E. 3D Printing All-Aromatic Polyimides Using Mask-Projection Stereolithography: Processing the Nonprocessable. *Adv. Mater.* **2017**, *29* (31), 1701240.

(22) Herzberger, J.; Meenakshisundaram, V.; Williams, C. B.; Long, T. E. 3D Printing

All-Aromatic Polyimides Using Stereolithographic 3D Printing of Polyamic Acid Salts. *ACS Macro Lett.* **2018**, *7* (4), 493–497.

(23) Hoyle, C. E.; Bowman, C. N. Thiol-Ene Click Chemistry. *Angew. Chemie Int. Ed.* **2010**, *49* (9), 1540–1573.

(24) Sycks, D. G.; Wu, T.; Park, H. S.; Gall, K. Tough, Stable Spiroacetal Thiol-ene Resin for 3D Printing. *J. Appl. Polym. Sci.* **2018**, *135* (22), 46259.

(25) Sycks, D. G.; Safranski, D. L.; Reddy, N. B.; Sun, E.; Gall, K. Tough Semicrystalline Thiol–Ene Photopolymers Incorporating Spiroacetal Alkenes. *Macromolecules* **2017**, *50* (11), 4281–4291.

(26) Alim, M. D.; Childress, K. K.; Baugh, N. J.; Martinez, A. M.; Davenport, A.; Fairbanks, B. D.; McBride, M. K.; Worrell, B. T.; Stansbury, J. W.; McLeod, R. R.; Bowman, C. N. A Photopolymerizable Thermoplastic with Tunable Mechanical Performance. *Mater. Horizons* **2020**, *7* (3), 835–842.

(27) Childress, K. K.; Alim, M. D.; Hernandez, J. J.; Stansbury, J. W.; Bowman, C. N. Additive Manufacture of Lightly Crosslinked Semicrystalline Thiol–Enes for Enhanced Mechanical Performance. *Polym. Chem.* **2020**, *11* (1), 39–46.

(28) Monzón, M.; Ortega, Z.; Hernández, A.; Paz, R.; Ortega, F. Anisotropy of Photopolymer Parts Made by Digital Light Processing. *Materials* **2017**, *10*, 64.

(29) Meijs, G. F.; Morton, T. C.; Rizzardo, E.; Thang, S. H. The Use of Substituted Allylic Sulfides to Prepare End-Functional Polymers of Controlled Molecular Weight by Free-Radical Polymerization. *Macromolecules* **1991**, *24* (12), 3689–3695.

(30) Scott, T. F.; Schneider, A. D.; Cook, W. D.; Bowman, C. N. Photoinduced Plasticity in Cross-Linked Polymers. *Science* **2005**, *308* (5728), 1615–1617.

(31) Evans, R. A.; Rizzardo, E. Free-Radical Ring-Opening Polymerization of Cyclic Allylic Sulfides. *Macromolecules* **1996**, *29* (22), 6983–6989.

(32) Evans, R. A.; Rizzardo, E. Free-Radical Ring-Opening Polymerization of Cyclic Allylic Sulfides. 2. Effect of Substituents on Seven- and Eight-Membered Ring Low Shrink Monomers. *Macromolecules* **2000**, *33* (18), 6722–6731.

(33) Evans, R. A.; Rizzardo, E. Free Radical Ring-Opening Polymerization of Cyclic Allylic Sulfides: Liquid Monomers with Low Polymerization Volume Shrinkage. *J. Polym. Sci. Part A Polym. Chem.* **2001**, *39* (1), 202–215.

(34) Pritchard, Z. D.; Beer, M. P.; Whelan, R. J.; Scott, T. F.; Burns, M. A. Modeling and Correcting Cure-Through in Continuous Stereolithographic 3D Printing. *Adv. Mater. Technol.* **2019**, *4* (12), 1900700.

(35) Lovell, L. G.; Berchtold, K. A.; Elliott, J. E.; Lu, H.; Bowman, C. N. Understanding the Kinetics and Network Formation of Dimethacrylate Dental Resins. *Polym. Adv. Technol.* **2001**, *12* (6), 335–345.

(36) Anslyn, E. V.; Dougherty, D. A. *Modern Physical Organic Chemistry*; University Science Books: Sausalito, CA, 2005.

(37) Lee, T. Y.; Roper, T. M.; Jönsson, E. S.; Guymon, C. A.; Hoyle, C. E. Influence of Hydrogen Bonding on Photopolymerization Rate of Hydroxyalkyl Acrylates. *Macromolecules* **2004**, *37* (10), 3659–3665.

(38) Scott, T. F.; Cook, W. D.; Forsythe, J. S. Photo-DSC Cure Kinetics of Vinyl Ester Resins II: Influence of Diluent Concentration. *Polymer* **2003**, *44* (3), 671–680.

(39) Goodner, M. D.; Lee, H. R.; Bowman, C. N. Method for Determining the Kinetic Parameters in Diffusion-Controlled Free-Radical Homopolymerizations. *Ind. Eng. Chem. Res.* **1997**, *36* (4), 1247–1252.

(40) Li, L.; Sun, X.; Lee, L. J. Low Temperature Cure of Vinyl Ester Resins. *Polym. Eng. Sci.* **1999**, *39* (4), 646–661.

(41) Cook, W. D. Thermal Aspects of the Kinetics of Dimethacrylate Photopolymerization. *Polymer* **1992**, *33* (10), 2152–2161.

(42) Kloosterboer, J. G.; Bressers, H. J. L. Evidence for Two Gel Effects during the Bulk Polymerization of Ethyl Acrylate from DSC, Rayleigh and Brillouin Scattering. *Polym. Bull.* **1980**, *2* (3), 205–210.

(43) Bressers, H. J. L.; Kloosterboer, J. G. Thermally and Light-Induced Polymerization of Ethyl Acrylate and Methyl Methacrylate, Studied by DSC. *Polym. Bull.* **1980**, *2* (3), 201–204.

(44) Mandelkern, L. *Crystallization of Polymers:Volume 2, Kinetics and Mechanisms*; Cambridge University Press, 2004.

(45) Scott, T. F.; Kloxin, C. J.; Draughon, R. B.; Bowman, C. N. Nonclassical Dependence of Polymerization Rate on Initiation Rate Observed in Thiol−Ene Photopolymerizations. *Macromolecules* **2008**, *41* (9), 2987–2989.

(46) Fox, T. G. Influence of Diluent and of Copolymer Composition on the Glass Transition Temperature of a Polymer System. *Bull. Am. Phys. Soc.* **1956**, *1*, 123.

(47) Young, R. J.; Lovell, P. A. *Introduction to Polymers*, 3rd ed.; CRC Press: Boca Raton, FL, 2011.

(48) *About #3DBenchy*. https://www.3dbenchy.com/about/.

(49) *Monocure 3D Calibration Models*. https://monocure3d.com/pages/calibration-models.

# Chapter 4 Fabrication of Tough Semi-crystalline Polymers via Radical-mediated Ring Opening Photopolymerization

## 4.1 Abstract

Radical ring-opening photopolymerization of cyclic allylic sulfide monomers has proven to be a useful method for producing thermoplastic stereolithographic objects. The previously studied 7- and 8-membered CAS monomers all produce highly crystalline and thus brittle polymers. Here we investigate the photopolymerization kinetics and mechanical properties of larger 11- (CAS11) and 15-membered (CAS15) CAS monomers. While the homopolymers from the larger rings resulted in weaker mechanical properties, the copolymers of the newly synthesized larger rings with the 8-membered CAS monomer yielded genuinely tough semi-crystalline polymers. The polymerization and crystallization kinetics and mechanical properties of all (co)polymers of the four different sized semi-crystalline CAS monomers is further evaluated and discussed.

## 4.2 Introduction

Thermoplastic polymers have long had advantages over their cross-linked, thermoset counterparts owing to their capacity for post-synthetic processing, welding, and recycling;[1] nevertheless conventional molding techniques require high temperatures and pressures to impregnate molds with high viscosity polymer melts.[2] Thus, necessitating the polymerization of thermoplastics *in situ* with low viscosity resins that more efficiently impregnate glass or carbon-fiber matrices to produce polymer composites. Current

approaches are mainly limited to thermally-initiated anionic ring-opening polymers including ε-caprolactone (PCL), L-lactide (PLA), ε-caprolactam (PA-6), and ω-laurolactam (PA-12).[1,3]

Low temperature *in situ* photopolymerization of tough thermoplastics have been examined for stereolithography and have so far been mostly focused on tough thiol-ene polymers[4–7] and rapid curing, high $T_g$ amorphous photopolymers[8]. A previous study by our group described one of the only instances of a radical ring-opening photopolymerization producing a thermoplastic *in situ*. The cyclic allylic sulfide (CAS) monomers described were successfully used as thermoplastic resins for stereolithographic (SLA) 3D printing. Owing in large part to their addition-fragmentation chain transfer (AFCT) mechanism, they are well suited monomers for thermoplastic stereolithography where limited interlayer adhesion of semi-crystalline polymers remains a significant challenge. Limited interlayer adhesion and internal stresses are two main challenges that limited the utility of certain SLA resins and appear to contribute to the degradation of mechanical properties in printed parts.[6,7] However, AFCT chain transfer allows for the rearrangement of the network topology thus releasing built up internal stresses[9] and allows for increased rearrangement of bonds in adjacent printed layers to help bridge the interface between layers. However, the high crystallinity of 7- and 8-membered CAS monomers makes them hard to process with solvents and the resulting homopolymers are quite brittle[10].

Semi-crystalline polymers like poly(lactic acid) (PLA) are also brittle as homopolymers and limit their applications without further modifications.[11] Studies on the toughening of brittle polymers like PLA found that modifications like addition of crosslinkers[12,13], plasticizers[14], or copolymerization[13,15] produced polymers with increased

toughness. Copolymers have been attractive materials in industry, often used to combine different properties from the comonomers into a single polymer which can be altered by varying the comonomer composition. Crystalline copolymers add a layer of complexity as the degree of crystallization also affects the mechanical properties and the crystallization behavior of copolymers can vary widely depending on the structures of the comonomers. Although semi-crystalline CAS monomers possess a lot of intriguing characteristics[16], they are very much less studied and used than amorphous CAS monomers.[17–20] Other than 7- and 8-membered CAS monomers, it is also possible to synthesize different sized rings by varying the length of the dithiol used in the ring synthesis. Larger rings have the added benefit of lower vapor pressure and less unpleasant odor that is present in CAS7 and CAS8.

In this work, we expand on our previous work on photopolymerized cyclic allyl sulfides by synthesizing and examining the photopolymerization of new, larger 11- and 15-membered cyclic allylic sulfides (Figure 4.1). We also establish a relationship between the comonomer composition and the resulting photopolymerization and crystallization kinetics. Differential scanning calorimetry (DSC) and x-ray diffraction (XRD) were used to characterize copolymer crystallization behavior and examined the relationship between crystallinity and mechanical properties.

## 4.3 Experimental

### *4.3.1 Materials*

Photopolymerizable resins were formulated using a mixture of synthesized cyclic allylic sulfide monomers and 0.5 wt% bis(2,4,6-trimethylbenzoyl)-phenylphosphineoxide (Irgacure 819, Ciba Specialty Chemicals Inc., Basel, Switzerland) as a violet-active photoinitiator. All cyclic allylic sulfides were synthesized as described below *via* a single

step ring-closing reaction between 3-chloro-2-(chloromethyl)-1-propene (Aaron Chemicals, San Diego, CA) and an alkyl dithiol. 6-Methylene-1,4-dithiepane (CAS7) and 3-methylene-1,4-dithiacyclooctane (CAS8) were synthesized as described previously in Chapter 3. 1,6-Hexanedithiol (Sigma Aldrich) and 1,10-decanedithiol (Chem Supply Pty Ltd., Gillman, AUS) were sourced commercially and used as received. All other reagents were obtained from Sigma Aldrich.

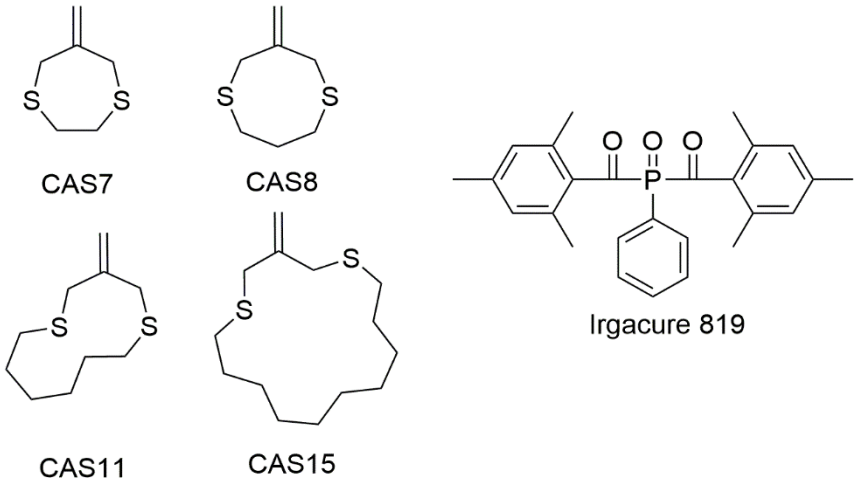


***Figure 4.1 Structures of CAS monomers and photoinitiator (Irgacure 819) used in tougher copolymers***

### *4.3.2 Methods*

#### *4.3.2.1 Polymer film Preparation*

All CAS polymer and copolymer samples were photopolymerized. CAS Monomer/s was mixed with 0.5 wt% of Irgacure 819 which dissolved well in all monomers. The resin was then pipetted in between glass slides with a 250 µm spacer and held together with binder clips. The films were cured using a 405 nm LED (Thorlabs ) which was adjusted to output 10 mW/cm$^2$ intensity and cured for 10 minutes.

#### *4.3.2.2 Calorimetry*

Differential scanning calorimetry (DSC) was performed using a Perkin Elmer DSC 8500 equipped with an intracooler. Polymer samples (approximately 3 mg) were cut from sheets that were produced using 10 mW/cm$^2$ light (405 nm, 10 min). Samples were subject to a temperature ramp from -50°C to 150°C at 10°C/min under flowing nitrogen gas.

Isothermal photocalorimetry was performed by using the Perkin Elmer DSC 8500 equipped with a photocalorimeter accessory. Light from an Omnicure 2000 mercury arc lamp equipped with a 400-500 nm band pass filter was directed through a bifurcated light guide to irradiate both sample and reference pans via quartz windows. The thermal imbalance of the sample and reference pans was corrected by repeating the irradiation of the cured pans in a second run and subtracting the data from the first run. The irradiation intensity was measured by measuring the heat flow increase under irradiation of a graphite disk and dividing the heat flow by the known surface area of the disk. All samples were cured at 25°C under flowing nitrogen with an irradiation intensity that was 10 mW/cm$^2$.

#### *4.3.2.3 Mechanical testing*

Molds for bulk samples were prepared using 0.50 mm thick silicone sheet cut with an ASTM D1708 dog bone cutting die. To fabricate bulk dog bone samples, the silicone molds were sandwiched between glass microscope slides and injected with formulated resin which was then cured under 10 mW/cm$^2$ LED light (405 nm) for 10 minutes. All samples were stored in the dark overnight before loading them into a uniaxial tensile tester (Mini Instron ElectroPuls E3000) equipped with a 3 kN load cell. Tests took place at ambient conditions and a strain rate of 1 mm/min.

#### *4.3.2.4 Dynamic mechanical analysis (DMA)*

DMA rectangular samples (20 mm x 4 mm) were cut from 250 µm films that were photocured using a 405 nm LED (Thorlabs) at 10 mW/cm$^2$ and loaded into a TA Instrument Q850 Discovery. The samples were preloaded with 1 N and an applied strain of 0.1% strain at 1 hz then a temperature sweep was applied with a 5 min soak time at -60℃ and then ramped at 3℃/min from -60℃ to a final temperature of 5℃ below the $T_m$.

#### *4.3.2.5 X-ray diffraction*

X-ray samples were produced by photopolymerization of resin between glass slides cut to a size of approximately 20 mm x 20 mm with 500 µm silicone spacers. X-ray diffractograms were collected on a Bruker D8 Advance A25 X-ray diffractometer with Cu Kα radiation (1.54056λ, 40kV, 40mA) equipped with a Lynx Eye XE-T detector. 2θ scans were collected from 5° - 40° at a step size of 0.05° and 1.5s per time step.

### *4.3.3 Synthesis*

#### *4.3.3.1 Synthesis of 6-methylene-1,4-dithiepane (CAS7)*

As described earlier, methanolic solutions of 3-chloro-2-(chloromethyl)-1-propene (3.94 g, 31.5 mmol) and 1,2-ethanedithiol (2.97 g, 31.5 mmol) were added simultaneously to a refluxing solution of sodium metal (1.52 g, 66.2 mmol) in methanol (200 mL) under argon protection. After completion of the addition, it was left to reflux for 4 hours and let to cool and filtered. The solvent was evaporated, water added and extracted with diethyl ether. The ether extracts were pooled, dried with sodium sulfate, and ether evaporated, affording 3.5 g of pale amber liquid. This material was then bulb-to-bulb distilled (55°C, 0.2 mmHg) to yield a clear oil (2.4 g, 16.4 mmol, 52%). $^{1}$H NMR (400 MHz, $CDCl_3$, 25°C) δ 3.01 (s, 4H, SC**H**$_2$C**H**$_2$S), 3.64 (s, 4H, =CC**H**$_2$S), 4.84 (pent., $J$ = 1.1 Hz, 2H, =C**H**$_2$) ppm.

#### *4.3.3.2 Synthesis of 3-methylene-1,4-dithiacyclooctane (CAS8)*

As described earlier, methanolic solutions of 3-chloro-2-(chloromethyl)-1-propene (3.94 g 31.5 mmol) and 1,3-propanedithiol (3.40 g, 31.5 mmol) were added to a refluxing solution of sodium metal (1.52 g, 66.2 mmol) in methanol (200 mL) under argon protection. After addition and an additional 4 hours under reflux, the mixture was filtered, solvent evaporated, water added, and extracted with ether. The ether extracts were pooled, dried and the ether evaporated, affording 4.02 g of pale amber liquid. A final bulb-to-bulb distillation (65°C, 0.2 mmHg) yielded a clear oil (3.0 g, 18.7 mmol, 59%). $^{1}$H NMR (400 MHz, $CDCl_3$, 25°C) δ1.79 (m, $J$ = 6.2 Hz, 2H, $SCH_2C$**H**$_2CH_2S$), 2.88 (t, $J$ = 6 Hz, 4H, SC**H**$_2CH_2C$**H**$_2$S), 3.25 (s, 4H, =CC**H**$_2$S), 5.19 (s, 2H, =C**H**$_2$) ppm.

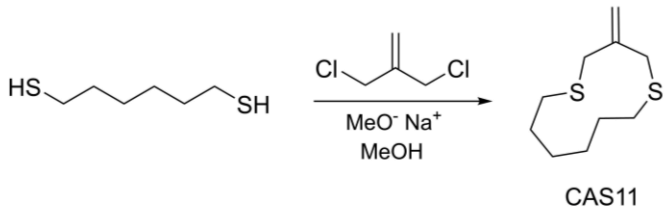


***Scheme 4.1 Synthesis of 3-methylene-1,5-dithiacycloundecane (CAS11)***

#### *4.3.3.3 Synthesis of 3-methylene-1,5-dithiacycloundecane (CAS11)*

Using a similar procedure to the other CAS monomers, 3-chloro-2-(chloromethyl)-1-propene (19.70 g 157.5 mmol) and 1,6-hexanedithiol (23.67 g, 157.5 mmol) were each made up into separate 60 mL solutions with methanol. These two solutions were then added simultaneously and separately by syringe pump at a rate of 2 mL/h to a refluxing solution of sodium metal (7.6 g, 331 mmol) in methanol (1400 mL) under argon protection. Upon the completion of the addition, the reaction mixture remained under reflux for 4 hours, then the mixture was filtered to remove the precipitate formed during the reaction. The solvent was then evaporated, water added, and the mix extracted twice with diethyl ether. The ether extracts were pooled, dried with sodium sulfate and the ether evaporated. This material was then bulb-to-bulb distilled (95 °C, 0.2 mmHg) to give a clear oil (4.85 g, 15%).$^{1}$H NMR (400 MHz, $CDCl_3$, 25°C) δ1.45(m, 4H, C**H**$_2$C$H_2$C$H_2$S), 1.63(m, 4H,C$H_2$C**H**$_2$C$H_2$S), 2.68(s, 4H,C$H_2$C**H**$_2$S), 3.29(s, 4H, =CC**H**$_2$S), 5.27(s, 2H, =C**H**$_2$) ppm.

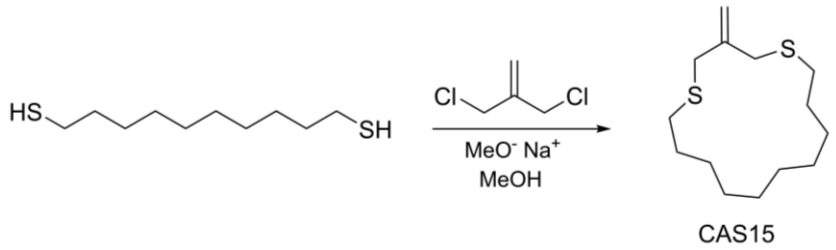


***Scheme 4.2 Synthesis of 3-methylene-1,5-dithiacyclopentadecane (CAS15)***

#### *4.3.3.4 Synthesis of 3-methylene-1,5-dithiacyclopentadecane (CAS15)*

Using a similar procedure to other CAS monomers, 3-chloro-2-(chloromethyl)-1-propene (15.76 g 126 mmol) was made up in a 60 mL methanol solution while 1,10-decanedithiol (26.01 g, 126 mmol) was made up into a 60 mL solution in 1-butanol. These two solutions were then added simultaneously and separately by syringe pump at a rate of 1.5 mL/h to a refluxing solution of sodium metal (6.1 g, 265 mmol) in methanol (1400 mL) under argon protection. Upon the completion of the addition, it remained under reflux for 4 hours, then the mixture was filtered. The solvent was then evaporated, water added, and the mix extracted twice with diethyl ether. The ether extracts were pooled, dried with sodium sulfate and the ether evaporated. This material was then bulb-to-bulb distilled (110 °C, 0.2 mmHg) to give a clear oil (3.6 g, 11%). $^{1}$H NMR (400 MHz, $CDCl_3$, 25°C) δ1.37(m, 12H, $CH_2C\mathbf{H}_2CH_2$), 1.63(m, 4H,$CH_2C\mathbf{H}_2CH_2S$), 2.53(t, *J* = 7.1 Hz, 4H,$CH_2C\mathbf{H}_2S$), 3.28(t, *J* = 0.9 Hz, 4H, $=CC\mathbf{H}_2S$), 5.15(s, 2H, $=C\mathbf{H}_2$) ppm.

## 4.4 Results and Discussion

Previously reported cyclic allylic sulfide monomers have been limited to 7- and 8-membered rings with most of the subsequent research utilizing various amorphous versions of the 7- and 8- membered CAS monomer.[17–19,21,22] Nevertheless, the synthesis of larger rings *via* the co-addition of allyl dichloride and a relatively long alkyl dithiol to refluxing sodium methoxide, where the length of the alkyl dithiol dictates the size of the ring, remains conceivable. The deficiency of this approach is that it relies upon high dilution reaction conditions to ensure successful ring closure yielding the target product rather than chain extension that would generate oligomeric species. Previous cyclic allyl sulfide monomer syntheses employed a simultaneous reagent addition rate of 4 mL/hr; however, although the general reaction conditions were maintained, an addition rate of 2 mL/hr was employed here to further dilute the reaction to promote ring closure for larger alkyl dithiols. The yields of the larger rings were significantly lower than the smaller rings as expected but provided sufficient material for use in polymer film fabrication.

The ring-opening photopolymerization kinetics of cyclic allyl sulfide monomers are strongly dependent on the size of the ring with the ring strain dictating a large contribution to the exotherm generated upon polymerization. The 7- and 8-membered CAS monomers ring opened rapidly but as the rings get above 11 members, the ring strain becomes almost negligible.[23] Thus, the kinetics of ring-opening polymerization of the 11- and 15-membered rings is crucial to the successful photopolymerization.

Isothermal photoDSC was employed to investigate the polymerization and crystallization kinetics of CAS monomers as the more typical method of FTIR is limited by the lack of a functional group change during ring-opening. The exothermic heat flow of

CAS monomers during polymerization was monitored using isothermal photoDSC at 25°C during 10 mW/cm$^2$ of 405 nm irradiation (see Figure 4.2, summarized in Table 4.1). CAS7 and CAS11 exotherms have the same trajectory at the onset of irradiation along with the copolymers, this initial rate of heat flow is understood to be the polymerization. CAS7 and CAS11 deviate in their trajectories after about 10 secs of irradiation when the rate of both exotherms change (Figure 4.2a). The change in the heat flow after 10 seconds is reflective of the beginning of crystallization and reveals that the two monomers crystallize at different rates leading to differences in heat evolution after crystallization begins. Interestingly, the overall heat generated by CAS11 after 10 minutes is slightly higher than CAS7 which suggests that CAS7 may crystallize sooner, but the slower crystallizing CAS11 may crystallize to a greater degree. This would only hold true if the heats of polymerization of CAS11 and CAS7 were indeed equal, but it is impossible to fully separate the two phenomena.

While CAS7 and CAS11 exotherms are fairly similar, CAS8 is an outlier with rapid polymerization and crystallization leading to an exceedingly large exotherm. The max heat flow is around 2 times higher than any other sized ring and occurs in less than 20 secs of irradiation. This contrasts with CAS15 which displays a max heat flow peak that occurs earlier in time but much lower in magnitude than the other sized rings. This may explain why the CAS8:CAS15 copolymers behave differently than CAS8:CAS11 copolymers. In Figure 4.2a, the CAS8:CAS11 copolymers display long delay times after polymerization but before crystallization. All these copolymers have heat flows that decrease in magnitude for over 30 seconds before the magnitude of heat flow increases during crystallization even for the 75 wt% CAS8 copolymer. However, in Figure 4.2b, the CAS8:CAS15 copolymers

display much shorter delay times with only minor pauses in heat flows and for 75 wt% CAS8 with CAS15, the heat flow magnitude never decreases before maxing out during crystallization.

All homopolymers besides CAS15 appear to have similar polymerization rates in the first 10 seconds of irradiation but differ drastically after the onset of crystallization. In comparison, the CAS15 appears to be more delayed in the polymerization phase which could arise from a less energetically favored ring-opening and the low overall heat evolution supports that CAS15 may not polymerize or crystallize to the extent of the other monomers. In terms of ring-opening thermodynamics, rings around 8-10 members in size generally have favorable Gibbs free energy of polymerization with a dominant enthalpy term coming from considerable ring strain[24]. So, it is perhaps unsurprisingly that CAS8 appears to have greater heat evolved than other sized rings and CAS15 is the lowest, although at least some of this heat is explained by heat of crystallization and not just heat of polymerization.

In addition to lower crystallinity, it also appears that CAS11 and CAS15 do not fully polymerize. Compared to poly(CAS7) and poly(CAS8), the solubility is greater and allowed for some dissolution in chloroform under reflux. After 15 minutes of photopolymerization of poly(CAS11) and poly(CAS15) under 405 nm light, the polymers were dissolved in $CDCl_3$ under reflux and the conversion of CAS11 and CAS15 were interpreted from NMR. The polymer samples of poly(CAS11) show around 6% residual monomer (Figure 4.3a) and poly(CAS15) show around 12% residual monomer (Figure 4.3b). This lower conversion of monomer likely dictates many of the properties of the

larger rings, including the lower heats evolved during irradiation and the weaker mechanical properties that the CAS11 and CAS15 homopolymers possess.

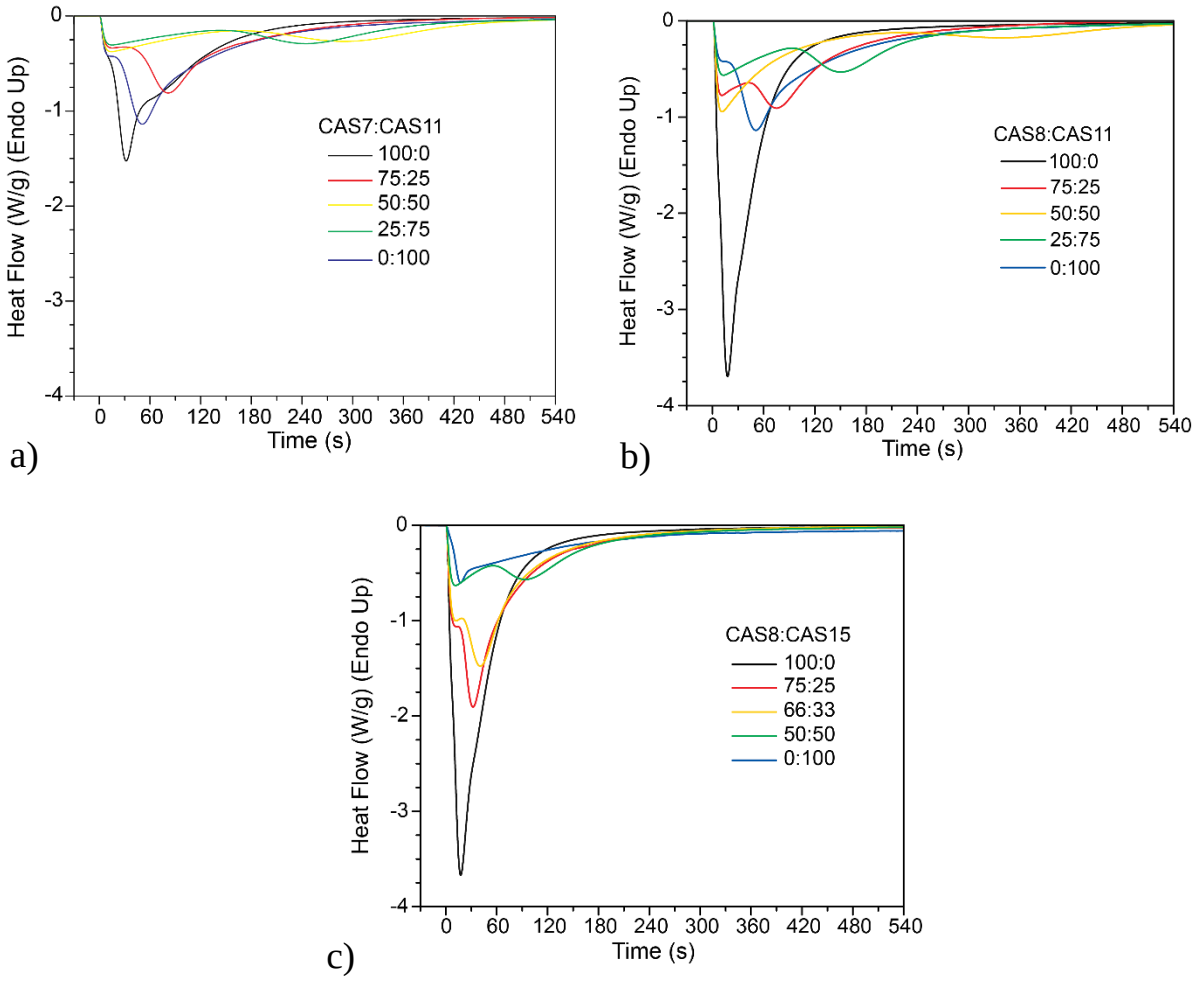


***Figure 4.2 Isothermal photoDSC traces for cyclic allyl sulfide resins (as shown) formulated with 0.5 wt% Irgacure 819 and irradiated with 405 nm light at 10 mW/cm$^2$ and at 25°C. Heat flow versus time for the photopolymerization of resins formulated from a) CAS7 and CAS11, b) CAS8 and CAS11, and c) CAS8 and CAS15, upon 405 nm irradiation at t=0.***

***Table 4.1 Summary of CAS resin photocalorimetry.***

| Semi-crystalline resin formulation | $\Delta H_{p,\ semicryst.}$ (J/g) |
|---|---|
| CAS7 | 130 ± 3 |
| CAS8 | 187.8 ± 1.1 |
| CAS11 | 141.6 ± 1.4 |
| CAS15 | 64 ± 16 |
| 75:25 CAS7:CAS11 | 115 ± 3 |
| 50:50 CAS7:CAS11 | 96.3 ± 1.6 |
| 25:75 CAS7:CAS11 | 94 ± 2 |
| 75:25 CAS8:CAS11 | 121 ± 4 |
| 50:50 CAS8:CAS11 | 113.9 ± 1.9 |
| 25:75 CAS8:CAS11 | 117.6 ± 1.8 |
| 75:25 CAS8:CAS15 | 153.3 ± 0.2 |
| 66:33 CAS8:CAS15 | 137.3 ± 0.9 |
| 50:50 CAS8:CAS15 | 100.7 ± 0.7 |

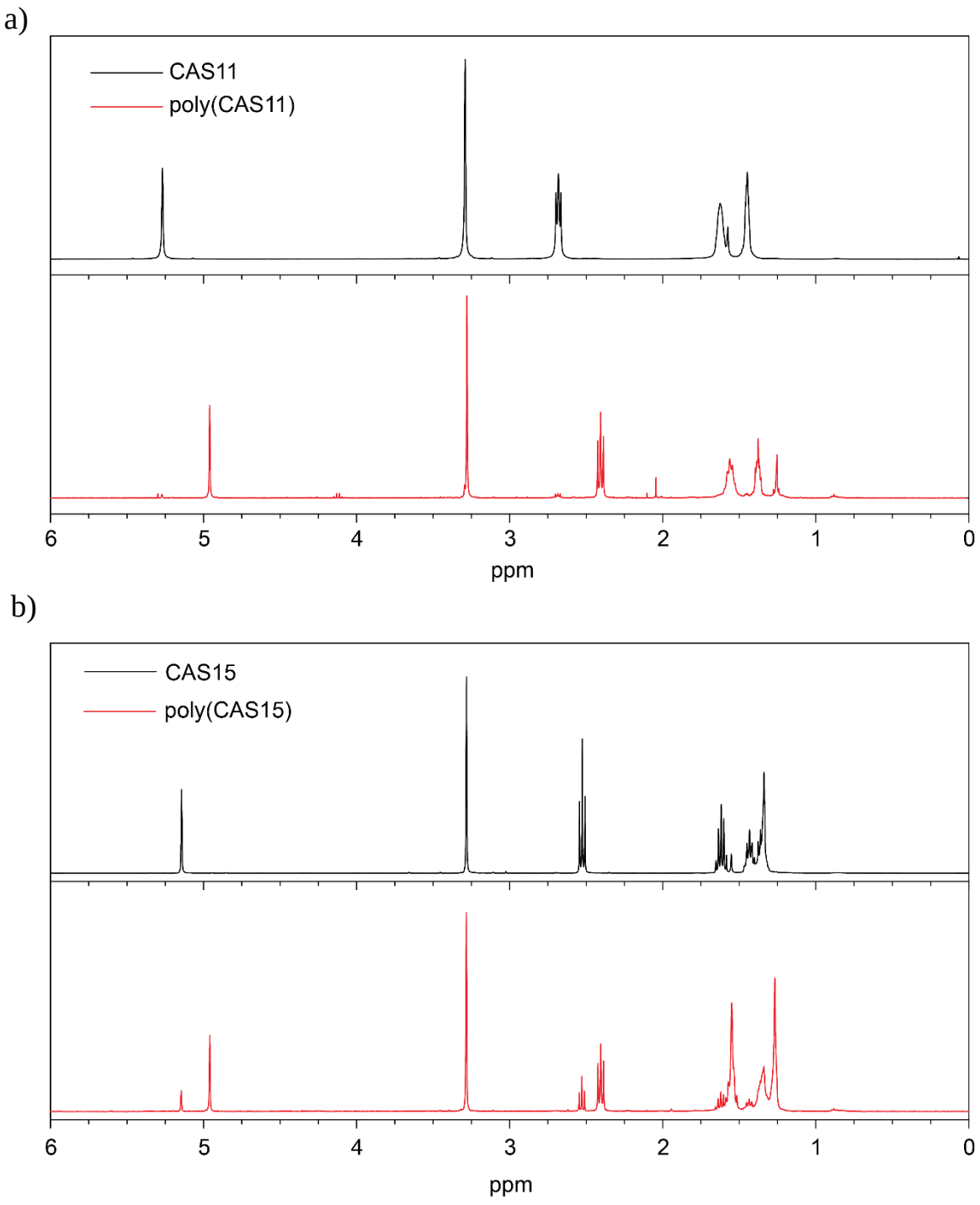


***Figure 4.3 NMR spectra in $CDCl_3$ (7.26 ppm) of monomer (top, black) and polymer after 10 minute photopolymerization under 405 nm irradiation (bottom, red) of a) CAS11 and b) CAS15.***

The homopolymers from the CAS11 and CAS15 monomers were quite brittle after photopolymerization at room temperature like CAS7 and CAS8. However, the polymers were softer than the polymers from smaller rings potentially in part to the lower monomer conversion in the larger rings. The weak mechanical properties of the new polymers do not lend themselves to use in stereolithography yet the copolymers from these monomers displayed properties that deviated considerably from the homopolymers. The mechanical properties of the larger rings, including ultimate tensile strength (UTS), Young's modulus, and tensile toughness (area under the stress-strain curve) were further investigated through uniaxial tensile testing with 500 μm thick ASTM D1708 microtensile dog bones tested at 1 mm/min. Seen in Figure 4.4 and summarized in Table 4.2, the UTS of CAS11 and CAS15 are both less than half of CAS8 (24 MPa compared to 10 and 3.6 MPa) and significantly lower than CAS7 (18.1 MPa). The lower UTS and Young's modulus confirms that the larger rings produce softer polymers and corresponds well to the lower conversion seen in NMR. The polymers still are much too brittle to be elongated significantly more than the original 7- and 8-membered homopolymers so possess lower tensile toughness values. CAS15 is especially low with a toughness of 47 $kJ/m^3$ compared to CAS11 with a toughness over 3 times higher at 170 $kJ/m^3$ and both are much lower than the original CAS7 and CAS8 at 250 and 430 $kJ/m^3$, respectively.

Being both brittle and soft, the CAS11 and CAS15 homopolymers are not ideal for commercial usage in any type of application, but the softer properties may be beneficial in a copolymer as a diluent with a more rigid polymer. Previous copolymers between CAS7 and CAS8 displayed a reduction in crystallinity and an increase in maximum elongation over the homopolymers. The four different CAS monomers were mixed into a resin and

photopolymerized to produce all combinations of copolymers. The copolymers between CAS11 and CAS15 were extremely brittle and fell apart too easily to test and the copolymer between CAS7 and CAS15 was similarly too brittle to test. The CAS7 copolymer with CAS11 was slightly tougher but neither the toughness nor the UTS was improved over the homopolymers. The toughness of CAS7:CAS11 copolymers are actually lower than the CAS11 homopolymers which is completely undesirable (Figure 4.4a).

On the other hand, the CAS8:CAS11 copolymers increased in tensile toughness as the amount of CAS11 was increased (Figure 4.4b). While the toughness increases with increasing comonomer content, the modulus decreases with increasing comonomer. The 50 wt% copolymer of CAS8:CAS11 was much tougher than any other polymer produced with a 10-fold higher toughness compared to all other (co)polymers and was reminiscent of a tough elastic polymer and not like either of the brittle homopolymers. The next toughest (co)polymer was the 50 wt% copolymer of CAS8:CAS15 at 1200 $kJ/m^3$ which produced polymers that necked on some runs but still only displayed 10% of the toughness of CAS8:CAS11 50:50.

CAS8 copolymers displayed better toughness overall than CAS7 copolymers which is not unsurprising considering the tougher properties of CAS8 homopolymers. The toughest (co)polymers were 50 wt% of CAS8 and CAS11 or CAS15 and this composition range plays a key role in the mechanical properties of the copolymer. Previously in Chapter 3, we determined that the composition range influences the crystallinity with a minimum in crystallinity occurring around 50 wt%. To fully characterize the morphology and elucidate the crystallinity as a function of composition, the copolymers were examined using non-isothermal DSC.

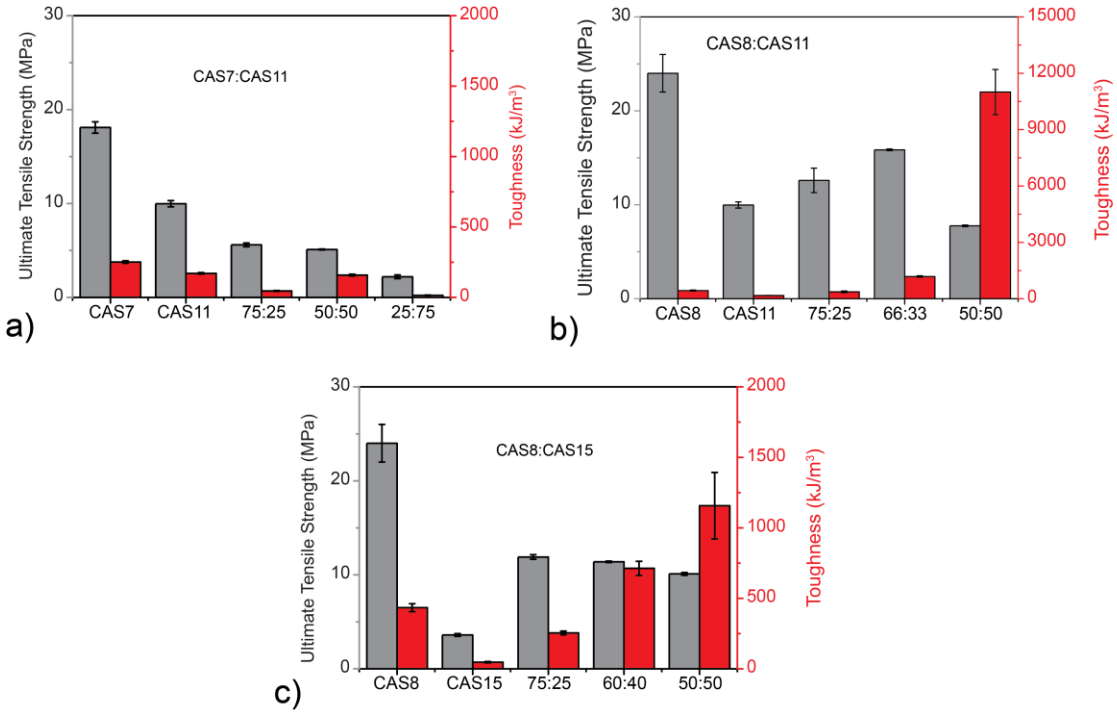


***Figure 4.4 Ultimate tensile strength and toughness as a function of comonomer mass fraction for copolymers a) CAS7:CAS11 b) CAS8:CAS11 c) CAS8:CAS15.***

***Table 4.2 Mechanical Properties of bulk CAS copolymers using ASTM D1708 tensile test at 1 mm/min.***

| Semi-crystalline resin formulation | Ultimate Tensile Strength (MPa) | Young's Modulus (MPa) | Tensile Toughness ($kJ/m^3$) |
|---|---|---|---|
| CAS7 | 18.1 ± 0.6 | 1006 ± 6 | 251 ± 9 |
| CAS8 | 24 ± 2 | 1407 ± 6 | 430 ± 30 |
| CAS11 | 10.0 ± 0.3 | 463 ± 6 | 171 ± 5 |
| CAS15 | 3.6 ± 0.2 | 170.0 ± 0.4 | 47 ± 5 |
| 75:25 CAS7:CAS11 | 5.6 ± 0.2 | 417 ± 1 | 46 ± 3 |
| 50:50 CAS7:CAS11 | 5.1 ± 0.1 | 183 ± 0.7 | 159 ± 7 |
| 25:75 CAS7:CAS11 | 2.2 ± 0.2 | 242 ± 3 | 15 ± 2 |
| 75:25 CAS8:CAS11 | 12.6 ± 1.3 | 571 ± 3 | 370 ± 50 |
| 66:33 CAS8:CAS11 | 15.9 ± 0.1 | 388 ± 2 | 1180 ± 40 |
| 50:50 CAS8:CAS11 | 7.76 ± 0.09 | 152 ± 2 | 11,000 ± 1000 |
| 75:25 CAS8:CAS15 | 11.9 ± 0.2 | 422.0 ± 0.6 | 255 ± 10 |
| 60:40 CAS8:CAS15 | 11.4 ± 0.1 | 277 ± 2 | 710 ± 50 |
| 50:50 CAS8:CAS15 | 10.1 ± 0.2 | 246 ± 2 | 1200 ± 200 |

Using non-isothermal scanning DSC, the first heating scans are recorded as evidence of the photopolymerized microstructure present in the samples. All combinations of CAS7, CAS8, CAS11, and CAS15 crystallized along the entire range of compositions (Figure 4.5, summarized in Table 4.3). The melting peaks in each scan provide evidence for the crystallization and the trend of depressed melting temperatures for the copolymers is similar to CAS7:CAS8 copolymers (see Figure 3.3b). This trend can be seen more clearly

in Figure 4.6 where the heat of fusion ($\Delta H_m$) and melting temperature ($T_m$) are plotted as a function of comonomer content. The melting point and heat of fusion values over the composition range show the depressed values at near equimolar compositions. The heat of fusion is used as a measure of degree of crystallinity by comparing the sample heat of fusion with an 100% crystalline reference sample. The lack of a 100% crystalline reference value for CAS monomers means that the exact degree of crystallinity cannot be calculated, but the trend of heat of fusion values over the composition do indicate the lower crystallinity of the near equimolar compositions compared to the homopolymers. The greatest depression of $T_m$ and $\Delta H_m$ was in the CAS8:CAS11 copolymer and the lowest crystallinity was the extremely tough CAS8:CAS11 50wt% copolymer. Clearly this reduction in crystallinity in these copolymers is advantageous for increasing toughness. Compared to other CAS8 copolymers, the CAS11 copolymers produced tougher copolymers than CAS7 or CAS15 so both comonomer choice and composition influence the mechanical properties.

The low crystallinity as indicated by low melting temperatures and enthalpies at intermediate compositions giving a "pseudo-eutectic trend" indicates that the copolymers have an isodimorphic behavior.[25] This means that the comonomer can be partially included in the crystal lattice of the majority component. As more comonomer is added, the crystallization decreases as not all comonomer can be included in the crystal lattice of the major component. The structure of the crystal lattices can be inferred through x-ray diffraction scans and further confirm the presence of crystallinity. Supporting the results obtained by DSC, the crystallinity appears to decrease from homopolymers to intermediate copolymers (Figure 4.7). The presence of characteristic peaks from the crystal lattice of

both homopolymers in intermediate compositions indicate that some (co)crystallization occurs at these compositions. In all formulations, the peaks broaden from the homopolymers towards intermediate compositions as less crystallization occurs and more comonomer is excluded from the crystal lattice. This confirms the isodimorphic nature of the CAS copolymers and explains the reduced crystallinity with increasing comonomer content.

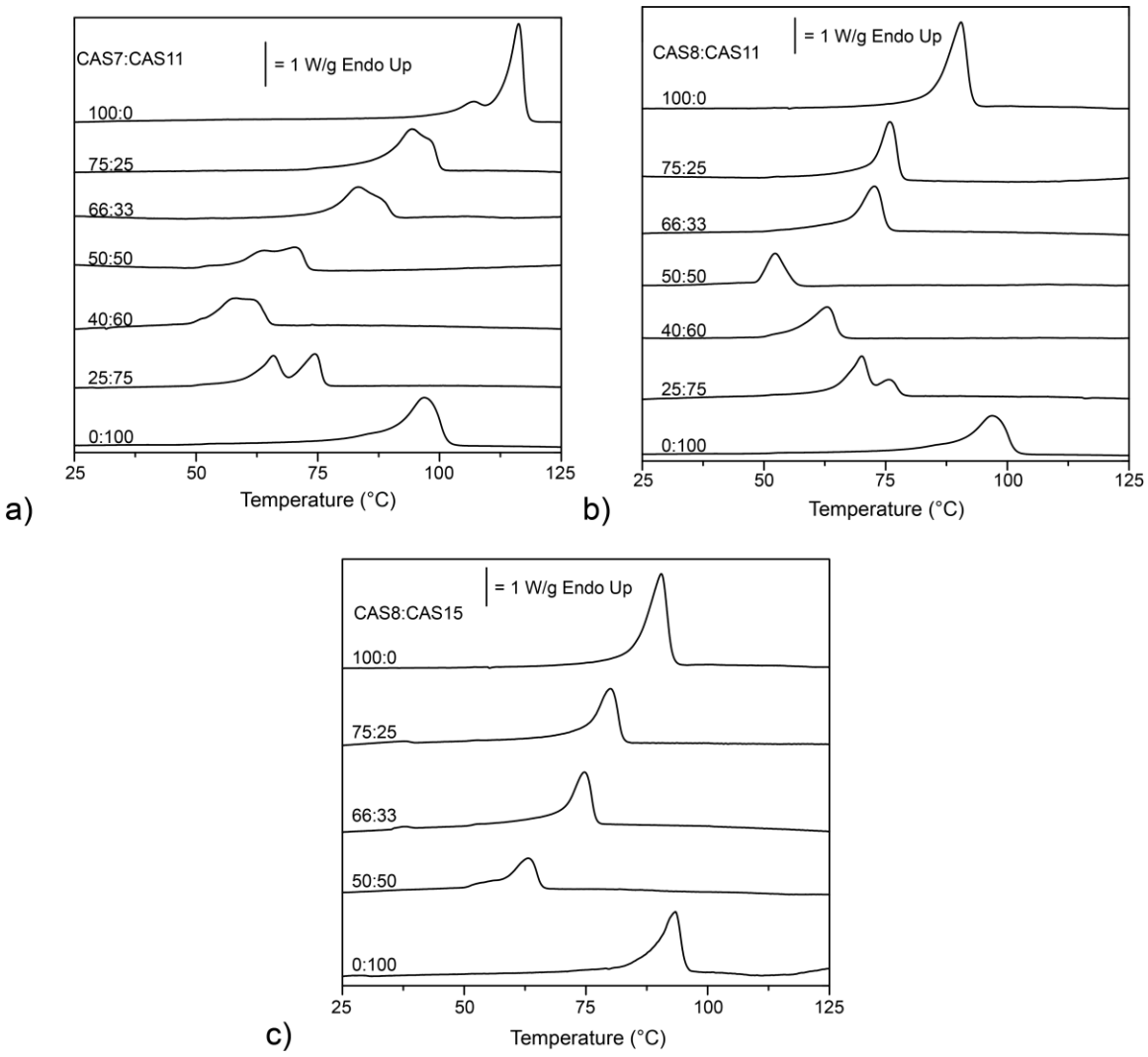


***Figure 4.5 Non-isothermal DSC scans over a range of compositions for a) CAS7:CAS11, b) CAS8:CAS11, and c) CAS8:CAS15.***

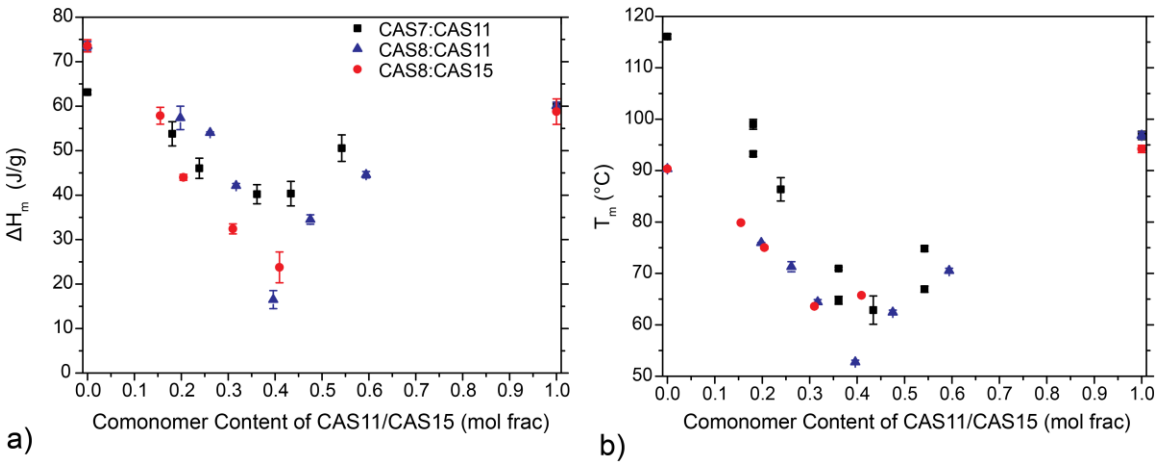


***Figure 4.6 Differential scanning calorimetry measured values for the a) heat of fusion and b) peak melting temperatures for CAS7:CAS11 (black squares), CAS8:CAS11 (blue triangles), and CAS8:CAS15 (red circles) plotted as a function of the CAS11 or CAS15 mole fraction where a minimum in both values occurs around 40% comonomer. Note: CAS 7/11 copolymers displayed multiple separate melting peaks at multiple compositions so both are plotted.***

*Table 4.3 Summary of non-isothermal DSC scans for CAS (co)polymers*

| **Semi-crystalline resin formulation** | **Mole fraction** | **$T_m$ (°C)** | **$\Delta H_m$ (J/g)** |
|---|---|---|---|
| CAS7 | 100:0 | 116.1 ± 0.5 | 63.1 ± 0.5 |
| CAS8 | 100:0 | 90.3 ± 0.1 | 74 ± 1 |
| CAS11 | 0:100 | 96.9 ± 0.8 | 60.1 ± 0.8 |
| CAS15 | 0:100 | 94.2 ± 0.7 | 59 ± 3 |
| 75:25 CAS7:CAS11 | 82:18 | 93.2 ± 0.5, 99 ± 1 | 54 ± 3 |
| 66:33 CAS7:CAS11 | 76:24 | 86 ± 2 | 46 ± 2 |
| 50:50 CAS7:CAS11 | 64:36 | 64.8 ± 0.8, 70.9 ± 0.3 | 40 ± 2 |
| 40:60 CAS7:CAS11 | 57:43 | 63 ± 3 | 40 ± 3 |
| 25:75 CAS7:CAS11 | 46:54 | 66.9 ± 0.6, 74.8 ± 0.6 | 51 ± 3 |
| 75:25 CAS8:CAS11 | 80:20 | 76.0 ± 0.1 | 57 ± 3 |
| 66:33 CAS8:CAS11 | 74:26 | 71 ± 1 | 54.0 ± 0.2 |
| 60:40 CAS8:CAS11 | 68:32 | 64.4 ± 0.5 | 42.1 ± 0.5 |
| 50:50 CAS8:CAS11 | 60:40 | 52.8 ± 0.4 | 17 ± 2 |
| 25:75 CAS8:CAS11 | 41:59 | 70.5 ± 0.5 | 44.6 ± 0.7 |
| 75:25 CAS8:CAS15 | 84:16 | 79.9 ± 0.2 | 58 ± 2 |
| 66:33 CAS8:CAS15 | 80:20 | 75.0 ± 0.3 | 44.0 ± 0.7 |
| 50:50 CAS8:CAS15 | 69:31 | 63.6 ± 0.3 | 32 ± 1 |
| 33:66 CAS8:CAS15 | 59:41 | 65.73 ± 0.01 | 24 ± 3 |

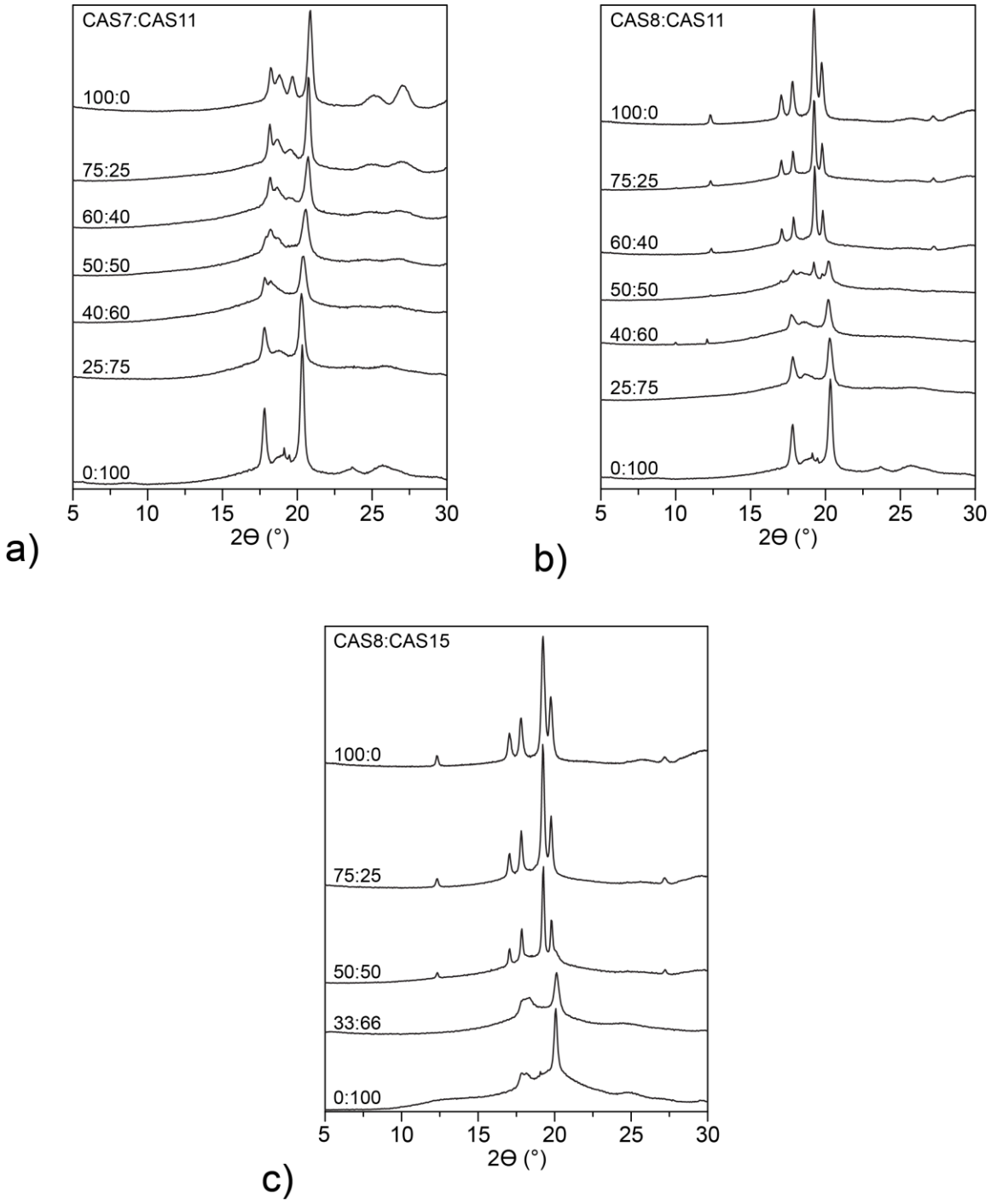


***Figure 4.7 Qualitative X-ray diffractograms of photopolymerized cyclic allyl sulfide (co)polymers a) CAS7:CAS11, b) CAS8:CAS11, and c) CAS8:CAS15.***

Random copolymers tend to have glass transition temperatures ($T_g$) that follow he Fox equation which indicates that it can be calculated based on the mass fraction of each homopolymer and the respective $T_g$ of each homopolymer.[26] The $T_g$ of CAS (co)polymers were measured using the peak of Tan δ from a DMA temperature scan and plotted as a function of large ring comonomer mole fraction for each of the three combinations (see Figure 4.8). The homopolymers had glass transition temperatures above -15°C with CAS7 being the highest at 1°C and CAS11 having the lowest at -13°C. However, none of the copolymers had a $T_g$ above -25°C indicating deviation from the Fox equation where the $T_g$ would be predicted to be between the $T_g$ of the homopolymers. The deviation is similar to the deviation in CAS7:CAS8 copolymers and the trend in $T_g$ follows the same pattern of depressed values at intermediate compositions as the melting temperature and enthalpy values.

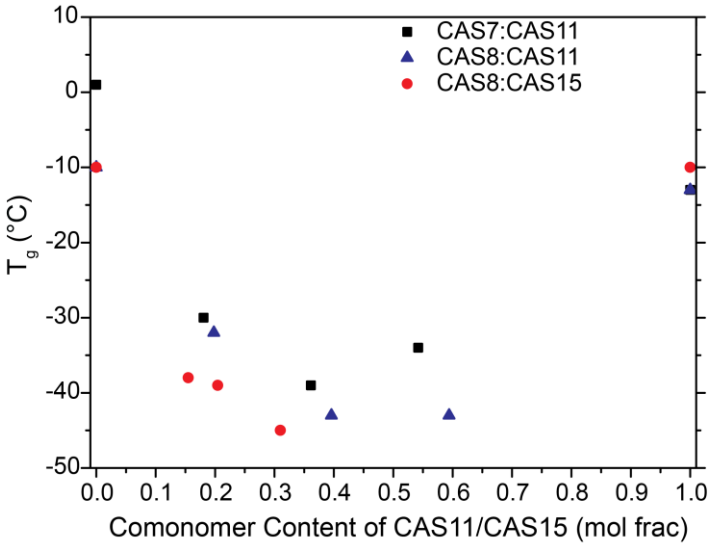


***Figure 4.8 Glass transition temperatures ($T_g$) calculated using the peak of Tan δ measured by DMA and plotted as a function of the CAS11 or CAS15 mole fraction.***

## 4.5 Conclusions

CAS monomers of ring size 11 and 15 were synthesized and photopolymerized into films. We have demonstrated the versatile mechanical properties of photopolymerized cyclic allylic sulfides. The comonomer ratio of cyclic allylic sulfides affects both the kinetics and degree of crystallization which dictates the thermal and mechanical properties of the copolymer. While CAS homopolymers displayed highly brittle nature, the copolymerization of CAS7 or CAS8 with CAS11 or CAS15 produced mechanically robust polymers at near-equimolar comonomer ratios.

## 4.6 References


(1) Miranda Campos, B.; Bourbigot, S.; Fontaine, G.; Bonnet, F. Thermoplastic Matrix-Based Composites Produced by Resin Transfer Molding: A Review. *Polym. Compos.* **2022**, No. February, 2485–2506.

(2) van Rijswijk, K.; Bersee, H. E. N. Reactive Processing of Textile Fiber-Reinforced Thermoplastic Composites – An Overview. *Compos. Part A Appl. Sci. Manuf.* **2007**, *38* (3), 666–681.

(3) Sibikin, I.; Karger-Kocsis, J. Toward Industrial Use of Anionically Activated Lactam Polymers: Past, Present and Future. *Adv. Ind. Eng. Polym. Res.* **2018**, *1* (1), 48–60.

(4) Sycks, D. G.; Safranski, D. L.; Reddy, N. B.; Sun, E.; Gall, K. Tough Semicrystalline Thiol–Ene Photopolymers Incorporating Spiroacetal Alkenes. *Macromolecules* **2017**, *50* (11), 4281–4291.

(5) Sycks, D. G.; Wu, T.; Park, H. S.; Gall, K. Tough, Stable Spiroacetal Thiol-ene Resin for 3D Printing. *J. Appl. Polym. Sci.* **2018**, *135* (22), 46259.

(6) Alim, M. D.; Childress, K. K.; Baugh, N. J.; Martinez, A. M.; Davenport, A.; Fairbanks, B. D.; McBride, M. K.; Worrell, B. T.; Stansbury, J. W.; McLeod, R. R.; Bowman, C. N. A Photopolymerizable Thermoplastic with Tunable Mechanical Performance. *Mater. Horizons* **2020**, *7* (3), 835–842.

(7) Childress, K. K.; Alim, M. D.; Hernandez, J. J.; Stansbury, J. W.; Bowman, C. N. Additive Manufacture of Lightly Crosslinked Semicrystalline Thiol–Enes for Enhanced Mechanical Performance. *Polym. Chem.* **2020**, *11* (1), 39–46.

(8) Deng, S.; Wu, J.; Dickey, M. D.; Zhao, Q.; Xie, T. Rapid Open-Air Digital Light 3D Printing of Thermoplastic Polymer. *Adv. Mater.* **2019**, *31* (39), 1903970.

(9) Kloxin, J. C.; Scott, F. T.; Bowman, N. C. Stress Relaxation via Addition Fragmentation Chain Transfer in a Thiol-Ene Photopolymerization. *Macromolecules* **2009**, *42* (7), 2551–2556.

(10) Evans, R. A.; Rizzardo, E. Free-Radical Ring-Opening Polymerization of Cyclic Allylic Sulfides. *Macromolecules* **1996**, *29* (22), 6983–6989.

(11) Hiijanen-vainio, M.; Varpomaa, P.; Seppala, J.; Tormala, P. Modification of Poly ( Lactides ) by Blending : Mechanical and Hydrolytic Behavior. *Macromol. Chem. Phys.* **1996**, *197*, 1503–1523.

(12) Nijenhuis, A. J.; Grijpma, D. W.; Pennings, A. J. Crosslinked Poly ( L-Lactide ) and Poly ( e-Caprolactone ). *Polymer* **1996**, *37* (13), 2783–2791.

(13) Grijpma, D. W.; Pennings, A. J. (Co)Polymers of L-Lactide, 2. Mechanical Properties. *Macromol. Chem. Phys.* **1994**, *195* (5), 1649–1663.

(14) Jacobsen, S. Plasticizing Polylactide-The Effect of Different Plasticizers on the Mechanical Properties. **1999**, No. 7, 1303–1310.

(15) Anderson, K.; Schreck, K.; Hillmyer, M. Toughening Polylactide. *Polym. Rev.* **2008**, *48* (1), 85–108.

(16) Evans, R. A.; Rizzardo, E. Free-Radical Ring-Opening Polymerization of Cyclic Allylic Sulfides. *Macromolecules* **1996**, *29* (22), 6983–6989.

(17) Evans, R. A.; Rizzardo, E. Free Radical Ring-Opening Polymerization of Cyclic Allylic Sulfides: Liquid Monomers with Low Polymerization Volume Shrinkage. *J. Polym. Sci. Part A Polym. Chem.* **2001**, *39* (1), 202–215.

(18) Evans, R. A.; Rizzardo, E. Free-Radical Ring-Opening Polymerization of Cyclic Allylic Sulfides. 2. Effect of Substituents on Seven- and Eight-Membered Ring Low Shrink Monomers. *Macromolecules* **2000**, *33* (18), 6722–6731.

(19) Harrisson, S.; Davis, T. P.; Evans, R. A.; Rizzardo, E. Chain Transfer in the Sulfur-Centered Free Radical Ring-Opening Polymerization of 3-Methylene-6-Methyl-1,5-Dithiacyclooctane. *Macromolecules* **2000**, *33* (26), 9553–9560.

(20) Scott, T. F.; Schneider, A. D.; Cook, W. D.; Bowman, C. N. Photoinduced Plasticity in Cross-Linked Polymers. *Science* **2005**, *308* (5728), 1615–1617.

(21) Harrisson, S.; Davis, T. P.; Evans, R. A.; Rizzardo, E. Pulsed Laser Copolymerization of Ring-Opening Cyclic Allylic Sulfide Monomers with Methyl Methacrylate and Styrene. *Macromolecules* **2002**, *35* (7), 2474–2480.

(22) Galli, P.; Evans, R. A.; Bertarelli, C.; Bianco, A. Cyclic Allylic Sulfide Based Photopolymer for Holographic Recording Showing High Refractive Index Modulation. *J. Polym. Sci.* **2021**, 1399–1413.

(23) Anslyn, E. V.; Dougherty, D. A. *Modern Physical Organic Chemistry*; University Science Books, 2005.

(24) Ivin, K. J. Thermodynamics of Addition Polymerization. **2000**, *38*, 2137–2146.

(25) Pérez-camargo, R. A.; Arandia, I.; Safari, M.; Cavallo, D.; Lotti, N.; Soccio, M.; Müller, A. J. Crystallization of Isodimorphic Aliphatic Random Copolyesters : Pseudo- Eutectic Behavior and Double-Crystalline Materials. *Eur. Polym. J.* **2018**, *101* (February), 233–247.

(26) Fox, T. G. Influence of Diluent and of Copolymer Composition on the Glass Transition Temperature of a Polymer System. *Bull. Am. Phys. Soc.* **1956**, *1*, 123.

# Chapter 5 Visible Light Photoinitiation and Photoinhibition of Cyclic Allylic Sulfides

## 5.1 Abstract

Thermoplastic stereolithography of cyclic allylic sulfides was previously demonstrated in a commercial DLP 3D printer. The process of layer-by-layer stereolithography can be a time-consuming process that has been recently improved with various continuous processes. Here, we examine the potential of cyclic allylic sulfides in a dual wavelength continuous stereolithographic process. Using photorheology, we determined that the kinetics of a typical visible light initiating system, CQ/EDAB, is inadequate for polymerizing CAS monomers requiring minutes of high intensity irradiation to produce solid films. A better alternative visible light photoinitiator was identified as H-Nu-640 affording polymerization in seconds with mild irradiation (~10 mW/cm$^2$). Photoinhibition of CAS using UV active photoinhibitors were evaluated and found to be inadequate for two-color photoinitiation/photoinhibition systems.

## 5.2 Introduction

The additive manufacturing of photopolymerizable resins through repeated, 2-dimensional, patterned polymer layers requires significant control of the cure depth of resin. Through polymerization inhibition of a thin volume adjacent to the transparent window, stereolithography can proceed in a continuous fashion without adherence to the window.[1,2] The early oxygen-inhibited continuous stereolithography system could achieve

significantly higher print speeds than were attainable at the time by allowing diffusion of oxygen through the transparent window. More recently in stereolithography, latent, photo-activated inhibitors have been used actively to generate stable inhibiting radicals *in situ* to generate a controlled inhibition zone along the irradiation window, effectively removing the need to produce objects in discrete layers.[3] Combining an initiating wavelength and an inhibiting wavelength, this method allows for continuous additive manufacturing using simultaneous dual-wavelength irradiation at enhanced print rates.

Current dual wavelength stereolithography systems are dependent on the orthogonality of a visible light active photoinitiator and an ultraviolet active photoinhibitior. Camphorquinone (CQ), a common Norrish type II blue-light photoinitiator used in dental applications[4] is also commonly used as a visible light initiator in dual wavelength curing systems.[5–7] In these studies the photoinhibition species were chosen for their optical compatibility with CQ, which has a maximum absorbance ($\lambda_{max}$) at 470 nm, and negligible absorption between 340 and 380 nm.

Scott *et al*. described the optical compatibility of using tetraethylthiuram disulfide (TED) as a photoinhibitor for sub diffraction direct-write lithography with CQ as the visible light initiator.[5] Whilst the photoorthogonality of CQ and TED afforded spatiotemporal control of the polymerization, TED participates in chain transfer with propagating radicals leading to stunted polymerization rates with or without the photoinhibiting irradiation.[8] In response to the limitations of TED, other photoinhibiting species were found that didn't affect the polymerization rates under exclusive initiating wavelengths. Stable lophyl radicals generated from bis[2-(*o*-chlorophenyl)-4,5-diphenyl imidazole] (*o*-Cl-HABI)[3] and inhibiting radicals produced from the photolysis of butyl nitrite (BN)[9] were both

successfully used with dual wavelength irradiation to produce 3-dimensional shapes in a single step that are not possible with any other conventional manufacturing method.

The previous demonstrations of photoinhibition systems for continuous 3D printing have been limited to methacrylate formulations while *o*-Cl-HABI was also demonstrated with acrylate and vinyl ether/maleimide systems.[3] Acrylates and methacrylates comprise a majority of stereolithographic which produce non-recyclable thermosets, however, stereolithography of more processable thermoplastics has been recently described using thiol-ene step-growth polymerizations.[10–12] Moreover, we have described a stereolithography resin based on the radical ring-opening cyclic allylic sulfide (CAS) monomers for use in thermoplastic additive manufacturing but the print speeds of current thermoplastic systems remain sluggish. The photoinhibition of novel cyclic allylic sulfides has never been examined with the goal of using the thermoplastic resins in dual wavelength continuous stereolithography to increase the maximum print speed. Here the photoinhibition of thermoplastic CAS stereolithographic resins is examined for its potential in dual wavelength continuous stereolithography. This includes studying the kinetics of various visible light photoinitiator and photoinhibitor combinations.

## 5.3 Experimental

### *5.3.1 Materials*

3-Methylene-1,4-dithiacyclooctane (CAS8) was synthesized as described earlier and used after bulb-to-bulb distillation. Photoinitiator Irgacure 819 was obtained from Ciba Specialty Chemicals (Basel, Switzerland), 1-butyl-2-[5-(1-butyl-1,3-dihydro-3,3-dimethyl-2H-indol-2-ylidene)-penta-1,3-dienyl]-3,3-dimethyl-3H-indolium butyltripehnylborate (H-Nu-640) and 2-

butanoyloxyethyl(trimethyl)azanium;butyl(triphenyl)boranuide (borate V) were obtained from Spectra Photopolymers Inc. (Millbury, OH), and camphorquinone (CQ) and ethyl 4-dimethylaminobenzoate (EDAB) were obtained as a sample from Esstech (Essington, PA). Inhibitors tetraethylthiuram disulfide (TED), butyl nitrite (BN), and (2,2,6,6-Tetramethylpiperidin-1-yl)oxyl (TEMPO) were obtained from Sigma-Aldrich (St. Louis, MO) and 2,2'-Bis(2-chlorophenyl)-4,4',5,5'-tetraphenyl-1,2'-biimidazole (*o*-Cl-HABI) was obtained by Chem Supply Pty. Ltd. (Gillman, AUS).

CAS8 was used a model CAS monomer and was formulated with CQ/EDAB, H-Nu-640/Borate V or Irgacure 819 as the photoinitiating system (Figure 5.1). Owing to the limited solubility of Borate V and H-Nu-640 in CAS monomers, the borate V was dissolved in a small amount of DCM before being added to the resin while mixing and light heating to dissolve solids and remove excess DCM. UV active photoinhibitors TED, butyl nitrite (BN), and *o*-Cl-HABI were used for photo controlled inhibition experiments (Figure 5.2).

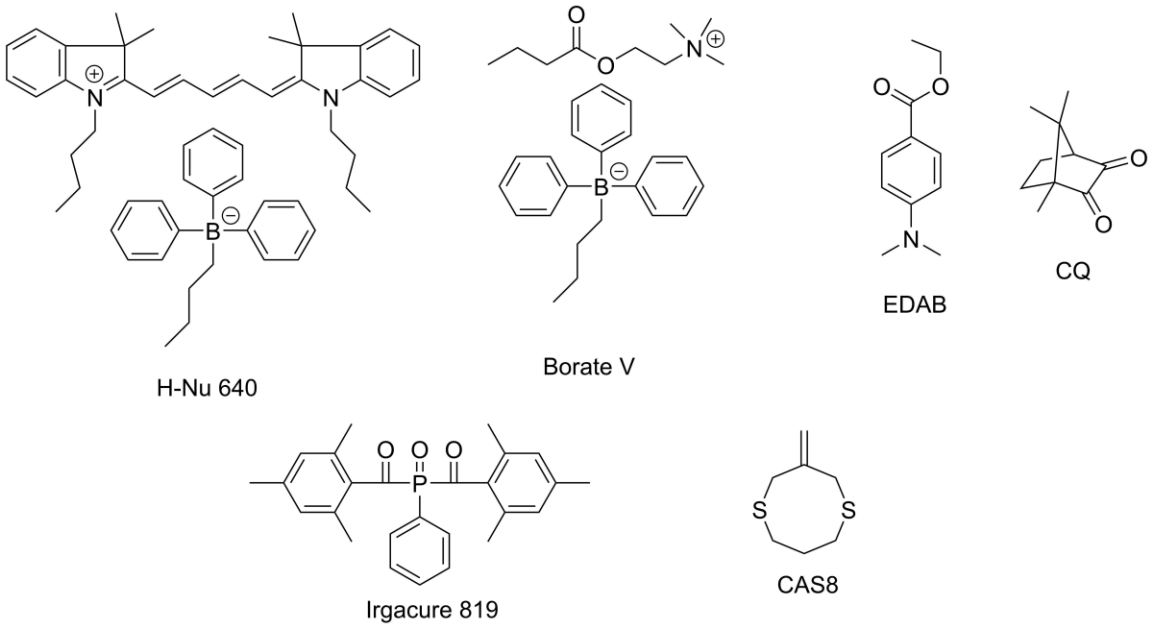


***Figure 5.1 Visible light photoinitiators (H-Nu-640, CQ, Irgacure 819) , coinitiators (Borate V, EDAB) and model CAS monomer (CAS8) used in this study.***

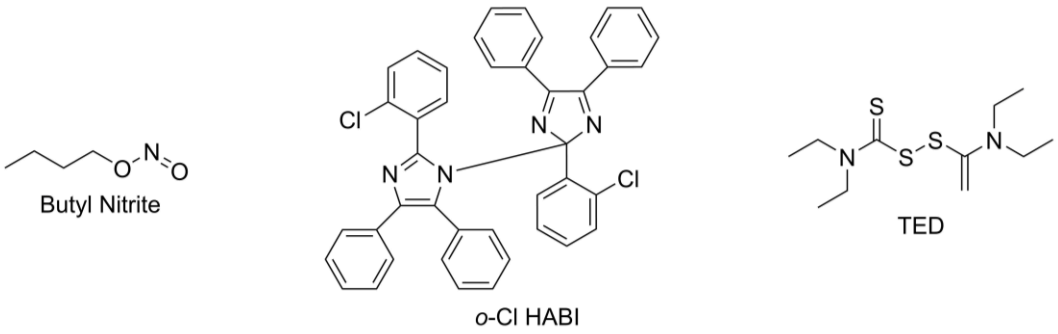


***Figure 5.2 UV active photoinitiators examined in this study***

### *5.3.2 Methods*

#### *5.3.2.1 Rheometry*

Rheometry data was collected using an Anton Paar 702e rheometer with parallel plates. The top plate was 15 mm diameter in size and the bottom plate was made of quartz. UV irradiation and blue irradiation was provided through a liquid light guide fixed below the quartz plate that allowed for radiation from an Omnicure 2000 lamp equipped with a 365 nm wavelength filter for UV or a 400-500 nm bandpass filter for blue light which was calibrated to emit either 10 or 2 $mW/cm^2$ irradiation intensity (as labeled in the experiments) using an International Light IL 1400A radiometer. Red irradiation was supplied using a 660 nm centered LED lamp (ThorLabs). Resin was dropped onto the bottom plate and the top plate moved down to a gap of 0.050 mm. Tests were conducted by applying a 1% strain and 1 Hz frequency on the resin for a total of 5 min, consisting of a 30 sec dark period creating an initial baseline after which the shutter was opened, and the resin was cured under the radiation for the remaining 4.5 min.

## 5.4 Results and Discussion

The radical polymerization of cyclic allylic sulfides was first identified by CSIRO[12,13] before we recently characterized the rapid photopolymerization and demonstrated the stereolithographic potential of CAS monomers. The photoinitiator used in the sterolithographic printing of CAS, Irgacure 819, is a phosphine oxide radical initiator that absorbs in both the UV and violet spectrum. However, the strong absorption in the UV spectrum is incompatible with most studied photoinhibitors which absorb exclusively in

the UV region and are traditionally used in combination with exclusive visible light photoinitiators like camphorquinone (CQ) in photoorthongonal initiation/inhibition systems.[3,5,6] Thus, Irgacure 819 is not orthogonal with known UV-active photoinhibiting systems. Here, the photopolymerization kinetics under visible light is examined to determine a suitable orthogonal visible light photoinitiator. The first choice of photoinitiator is the CQ/EDAB visible light initiator which has been used in previous dual wavelength photoinitiation/photoinhibition systems. However, the real-time modulus development of CQ/EDAB initiating system with CAS8, as recorded by photorheometry, was extremely slow both at 2 mW/cm$^2$ and 10 mW/cm$^2$ (Figure 5.3). Irgacure 819 under the same irradiation conditions has an almost instantaneous rise in storage modulus (G′), corresponding to rapid polymerization and crystallization. Even after 5 minutes of irradiation, the CQ/EDAB system has not achieved full solidification with partially liquid areas and any solids formed are easily fractured and the corresponding G′ still under $10^2$ Pa. The limited polymerization precluded CQ/EDAB from being used as a visible light initiator for CAS monomers.

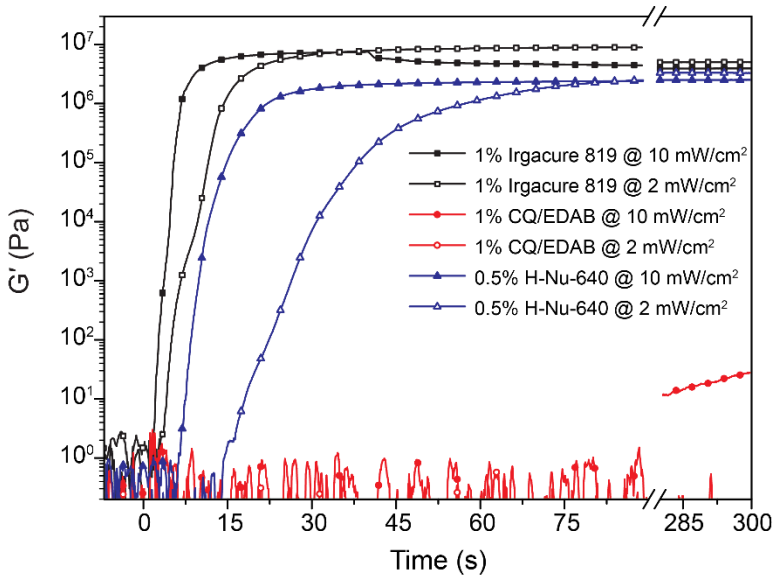


***Figure 5.3 Shear storage modulus trajectories of CAS8 resin at both 10 mW/cm$^2$ (solid) and 2 mW/cm$^2$ (open) with photoinitiating system Irgacure 819 (black), CQ/EDAB (red), and H-Nu-640 (blue).***

H-Nu-640 is also a visible light radical initiator with an absorption spectrum centered at 640 nm and limited absorption below 600 nm. When 0.5 wt% of H-Nu-640 was added to CAS and polymerized using 660 nm light, the polymerization of H-Nu-640 is significantly faster than CQ/EDAB and produces a solid film in less than a minute of irradiation. Even low intensity red light at 2 mW/cm$^2$ displays relatively fast modulus development reaching $10^6$ Pa in around 60 secs while CQ/EDAB at 10 mW/cm$^2$ didn't reach $10^2$ Pa in 5 minutes. Even though CQ/EDAB is typically used in dual wavelength systems, the polymerization, as determined by rheology, is much faster using H-Nu-640 and the low blue absorptivity makes it orthogonal with near-UV photoinhibitors.

The concentration of H-Nu-640 was also evaluated to assess the optimal concentration for both rapid kinetics and sufficiently solid films. Due to the absorbance of H-Nu-640, using a concentration over 1 wt% negatively affects cure through (Figure 5.4).

At a concentration of 2 wt%, the kinetics are significantly slower due to the large gradient caused by the strong absorption of the photons delaying the curing through the full 50 µm gap. The high absorption causes low cure through, and the higher concentration is less soluble in CAS monomers so not desirable for stereolithography applications. At low H-Nu-640 concentration of 0.25 wt%, the G′ at equilibrium is below $10^6$ Pa compared to the $10^7$ Pa of the 2 wt% formulation and this difference correlates well to the initiator concentration as expected. Moderate concentrations of 0.5 wt% and 1 wt% both cure through completely and produced cured materials that displayed similar G′ values as Irgacure 819 did. With both 0.5 wt% and 1 wt% having similar modulus trajectories and equilibrium modulus values, the lower concentration of 0.5 wt% was chosen as the concentration to further test the photoinitiation and photoinhibition character.

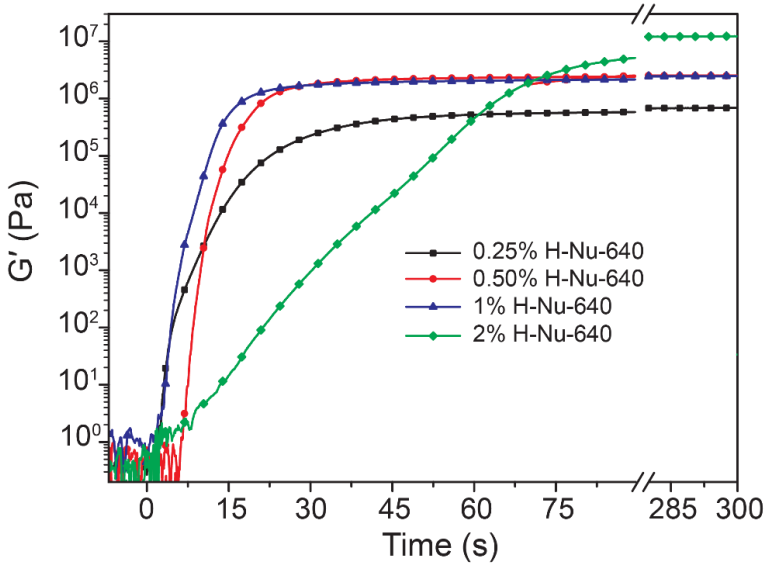


***Figure 5.4 Photopolymerization of H-Nu-640 using 660 nm LED lamp at 10 mW/cm$^2$***

Tetraethylthiuram disulfide (TED) photocleaves into 2 dithiocarbamyl radicals that can react with propagating carbon radicals and cause termination.[8] The ability of the dithiocarbamyl radicals to terminate polymers was exploited in two-color sub-diffraction lithography.[5] Here, TED is used as a UV-active inhibitor paired with H-Nu-640, which has limited near-UV absorption similar to the CQ/EDAB system used with TED previously. When irradiated with exclusive 660 nm light, the polymerization of CAS8 should be unhindered by the UV-active inhibitor. However, using 1 wt% of TED at 660 nm severely inhibits the polymerization as seen by the lack of storage modulus development (Figure 5.5a). When the concentration is reduced to 0.5 wt% the inhibition is reduced and the modulus reaches $10^4$ Pa after 5 minutes of irradiation but still below the value that would result in a solid robust film seen previously in the CAS8 films cured by Irgacure 819. Under exclusive 365 nm irradiation, the polymerization is also strongly inhibited at 1 wt% TED but initiates in the first minute at 0.5 wt% TED (Figure 5.5b). The TED concentration does influence the inhibition of the polymerization, but the behavior is almost identical under UV or red irradiation precluding the use in a dual-wavelength photoinitiation and photoinhibition system. Regardless of the photoinhibiting abilities, the presence of TED interferes with any polymerization at all wavelengths including exclusive initiating wavelengths. Along with the cleaved dithiocarbamyl radicals, TED itself can also participate in chain transfer reactions with propagating radicals. The chain transfer regardless of whether TED or dithiocarbamyl radicals are present could explain the photoinhibition occurring regardless of wavelength.

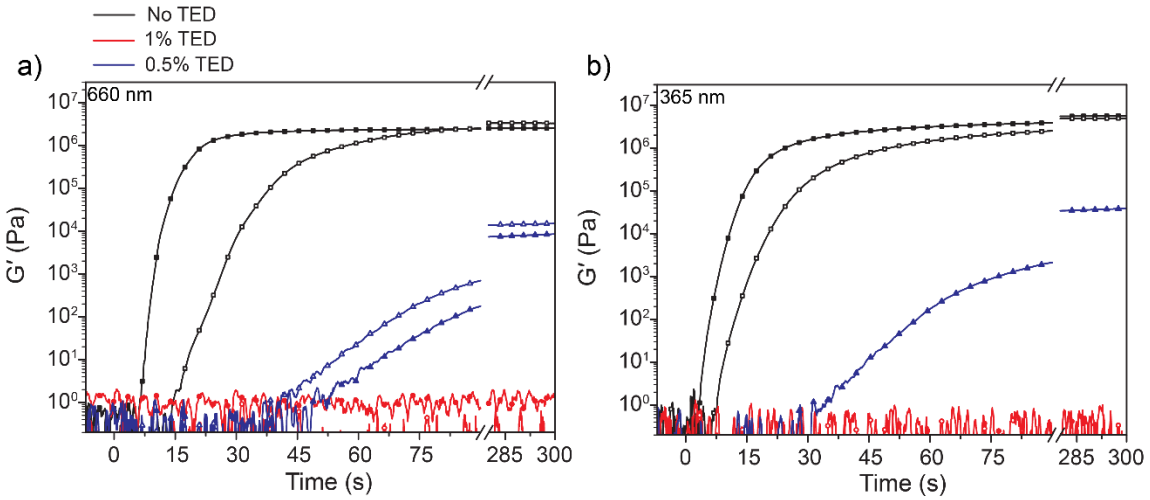


***Figure 5.5 Shear storage modulus trajectories of CAS8 with H-Nu-640 photoinitiator with TED as photoinhibitor at concentrations of 1 wt% (red), 0.5 wt% (blue), or 0 wt% TED (black) using a) 660 nm irradiation and b) 365 nm irradiation at both 10 mW/cm$^2$ (solid) and 2 mW/cm$^2$ (open) light intensity.***

Owing to the proclivity of TED to participate in deleterious chain transfer, UV-active *o*-Cl-HABI was studied as an alternative for photoinhibition. The inhibition of (meth)acrylates using lophyl radicals produced by photolabile o-Cl-HABI do not initiate (meth)acrylate polymerizations by themselves but can terminate growing radical chains to inhibit polymerization.[3] Here, o-Cl-HABI is used as the UV photoinhibitor with H-Nu-640 being the visible photoinitiator. In contrast to TED, polymerization of CAS8 at 660 nm is unaffected by the addition of the photoinhibitor as expected, HABI doesn't participate in the same deleterious chain transfer of the propagating radicals leading to the polymerization rate being similar with and without HABI (Figure 5.6a). However, under exclusive UV light, the polymerization of CAS behaves similar to the exclusive red light polymerization (Figure 5.6b). The polymerization at 365 nm suggests that the generated lophyl radicals do not hinder the polymerization in any way and when compared to the photoinhibition of acrylates, methacrylates, and vinyl ether/maleimide systems[6], the

photoinhibition of CAS monomer with HABI is not effective at all. Thus, HABI is not a good choice for photoinhibition of CAS polymerizations.

HABI has been shown to be a poor initiator of (meth)acrylate polymerizations but is a capable initiator of radical thiol-ene initiator when paired with a hydrogen donor like a thiol.[14] In order to rule out any photoinitiating effects of HABI, CAS polymerization was observed under 365 nm without the H-Nu-640 photoinitiator. When CAS is polymerized with HABI, the storage modulus does not increase upon irradiation and the monomer remains liquid thus confirming that HABI does not initiate CAS ring opening polymerization (see Figure 5.6b).

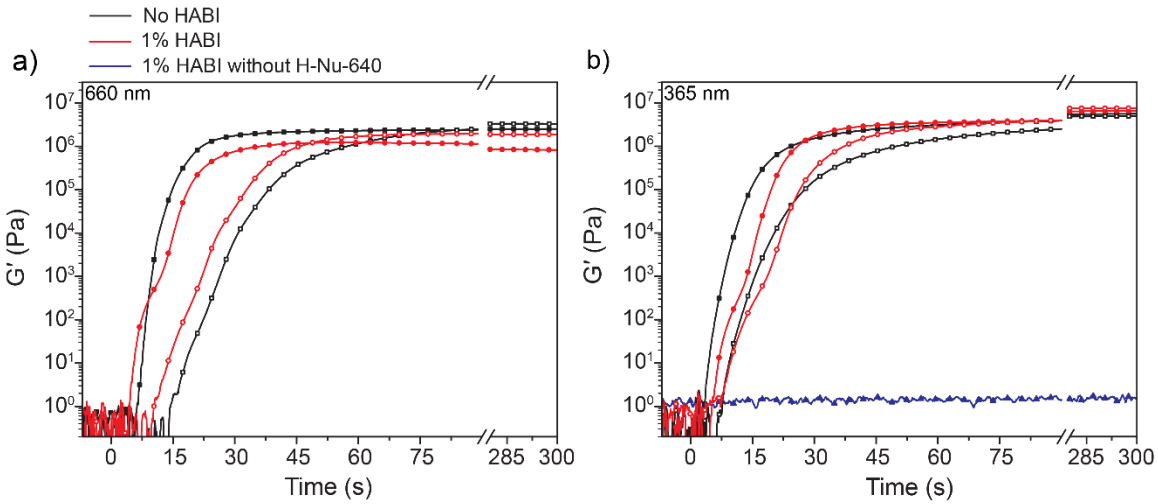


***Figure 5.6 Shear storage modulus trajectories of CAS8 with H-Nu-640 photoinitiator with o-Cl-HABI as photoinhibitor at concentrations of 1 wt% (red), or 0 wt% TED (black) using a) 660 nm irradiation and b) 365 nm irradiation at both 10 mW/cm$^2$ (solid) and 2 mW/cm$^2$ (open) light intensity. o-Cl-HABI at 1 wt% without H-Nu-640 did not have any initiation effects (blue).***

Similar to TED and HABI, butyl nitrite (BN) is a UV-active photoinhibitor that exhibits weak absorbance in the visible region thus complementing the visible light

initiator, H-Nu-640. BN cleaves under UV irradiation to generate nitric oxide and an alkoxy radical, while the alkoxy can initiate polymerization, the nitric oxide reacts with 3 propagating radicals in a series of inhibition events. The photoinhibition of free-radical acrylate polymerizations was found to be effective but the effectiveness was strongly dependent on the structure of the monomer.[6]

To identify the inhibiting potential of alkyl nitrites on CAS ring opening polymerizations, butyl nitrite was added to CAS8 resins with H-Nu-640 as an initiator and examined under exclusive visible red light and exclusive UV irradiation. The development of the storage modulus gives us an approximation of the polymerization that is occurring and the rate at which it is occurring. Under exclusive red light, the polymerization of CAS proceeds at a similar rate with or without the addition of BN (Figure 5.7a). The induction time is slightly reduced with the addition of BN while the actual rate of storage modulus increase is slightly lower. While the polymerization is unaffected under exclusive initiating irradiation, the polymerization is only slightly affected at exclusive inhibiting irradiation as well (Figure 5.7b). Notably, the inhibited 365 nm polymerization does lead to lower equilibrium G′ at both 2 and 10 mW/cm$^2$ and more clearly shows an inflection point which has been previously found to indicate the period between polymerization and crystallization processes. This may either be a result of lower molecular weights and slower crystallization due to slower development of larger molecular weight polymers or the result of BN affecting the crystal structure of CAS8. Since the visible light storage modulus development occurs more rapidly and displays a small inflection point, it is reasonable to assume that BN doesn’t affect the crystal structure but instead has a small inhibition effect at 365 nm. The inhibition effect is still much too slow to be useful in two color

photoinitiation/photoinhibition systems. To further rule out the photoinitiation of BN at inhibiting 365 nm wavelength, resin was formulated with only CAS8 and BN without H-Nu-640. The BN-only formulation did show modulus increase over time but the induction time in initiation indicates that the initiation has only a minor effect on the mechanical properties of the polymer.

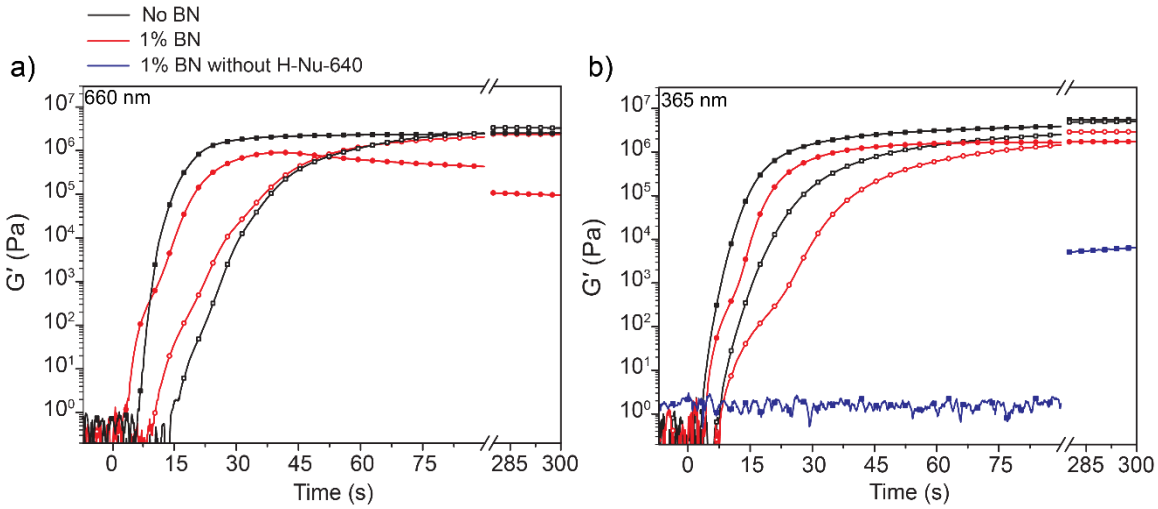


***Figure 5.7 Shear storage modulus trajectories of CAS8 with H-Nu-640 photoinitiator with BN as photoinhibitor at concentrations of 1 wt% (red), or 0 wt% TED (black) using a) 660 nm irradiation and b) 365 nm irradiation at both 10 mW/cm$^2$ (solid) and 2 mW/cm$^2$ (open) light intensity. BN at 1 wt% without H-Nu-640 had minor initiation effects after minutes of irradiation (blue).***

The inhibition of CAS using lophyl, and nitroxide radicals all are quite ineffective at inhibiting the radical polymerization of CAS8 and TED inhibits polymerization at all wavelengths. Other methods of inhibition include the traditional CLIP method which uses oxygen to inhibit radical polymerizations. Thiol-ene polymerizations are incompatible with CLIP due to the ability of peroxy radicals to initiate hydrogen abstraction reactions but oxygen inhibition works well with typical step-growth radical polymerizations. Even

though CAS polymerization don't involve a hydrogen donating thiol, it has been suggested that the polymerization of CAS is less sensitive to oxygen than typical chain-growth radical polymerizations.[15] The photopolymerization of CAS in all tests is completed in an ambient atmosphere but does not preclude that there could be oxygen inhibition at the surface. The inhibition due to oxygen was evaluated by photopolymerizing a drop of CAS8 in open air. In radical polymerizations, the polymer surface can often feel sticky due to inadequate polymerization at the polymer-air interface where oxygen concentration is highest. Compared to acylate drops, the CAS drops had no sticky feel which led credence to the notion that CAS would be less compatible with the CLIP method than traditional radical polymers.

Nitroxide-mediated polymerization (NMP) is a technique using stable nitroxide radicals to control propagation by termination of propagating radicals and reversible cleavage to control polymer distribution. A common stable nitroxide radical and radical inhibitor is (2,2,6,6-Tetramethylpiperidin-1-yl)oxyl (TEMPO) and similar to lophyl radicals, the nitroxide radicals are stable through electron delocalization and steric hinderance of the recombined dimer. As opposed to HABI, TED, and BN, the TEMPO radicals are stable and don't recombine so they don't require UV light to produce the radicals. Using TEMPO's ability to trap and identify radicals, it was investigated to determine if nitroxide radicals could terminate polymerization more efficiently than lophy radicals or alkyl nitrite. When a small amount of TEMPO (0.15 wt%) was added to a resin with H-Nu-640 and CAS8 as described previously, the induction time of polymerization is significantly extended (Figure 5.8). Compared to inhibition with lophyl radicals or alkyl

nitrite, the TEMPO radicals show significant inhibition of polymerization at both 365 nm and 660 nm.

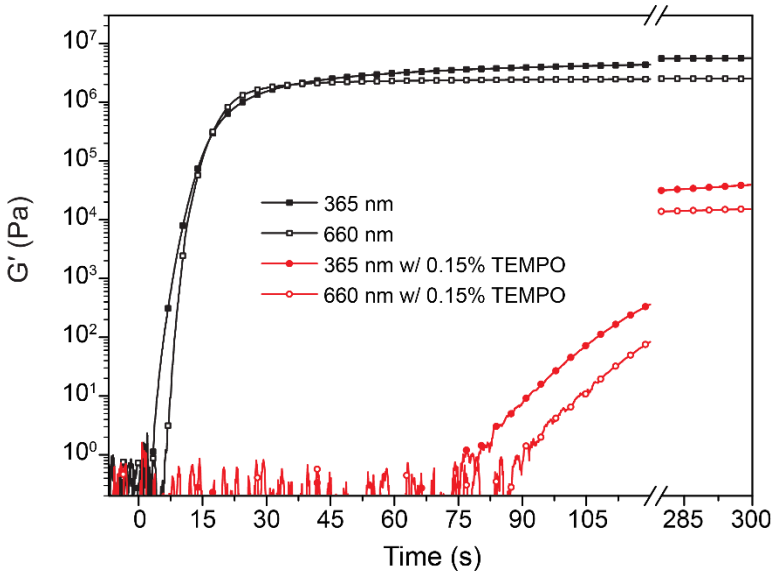


***Figure 5.8 Storage modulus trajectories of CAS8 with H-Nu-640 photoinitiator with 0.15 wt% TEMPO (red) and without TEMPO (black) using both 365 nm (solid) and 660 nm light (open).***

The inhibition by TEMPO showed the most promise for inhibiting CAS polymerization. The concentration was arbitrarily chosen to attempt to use as minimal as possible and a larger concentration of TEMPO would surely inhibit the polymerization longer. Since TEMPO is not photoactive, using TEMPO is not a strategy for two color photoinitiation/photoinhibition but instead shows that nitroxide radicals inhibit CAS polymerization better than common photoinhibitors. The inhibition of CAS using TEMPO leaves open the possibility for using CAS in dual wavelength stereolithography but other less common types of inhibiting radicals will have to be developed for use with CAS.

## 5.5 Conclusions

We have demonstrated that the radical ring-opening polymerization of CAS monomers is not as easily adapted to dual wavelength printing as has been demonstrated with (meth)acrylate and vinyl ether systems. The common visible light photoinitiator for dual wavelength additive manufacturing, camphorquinone, was found to initiate the polymerization of CAS too slowly to be used in additive manufacturing. H-Nu-640 was proposed as a better visible light photoinitiator for CAS polymerization under red irradiation and was shown to polymerize at comparable rates to previously studied near-UV initiator, Irgacure 819. The photoorthogonality of H-Nu-640 and near-UV photoinhibitors; TED, HABI, and BN made them good candidates for creating a photoinitiation and photoinhibition system. TED proved to interfere with polymerization at exclusive initiating wavelengths likely due to its ability to participate in chain transfer reactions with propagating radicals. HABI and BN both proved to be inefficient inhibitors for CAS polymerizations with minimal, if any, reduction of polymerization under exclusive inhibition wavelengths. Lastly, we propose a potential better type of inhibitor by showing the inhibition of CAS polymerization using TEMPO radicals. Although not UV-activated, the TEMPO radicals proved to be more efficient inhibitors than the radicals generated by HABI or BN. This study rules out and proposes potential methods for novel allylic sulfide photopolymer thermoplastics to be adapted to continuous dual wavelength additive manufacturing.

## 5.6 References


(1) Tumbleston, J. R.; Shirvanyants, D.; Ermoshkin, N.; Janusziewicz, R.; Johnson, A. R.; Kelly, D.; Chen, K.; Pinschmidt, R.; Rolland, J. P.; Ermoshkin, A.; Samulski, E. T.; DeSimone, J. M. Continuous Liquid Interface Production of 3D Objects. *Science* **2015**, *347* (6228), 1349–1352.

(2) Janusziewicz, R.; Tumbleston, J. R.; Quintanilla, A. L.; Mecham, S. J.; DeSimone, J. M. Layerless Fabrication with Continuous Liquid Interface Production. *Proceedings of the National Academy of Sciences of the United States of America*. 2016, pp 11703–11708.

(3) de Beer, M. P.; van der Laan, H. L.; Cole, M. A.; Whelan, R. J.; Burns, M. A.; Scott, T. F. Rapid, Continuous Additive Manufacturing by Volumetric Polymerization Inhibition Patterning. *Sci. Adv.* **2019**, *5*.

(4) Alvim, H. H.; Alecio, A. C.; Vasconcellos, W. A.; Furlan, M.; de Oliveira, J. E.; Saad, J. R. C. Analysis of Camphorquinone in Composite Resins as a Function of Shade. *Dent. Mater.* **2007**, *23* (10), 1245–1249.

(5) Scott, T. F.; Kowalski, B. A.; Sullivan, A. C.; Bowman, C. N.; McLeod, R. R. Two-Color Single-Photon Photoinitiation and Photoinhibition for Subdiffraction Photolithography. *Science* **2009**, *324* (5929), 913–917.

(6) Van Der Laan, H. L.; Burns, M. A.; Scott, T. F. Volumetric Photopolymerization Confinement through Dual-Wavelength Photoinitiation and Photoinhibition. *ACS Macro Lett.* **2019**, *8* (8), 899–904.

(7) Li, F.; Thickett, S. C.; Maya, F.; Doeven, E. H.; Guijt, R. M.; Breadmore, M. C. Rapid Additive Manufacturing of 3D Geometric Structures via Dual-Wavelength Polymerization. *ACS Macro Lett.* **2020**, *9* (10), 1409–1414.

(8) Lovell, L. G.; Elliott, B. J.; Brown, J. R.; Bowman, C. N. The Effect of Wavelength on the Polymerization of Multi(Meth)Acrylates with Disulfide/Benzilketal Combinations. *Polymer* **2001**, *42* (2), 421–429.

(9) Childress, K. K.; Alim, M. D.; Hernandez, J. J.; Stansbury, J. W.; Bowman, C. N. Additive Manufacture of Lightly Crosslinked Semicrystalline Thiol–Enes for Enhanced Mechanical Performance. *Polym. Chem.* **2020**, *11* (1), 39–46.

(10) Alim, M. D.; Childress, K. K.; Baugh, N. J.; Martinez, A. M.; Davenport, A.; Fairbanks, B. D.; McBride, M. K.; Worrell, B. T.; Stansbury, J. W.; McLeod, R. R.; Bowman, C. N. A Photopolymerizable Thermoplastic with Tunable Mechanical Performance. *Mater. Horizons* **2020**, *7* (3), 835–842.

(11) Sycks, D. G.; Wu, T.; Park, H. S.; Gall, K. Tough, Stable Spiroacetal Thiol-ene Resin for 3D Printing. *J. Appl. Polym. Sci.* **2018**, *135* (22), 46259.

(12) Evans, R. A.; Rizzardo, E. Free-Radical Ring-Opening Polymerization of Cyclic Allylic Sulfides. *Macromolecules* **1996**, *29* (22), 6983–6989.

(13) Evans, R. A.; Rizzardo, E. Free Radical Ring-Opening Polymerization of Cyclic Allylic Sulfides: Liquid Monomers with Low Polymerization Volume Shrinkage. *J. Polym. Sci. Part A Polym. Chem.* **2001**, *39* (1), 202–215.

(14) Ahn, D.; Sathe, S. S.; Clarkson, B. H.; Scott, T. F. Hexaarylbiimidazoles as Visible Light Thiol-Ene Photoinitiators. *Dent. Mater.* **2015**, *31* (9), 1075–1089.

(15) Yamada, S.; Goto, Y. Reduction of Oxygen Inhibition in Photopolymerization of Cyclic Allylic Sulfide Monomers. *J. Photopolym. Sci. Technol.* **2010**, *23* (1), 109–114.

# Chapter 6 Summary and Future Work

## 6.1 Research Summary

In this dissertation we first demonstrated hexaarylbimidazoles in two-stage reinforcing polymers using orthogonal nucleophilic and radical thiol-ene additions to generate thioethers. Functionalized hexaarylbimidazoles proved to be capable *in situ* initiators of thiol-ene radical polymerizations in the solid state using either UV light or mechanical stress as the stimulus. Later, we identified the thioether rearrangement in the radical-mediated ring opening polymerization of cyclic allylic sulfides to be useful for increasing layer adhesion in thermoplastic stereolithographic 3D printing. First, identifying and characterizing 7- and 8-membered cyclic allylic sulfides as rapid polymerizing and crystallizing photopolymers and demonstrating their use in stereolithography. Then, expanding the library of photopolymerizable cyclic allylic sulfides to include 11- and 15-membered cyclic allylic sulfides and their copolymers with 7- and 8-membered monomers to produce tougher polymers that encompass a wider range of mechanical properties. Finally, the radical polymerization of cyclic allylic sulfides using visible light initiators was examined along with their ability to be inhibited with known radical photoinhibitors.

In Chapter 2 we designed two-stage polymer films using the orthogonality of the nucleophilic and radical thiol-ene additions. Adapting polymeric materials to respond to their environment affords polymers with better safety and reliability, longer lifespans, and lower polymer waste.[1] Typical approaches to adaptable polymeric materials utilize stimuli-induced self-healing requiring additional energy input to the system for macroscopic

damage healing. Instead, we focused on using the typically destructive, mechanical stress as a stimulus to initiate *in situ* crosslinking. Mechanically triggered crosslinking has focused on proof-of-concept crosslinking in the liquid phase to cause gelation.[2,3] Although demonstrated in tough hydrogels,[4] the repeated mechanically-induced crosslinking has been a challenge due to both the complex mechanophore activation and crosslinking reactions in the solid state. For improved solid-state reactions, we employed orthogonal thiol-ene reactions that proceed efficiently under ambient conditions and without the need for solvent and proved to be capable of generating crosslinking thioethers *in situ* in the solid state. For triggering the radical thiol-ene reaction, we employed a functionalized HABI which has been previously shown to be a capable of mechanophore,[5] and thiol-ene initiator.[6] Without much optimization of the network, the mechanically triggered thiol-ene reaction afforded highly cross-linked polymers with higher $T_g$s and storage moduli capable of endless variation through the choice of monomers and stoichiometric ratios.

In Chapter 3 we examined the kinetics of the radical-mediated photopolymerization of cyclic allylic sulfides and demonstrated their utility as semi-crystalline thermoplastic polymers for stereolithography. Typical stereolithographic resins consist of thermosetting resins that afford highly crosslinked polymers that lack the processability or recyclability of thermoplastics. The thermoplastic resins previously developed using thiol-ene chemistry lacked strong interlayer adhesion and thus printability.[7–9] Cyclic allylic sulfides undergo radical ring-opening polymerization by way of an addition-fragmentation chain transfer mechanism which allows for chain transfer to polymerized chains in adjacent stereolithographic layers. First, the photopolymerization and crystallization kinetics of 7- and 8- membered CAS rings were examined for their use in stereolithographic additive

manufacturing. Then, using a commercial DLP 3D printer, the increased layer adhesion was demonstrated by 3D printing dogbone mechanical testing samples in different orientations and applying stress to the interlayer adhesions. The mechanical properties of printed parts were comparable to the bulk properties irrespective of the orientation in which they were printed.

In Chapter 4 we expanded the library of photopolymerized cyclic allylic sulfides by synthesizing 11- and 15-membered cyclic allylic sulfides. The previously examined 7- and 8-membered cyclic allylic sulfides polymerized and crystallized rapidly but the resulting properties were quite brittle. Several strategies for increasing toughness have been previously used for semi-crystalline ring-opening polymerizations of polyamides like 7-membered ε-caprolactam. The copolymerization of 7-membered ε-caprolactam with 13-membered ω-laurolactam lowered the crystallinity and increased ductility and toughness.[10] Inspired by larger polyamides, larger 11- (CAS11) and 15-membered (CAS15) cyclic allylic sulfides were synthesized successfully and reduced the crystallinity and increased the toughness when copolymerized with 8-membered cyclic allylic sulfides. Photopolymerization of all combinations CAS comonomers proceeded rapidly while the crystallization rate was related to the comonomer ratio. Compared to CAS8 homopolymers, CAS8:CAS11 copolymers displayed up to 2000% higher tensile toughness.

In Chapter 5 we studied the photoinhibition of cyclic allylic sulfides using hexaarylbimidazole (HABI), butyl nitrite (BN), and tetraethylthiuram disulfide (TED). Photoinhibition of radical chain-growth polymerization is a key foundation of dual wavelength continuous stereolithography.[11] Continuous stereolithography removes excessive steps required in stereolithography to separate each printed layer from the

transparent window and recoat the window with resin affording print speeds in excess of 1 m/hr.[12,13] HABI, BN, and TED have been demonstrated to photoinhibit radical chain-growth of acrylate and methacrylate monomers. However, the photoinhibition of radical ring-opening cyclic allylic sulfides has not been previously studied. The poor polymerization of typical visible light initiating system of camphorquinone (CQ) necessitated the use of other visible light initiators, we show that polymerization using the red-light active H-Nu-640 radical initiator is effective. However, the photoinhibition of H-Nu-640 polymerized CAS monomers was not as effective. BN and HABI did not sufficiently suppress polymerization at the inhibiting ultraviolet wavelengths any more than the polymerization at initiating red wavelengths. TED proved to inhibit polymerization at inhibiting wavelengths but also at initiating wavelengths, rendering it useless as an inhibitor for dual wavelength 3D printing.

The generation of thioethers using thiol-ene chemistry is a powerful tool for facile organic coupling. Thioethers may not be as strong as their ether counterparts but enable simpler generation and rearrangement which can be an incredible tool in polymer functional materials. The work in this thesis illustrates the utility of thioether chemistry from building the backbone of orthogonal two-stage polymers to thioether rearrangement in thermoplastic polymers during stereolithography.

### 6.2 Future Directions

The results in Chapter 2 demonstrate the potential of hexaarylbimidazoles as mechanophores in two-stage polymer films. While we described the proof-of-concept solid state thiol-ene initiation of HABI using orthogonal thiol-ene chemistry, we have yet to optimize the system for a wider range of applications. Optimization of both the toughness

and the force necessary to activate the mechanophore can be achieved to further tailor the films to different end-use applications. The toughness of the first stage and second stage film are important to dictate end use and we described how some of the mechanical properties can be tailored by changing the thiol monomers or the allyl:acrylate ratio in the formulation. Further diversifying the choice of monomers beyond the scope of the tested monomers is an available option to modify the mechanical properties. A preliminary test using a small percentage of urethane diacrylate monomer along with tetraacrylate HABI resulted in a noticeable improvement in mechanical properties of the first stage film. Adding in monomers with supramolecular interactions like urethane or urea groups with hydrogen bonding is a good starting point for creating tougher first stage films. Changing the toughness of the first stage film does have an additional effect on the activation of the mechanophore. With increased supramolecular bonding, the energy dissipation through the film would be increased and affect how the force is transferred through the film to the mechanically labile HABI bond.

Strategies to modify the force threshold of mechanophores have been previously described and rely mostly on modifying the connectivity of the mechanophore to the network or changing the architecture of the network itself. The connection of the mechanophore to the bulk polymer plays a large role in whether the mechanophore is activated and the extent of activation.[14] With this in mind, it would add value to be able to synthesize a library of HABI monomers with various functionalities to further optimize the activation of the HABI. An advantage of using HABI is the extensive research using HABI including various synthetic studies to produce functionalized HABI. Mechanophores are often placed in the middle of long linear polymers to increase the opposing forces on the

mechanically labile bond and cause scission. Difucntionalized HABI could offer a better transfer of force to the C-N bond over the tetrafunctional HABI. Using a different synthesis pathway, a di-functional HABI can be synthesized instead of the tetra-functional HABI and functionalized with an acrylate functional group in the same manner as the tetraacrylate HABI.[6] Instead of synthesizing difunctionalized benzil to generate the difunctionalized triarylimidazoles and tetrafunctionalized HABI, the benzaldehyde can be functionalized and then reacted with unsubstituted benzil to create monofunctionalized triarylimidazoles. These triarylimidazoles then dimerize to form the di-functionalized HABI (Figure 6.1).

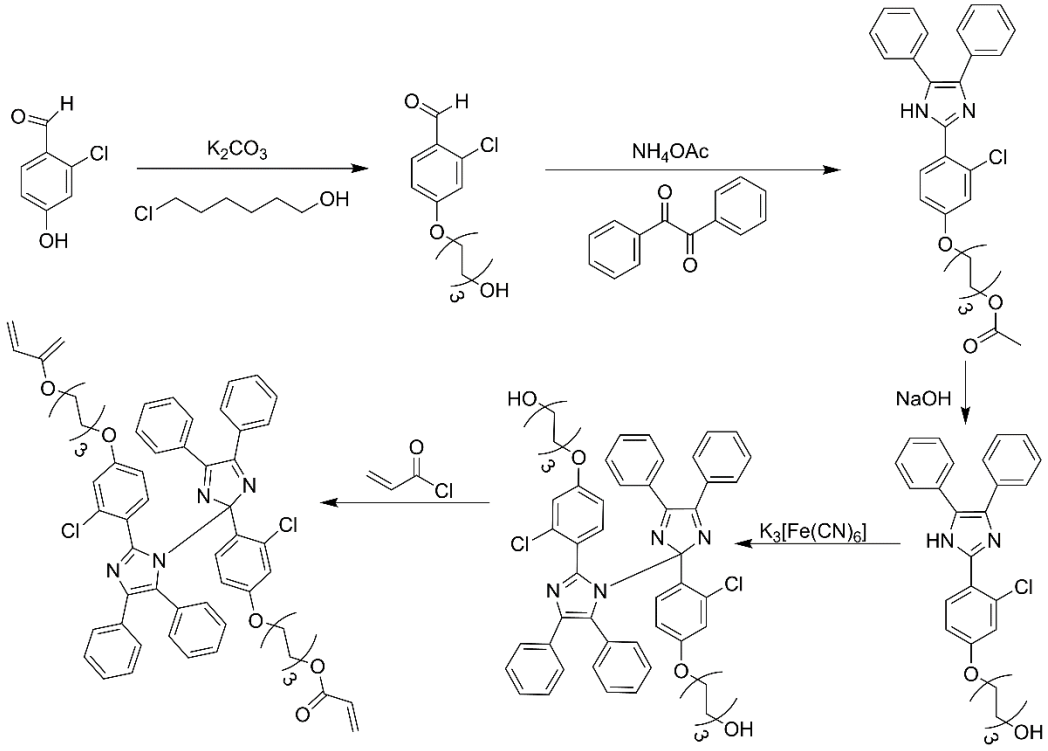


***Figure 6.1 Possible synthetic pathway for diacrylate HABI***

The results in chapters 3, 4, and 5 demonstrate the potential of using cyclic allylic sulfides in thermoplastic stereolithography with the rapid photopolymerization and mechanical tunability. The mechanical properties of semi-crystalline polymers depend on

the crystal structure and degree of crystallinity. Using light to polymerize CAS monomers, the control over the polymer molecular weight and orientation of the crystallites is minimal. Many common plastic products produced through processes like injection molding, film blowing, and fiber spinning are created with highly oriented crystallites. The orientation in the crystallites is caused by the axial strain put on the polymer melt during crystallite formation which increases the orientation of crystallites in the axial direction. This strain-induced crystallization increases the tensile properties of the semi-crystalline polymer in the direction of crystal orientation. In stereolithography, the printed materials tend to be anisotropic due to the weak points caused by the layer interfaces. Due to their semi-crystalline nature, oriented crystallites of CAS polymers can be produced in the axial direction to increase the tensile properties of the material. With the introduction of strain on the polymer during the delay that was seen between polymerization and crystallization during photocuring, the crystallites would form in a more highly oriented fashion and subsequently increase the tensile properties. The strain would have to be produced by a vertical movement of the build head or the resin bath at the exact time after polymerization to increase tension on the polymer after it adhered to both the build head and bottom of the resin bath. The strain on the polymer melt during crystallization should produce strain-oriented crystallites. While there are some challenges in accomplishing this, strain-induced crystallization of CAS polymers during stereolithography could greatly expand the potential opportunities for using thermoplastic stereolithography.

The radical-initiated polymerization using UV or near UV light yielded rapid polymerization rates and good mechanical properties. However, the polymerization using

visible light initiators was less effective with both slower rates and weaker properties. The visible light initiator that produced the best materials was H-Nu-640 but still had reduced mechanical properties and limited photoinhibition using known photoinhibitors. Other visible light photoinitiators are known as efficient visible light initiators with high quantum yield. Amine-free visible light photoinitiators that improve on the low absorptivity of camphoquinone (CQ) have been reported as suitable substitutes to CQ. Substitutes like modified germanium photoinitiators developed as an analog to the phosphine oxide initiators like Irgacure 819 and MAPO have shown promise as a one-component visible light initiators (Figure 6.2). The germanium initiator, dibenzoyldiethylgermane (DBDEGe), proved to have improved quantum yields to Irgacure 819 and generally showed better photoinitiating performance to Irgacure 819 or CQ/EDAB.[15,16] As an improved substitute for CQ, these one component visible light initiators could afford better initiating of CAS monomers under visible light conditions and potentially a better candidate for developing novel dual wavelength thermoplastic stereolithography.

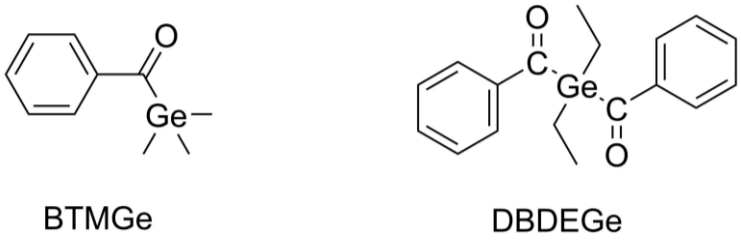


***Figure 6.2 Germanium-based one component visible light photoinitiators***

Instead of developing new photoinitiators, new photoinhibitors can be developed and tested with CAS monomers. TEMPO radicals showed potential in inhibiting CAS polymerizations but are too stable to exist as dimers and thus can't be photoactivated. An analog to TEMPO is the sulfur-substituted TEMPS which has been documented previously. The original synthetic method for producing TEMPS by J.E. Bennett in 1967 had many issues including low yield and difficult purification with a considerable amount of trisulfide products being produced (Figure 6.4).[17] A revised synthetic method for producing TEMPS in a two-step synthesis reduced the amount of trisulfide product produced to only trace amounts allowing for efficient purification and better yields.[18] TEMPS has been studied as a substitute for TEMPO in living/controlled radical polymerizations but the behavior is not exactly the same as TEMPO.[19] Nevertheless, the disulfide linkage in the dimer is reversible and the stable thionitroxyl radicals do have inhibiting properties that are more suitable for inhibiting propagating thiyl radicals and are worth investigating further.

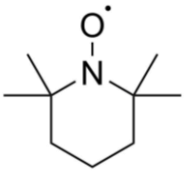


TEMPO

a)

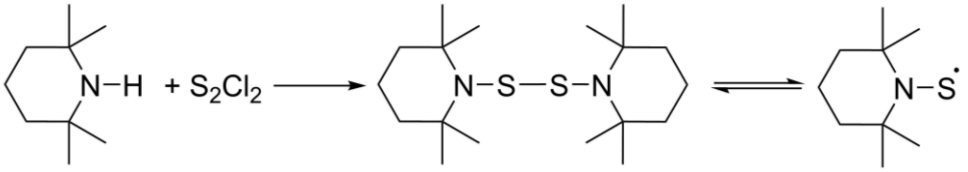


TEMPS

b)

***Figure 6.3 a) Radical inhibitor TEMPO and b) the one-step synthesis method and reversible dissociation of diTEMPS into the radical inhibitor TEMPS***

## 6.3 References


(1) Patrick, J. F.; Robb, M. J.; Sottos, N. R.; Moore, J. S.; White, S. R. Polymers with Autonomous Life-Cycle Control. *Nature* **2016**, *540* (7633), 363–370.

(2) Ramirez, A. L. B.; Kean, Z. S.; Orlicki, J. A.; Champhekar, M.; Elsakr, S. M.; Krause, W. E.; Craig, S. L. Mechanochemical Strengthening of a Synthetic Polymer in Response to Typically Destructive Shear Forces. *Nat. Chem.* **2013**, *5* (9), 757–761.

(3) Gordon, M. B.; Wang, S.; Knappe, G. A.; Wagner, N. J.; Epps, T.; Kloxin, C. Force-Induced Cleavage of a Labile Bond for Enhanced Mechanochemical Crosslinking. *Polym. Chem.* **2017**, 6485–6489.

(4) Matsuda, A. T.; Kawakami, R.; Namba, R.; Nakajima, T.; Ping, J. Mechanoresponsive Self-Growing Hydrogels Inspired by Muscle Training. *Science* **2019**, *363* (February), 504–508.

(5) Verstraeten, F.; Göstl, R.; Sijbesma, R. P. Stress-Induced Colouration and Crosslinking of Polymeric Materials by Mechanochemical Formation of Triphenylimidazolyl Radicals. *Chem. Commun.* **2016**, *52* (55), 8608–8611.

(6) Ahn, D.; Sathe, S. S.; Clarkson, B. H.; Scott, T. F. Hexaarylbiimidazoles as Visible Light Thiol-Ene Photoinitiators. *Dent. Mater.* **2015**, *31* (9), 1075–1089.

(7) Sycks, D. G.; Wu, T.; Park, H. S.; Gall, K. Tough, Stable Spiroacetal Thiol-ene Resin for 3D Printing. *J. Appl. Polym. Sci.* **2018**, *135* (22), 46259.

(8) Alim, M. D.; Childress, K. K.; Baugh, N. J.; Martinez, A. M.; Davenport, A.; Fairbanks, B. D.; McBride, M. K.; Worrell, B. T.; Stansbury, J. W.; McLeod, R. R.; Bowman, C. N. A Photopolymerizable Thermoplastic with Tunable Mechanical Performance. *Mater. Horizons* **2020**, *7* (3), 835–842.

(9) Childress, K. K.; Alim, M. D.; Hernandez, J. J.; Stansbury, J. W.; Bowman, C. N. Additive Manufacture of Lightly Crosslinked Semicrystalline Thiol–Enes for Enhanced Mechanical Performance. *Polym. Chem.* **2020**, *11* (1), 39–46.

(10) Kubota, H.; Nowell, J. B. Changes in the Morphology of Cast Nylon 6 through Copolymerization. *J. Appl. Polym. Sci.* **1975**, *19* (6), 1521–1538.

(11) de Beer, M. P.; van der Laan, H. L.; Cole, M. A.; Whelan, R. J.; Burns, M. A.; Scott, T. F. Rapid, Continuous Additive Manufacturing by Volumetric Polymerization Inhibition Patterning. *Sci. Adv.* **2019**, *5*.

(12) Tumbleston, J. R.; Shirvanyants, D.; Ermoshkin, N.; Janusziewicz, R.; Johnson, A. R.; Kelly, D.; Chen, K.; Pinschmidt, R.; Rolland, J. P.; Ermoshkin, A.; Samulski, E. T.; DeSimone, J. M. Continuous Liquid Interface Production of 3D Objects. *Science* **2015**, *347* (6228), 1349–1352.

(13) Janusziewicz, R.; Tumbleston, J. R.; Quintanilla, A. L.; Mecham, S. J.; DeSimone, J. M. Layerless Fabrication with Continuous Liquid Interface Production. *Proceedings of the National Academy of Sciences of the United States of America*. 2016, pp 11703–11708.

(14) Li, J.; Nagamani, C.; Moore, J. S. Polymer Mechanochemistry: From Destructive to Productive. *Acc. Chem. Res.* **2015**, *48* (8), 2181–2190.

(15) Ganster, B.; Fischer, U. K.; Moszner, N.; Liska, R. New Photocleavable Structures. Diacylgermane-Based Photoinitiators for Visible Light Curing. *Macromolecules* **2008**, *41* (7), 2394–2400.

(16) Moszner, N.; Fischer, U. K.; Ganster, B.; Liska, R.; Rheinberger, V. Benzoyl Germanium Derivatives as Novel Visible Light Photoinitiators for Dental Materials. *Dent. Mater.* **2008**, *24* (7), 901–907.

(17) Bennett, J. E.; Sieper, H.; Tavs, P. 2,2,6,6-Tetramethylpiperidyl-1-Thiyl. A Stable New Radical. *Tetrahedron* **1967**, *23* (4), 1697–1699.

(18) Jaitner, P.; Jager, K.; Dorfer, A.; Schwarzhans, K. Improved Synthesis of the Radical Source Bis[2,2,6,6-Tetramethylpiperidyl-(1)]-Disulfide and Photoinduced Reactions with M2(CO)10 (M = Mn, Re). *J. Organomet. Chem.* **2001**, *621*, 173–176.

(19) Bricklebank, N.; Pryke, A. 2,2,6,6-Tetramethylpiperidin-1-Ylthiyl, the Sulfur Analogue of TEMPO, as an Initiator for the Controlled Radical Polymerisation of Styrene. *J. Chem. Soc. Perkin Trans. 1* **2002**, *18* (18), 2048–2051.

(20) Kelly, B. E.; Bhattacharya, I.; Heidari, H.; Shusteff, M.; Spadaccini, C. M.; Taylor, H. K. Volumetric Additive Manufacturing via Tomographic Reconstruction. *Science* **2019**, *363* (6431), 1075–1079.